NOVEL PHOTOCATALYTIC REACTOR FOR THE DESTRUCTION OF AIRBORNE POLLUTANTS: DESIGN AND PERFORMANCE TESTING

by

Hadeel Ibrahim

Faculty of Engineering Science

Department of Chemical and Biochemical Engineering

Submitted in partial fulfillment of the requirements

for the degree of Master of Engineering Science

Faculty of Graduate Studies

The University of Western Ontario

London, Ontario, Canada

May, 1998

© Hadeel Ibrahim 1998

National Library of Canada
Acquisitions and Bibliographic Services
395 Wellington Street
Ottawa ON K1A 0N4
Canada

Bibliothèque nationale du Canada
Acquisitions et services bibliographiques
395, rue Wellington
Ottawa ON K1A 0N4
Canada

Your file Votre référence

Our file Notre référence

The author has granted a non-exclusive licence allowing the National Library of Canada to reproduce, loan, distribute or sell copies of this thesis in microform, paper or electronic formats.

L'auteur a accordé une licence non exclusive permettant à la Bibliothèque nationale du Canada de reproduire, prêter, distribuer ou vendre des copies de cette thèse sous la forme de microfiche/film, de reproduction sur papier ou sur format électronique.

The author retains ownership of the copyright in this thesis. Neither the thesis nor substantial extracts from it may be printed or otherwise reproduced without the author's permission.

L'auteur conserve la propriété du droit d'auteur qui protège cette thèse. Ni la thèse ni des extraits substantiels de celle-ci ne doivent être imprimés ou autrement reproduits sans son autorisation.

0-612-30696-8

Canada

ABSTRACT

The performance of a novel system that incorporates the UV/TiO_2 technology was used to examine the heterogeneous oxidation of toluene. Experiments were carried out using Photo-CREC-Air, a batch system with air recirculation. In Photo-CREC-Air, TiO_2 is supported on a filter mesh with optimized contacting of near UV light, TiO_2, and air.

In the present study, emphasis was given to the determination of the influence of water vapor content, model pollutant concentration, and temperature on the photoconversion rate. Runs with and without TiO_2 and UV were used to demonstrate that the photocatalytic conversion of toluene takes place to a significant extent at 100°C. At room temperature the extent of photoconversion was very low. Adsorption runs in Photo-CREC-Air (light source "off") showed that pollutant adsorption is not significant, thus a pseudo homogenous model for kinetics modeling is proposed.

Results obtained revealed that the initial rates of toluene photodegradation at 100°C and in the range of model pollutant concentrations and humidity levels studied, are 0.005-0.05 μmole/(gcat.s). Experimental data obtained also showed that the first order is suitable and this yields rate constant equal to 0.033±0.014 (h^{-1}). In terms of energy efficiency, apparent quantum yields were assessed and found to be as high as 450% at the higher toluene concentrations and higher humidity level studied.

DEDICATION

"May there never develop in me the notion that my education is complete but give me strength and leisure and zeal continually to enlarge my knowledge."-Moses Maimonides (1135-1204)

This work in dedicated to my parents Hosni and Fereal and my sisters Gehan, Rana, Reema and Leena without whose help, support, and encouragement throughout my education career this work could not have seen the light.

ACKNOWLEDGMENTS

I wish to express my sincere appreciation to my supervisor Dr. Hugo de Lasa for his guidance, support, enthusiasm, patience and dedication.

I owe very special thanks to Souheil Afara for his help assembling the reactor and his infinite support throughout the course of study.

The contributions of Enzo Peluso could not be forgotten and are highly appreciated.

Special thanks go as well to S. Al-Khattaf, T. El-Solh, P. Fournier, C. Galarraga, L. Hagey, K. Jarosch, L. Oraha, M. Salaices, and B. Serrano for their help, advice, friendship and for providing a great research working atmosphere. Extended thanks to Dr. S. Krol for his help in the physics and the optics of the present project.

Finally, thanks are given to the staff of the Engineering Library, the Engineering Stores, the Engineering Machine Shop, UWO-Research Office and NSERC for their help in making this project feasible.

TABLE OF CONTENTS

LIST OF FIGURES

LIST OF TABLES

LIST OF APPENDICES

NOMENCLATURE

A_f: total free area of holes (cm^2).

A_p: total sectional area of the perforated plate (cm^2).

C: gas phase reactant concentration, and speed of light in vacuum (2.997×10^{10}cm/s), also the orifice coefficient in Figure 4.9.

C_o: orifice coefficient.

C_{OI}: concentration of the oxidized intermediates ($\mu g/cm^3$).

C_p: is the gas phase concentration of the pollutant.

C_v: Venturi coefficient. Empirically determined and is about 0.98 for well designed Venturi of pipe diameter 2-8 in.

C_w: is the gas phase concentration of the water vapor.

C_T: toluene concentration at time t ($\mu g/cm^3$).

C_{To}: initial toluene concentration ($\mu g/cm^3$).

D: hole diameter (cm).

f(C): concentration function of the rate equation.

F_p and F_w: are factors for the competitive adsorption between the pollutant and the water for the same active site.

g_c: gravity dimensional constant (32.17 lb ft/$lb_f s^2$). If SI units are used then g_c=1.

h: Plank's constant (6.62×10^{-34} J.s).

I: light intensity at distance ($\mu W/cm^2$).

I_o: incident intensity.

k(I): intensity dependent apparent rate constant.

k: reaction rate constant, also the ratio of the specific heats C_p/C_v.

$k_{corrected}$: reaction rate constant corrected for UV decay.

k_o: reaction rate constant at the surface and also the constant of proportionality in the Langmuir-Hinshelwood bimolecular reaction form ($\mu mol.cm^{-2}h^{-1}$).

k_s: intrinsic reaction rate constant ($cm^3/gcat.h$).

$K_{(ads)}$: adsorption equilibrium constant which can be measured at the solid-gas interface.

K_1, K_2, K_3, and K_4: are the Langmuir adsorption equilibrium constants ($ppmv^{-1}$).

L: the complete length of the TiO_2 layer.

nm: nanometer.

N_A: Avogadro number (6.023×10^{23} molecules/mole).

p_1: fluid pressure under upstream conditions.

p_2: fluid pressure at the throat conditions.

P: hole pitch.

$Q_{m,abs}$: rate of light energy absorbed by the TiO_2 in the photocatalytic reactor (J.s) at 40 h of lamp operation (50 $\mu W/cm^2$).

r: rate of reaction, ratio of p_2/p_1 in the Venturi calculations, also is the oxidation rate ($\mu mol.cm^{-2}h^{-1}$).

r_{To} : the initial toluene photo-oxidation rate ($\mu mol/ gcat. s$).

$[r_{mp,o}]_{max}$: rate of model pollutant destruction based on the corrected kinetic constants and gas phase toluene concentration when light was turned on.

r_T: rate of toluene photo-oxidation.

t: plate thickness

T: transmittance.

TCE: trichloroethylene.

V: total gas hold up.

V_2: average fluid velocity at the throat of the Venturi.

W: mass flow rate,also the weight of the catalyst involved in the chemical reaction.

x: penetration depth into TiO_2 layer.

Y: dimensionless expansion factor for the flow of compressible fluid.

z: the axial distance through the TiO_2 layer.

Greek letters

ν: gas superficial velocity.

β: ratio of diameter of the Venturi throat to diameter of pipe, also the effective extinction coefficient of the photocatalyst.

λ: wavelength (nm).

ρ_1: density of the fluid under upstream conditions.

Δp: pressure drop across the plate.

Ω: a constant used to correct for the decay in the UV intensity when calculating the kinetic constant k.

θ: surface coverage of the reactant.

μ: the absorbance coefficient of powdered solids.

ΔC: the finite difference between the pollutant concentration at length C_L and its initial concentration C_o.

CHAPTER 1

INTRODUCTION

Legislation and environmental acts are placing more emphasis on the removal of the undesired organic contaminants from air streams or at least the reduction of their emission. One of the processes that has received attention lately for treating air streams is the assisted photocatalytic oxidation with the help of semi-conductors such as TiO_2.

Overall, TiO_2 photocatalytic oxidation seems to be an attractive technique. There are still however, key difficulties related to cost and scale up of this technology. Hence, improvements and modifications are needed to optimize this process and make it more feasible. As a result, intensive research is currently being developed to better understand the photocatalytic reactor design including: reactor geometry, configuration, type and size of photocatalyst, and finally, light intensity and absorption.

This thesis deals with the design and development of a novel photocatalytic reactor and the optimization of its performance in terms of fluid dynamics, illumination, catalyst loading, and quantum yield. This is achieved by studying the photodegradation of a model pollutant: toluene.

Potential uses of this device are either in industrial or residential areas where significant concentrations of chemical vapors can be found; and this includes: offices, buildings, painting shops, car manufacturing industry and coating industry. An application of this technology can also be found in refinery plants to treat gaseous streams which contain undesirable concentrations of organic chemicals, before they are vented.

1.1 Treatment of Polluted Air

1.1.1 Conventional Methods

Air pollutants of major concern belongs to three main classes: metals, organic and inorganic substances. Organic emissions represent a class of chemicals that can be produced during the incomplete consumption of fuels used for heating and transportation. These chemical species can be either totally mineralized or treated by absorption, adsorption, incineration, or condensation [Miller *et al.*, (1993)]. The adsorption process involves the contact of a polluted gaseous stream with activated carbon granules, thus allowing the organic molecules to adsorb onto the carbon particles resulting in a clean air effluent stream. However, this process does not involve complete destruction of the pollutants rather their transfer from the gaseous phase to the solid phase creating a solid disposal problem. In addition, this method is limited to streams with relatively low concentrations [Miller *et al.*, (1993)]. As well, carbon particles require regeneration and eventual disposal which represent an extra cost and difficulty to the process. Finally, this method does not suit all potential organic pollutants since not all of them have good adsorbability properties on the activated carbon particles.

Absorption is similar to adsorption in the sense of transferring the pollutant from one phase to another, liquid in this case, without destroying the pollutants. Condensation is not feasible since its potential use is well outside the limits set for organic pollutant concentrations. Finally, incineration whether direct or catalytic requires either high capital

or operating cost and this presents an important burden on the users of this technology [Miller *et al.*, (1993)].

On the other hand, total or complete mineralization of the organic pollutants may be achieved naturally or using an oxidation process. Natural organic degradation is initiated by sunlight and molecular oxygen, which are naturally abundant. However, this process is very slow and may take years to come to completion. As a result, new technologies are currently considered to speed up these processes using the Advanced Oxidation Processes or AOPs.

1.1.2 Photochemical Processes

AOPs treatment involve accelerated oxidation of the desired chemicals with the help of ultraviolet light and semi-conductors acting as catalysts. Once these processes have emerged, continuous improvements have been added to optimize performance and to increase yields. The main principle adopted by this process is the generation of hydroxyl radicals(·OH). As the ·OH radicals are formed, they attack the organic molecules and react with the pollutant in one of two ways. One possible path is the abstraction of a H atom forming a water molecule and another radical. Another possibility is the addition reaction which requires the addition of the ·OH group to the pollutant molecule forming a combined pollutant-OH radical. The process continues with a series of reaction steps giving water, carbon dioxide and inorganic salts as end products. Examples of the abstraction and addition reactions are reported by Luo and Ollis (1996) as follows:

Abstraction : $^{\cdot}OH + CHCl_2CCl(O) \longrightarrow {}^{\cdot}CCl_2Cl(O) + H_2O$ **(1.1)**

Addition : $^{\cdot}OH + CCl_2CHCl \longrightarrow {}^{\cdot}CCl_2CHClOH$ **(1.2)**

The AOPs are usually classified as homogeneous and heterogeneous processes. In the heterogeneous processes the surface of an illuminated semi-conductor acts, at ambient temperature, as a catalyst by using band gap light as a source of solid excitation" [Peral and Ollis (1992)]. On the other hand, the homogeneous process involves the UV photolysis of chemicals such as H_2O_2 and O_3, to produce $^{\cdot}OH$ radicals which are directly involved in the reaction [Bolton *et al.*, (1995)].

In summary, photocatalytic assisted oxidation requires the presence of oxygen, light of a specific wavelength and a semi-conductor photocatalyst. In this respect, it can be stated that titanium dioxide mineralization of various organic contaminants by illumination is effective for both the aqueous and the vapor phases. This process has been proven effective for the destruction of many classes of chemicals in the vapor phase including alcohols [Childs *et al.*, (1981)], ketones [Sauer and Ollis, (1994)], aromatic compounds [Blanco *et al.*, (1996)], nitrogen containing substances [Ibuski *et al.*, (1993)] and [Anderson *et al.*, (1993)], and halogenated hydrocarbons [Wang *et al.*, (1993)] and [Dibble *et al.*, (1992)].

This technology can be applied in many areas including:

•remediation of contaminated soils and groundwater [Yamazaki-Nishida *et al.*, (1994)].

•improvement of indoor or closed system air quality [Jacoby *et al.*, (1996), Obee *et al.*, (1995)].

•treatment of industrial process vents.

Regarding potential chemical pollutants that can be treated by photoreactors, there is a class of organic substances named Volatile Organic Compounds (VOCs). VOCs are characterized by having a boiling point ≤ 100°C and/or a vapor pressure >1mm Hg at 25 °C [Tchobanoglous and Burton, (1991)]. These compounds are of major concern because when they are in the vapor phase they are very mobile, which make their release to the environment more likely; in addition their presence in the atmosphere may cause a public health risk. VOCs are produced in various industrial operations such as paint drying, metal degreasing, printing, and air striping units. VOC effluents cannot be vented directly from the industrial and the commercial sites. Hence, photo-oxidation can be applied to help in reducing their concentration in the vented streams.

1.2 Photocatalysis Advantages and Limitations

The process of UV/TiO_2 suffers from several disadvantages that have been reported in the technical literature:

a) Mass transfer limitations, since the process is a heterogeneous reaction.

b) Rate inhibition due to humidity.

c) Catalyst deactivation due to the adsorption of intermediate species.

d) The hole-electron recombination process. Generated holes and electrons can recombine and the process of excitation can be reversed leading to inefficiencies in terms of wasted energy.

e) The incomplete photocatalytic oxidation of TCE and other chlorinated hydrocarbons. With high gas flow rates, this can produce significant quantities of undesirable and toxic byproducts such as phosgene [Milne *et al.*, (1992)].

On the other hand, UV/TiO_2 processes allow the purification of air and water with the following advantageous characteristics:

a) No chemical addition (other than the catalyst). There is no need for additives since electrons are strong reductants. Holes are as well strong oxidants.

b) Catalyst recovery or regeneration is possible.

c) Energy, particularly if sun light is used, is cheap, available, renewable and environmentally friendly.

Given the significance of TiO_2/UV technology for air treatment, the present study proposes a novel Photo-CREC-Air reactor design for pollutant degradation.

CHAPTER 2

LITERATURE REVIEW

The photoactivity of semi-conductors was first described in 1972 by the work of Fujishima and Honda who discovered that water "could be split (simultaneously oxidized and reduced) upon illuminating a TiO_2 single-crystal electrode to which small electrochemical bias had been applied", [Fujishima *et al.*, (1972)]. Since then, there is a growing interest in the organic photoconversion of organic pollutants in both aqueous and gaseous phase.

In order to understand the principles of photocatalysis, one should consider the differences between thermal reactions and photocatalysis reactions as explained by Formenti *et al.*, (1979). Photocatalysis requires the absorption of a specific wavelength radiation by a TiO_2 molecule promoting the fundamental step of the reaction: the transfer of an electron from the valence band to the conduction band producing what is known as the electron-hole formation mechanism. On the other hand, thermal processes take place under high temperatures with electrons remaining at the ground level. Thus, photocatalytic processes have, over thermal processes, the advantage of requiring lower temperatures usually close to ambient temperature, which translates into huge savings in fuel and hence process cost.

Until now, the chemistry behind the destruction process of organic pollutants by photocatalysis is not fully understood. Many questions still remain unanswered: Does photocatalysis really work for all classes of pollutants? Is there a limit on the pollutant concentrations? How do catalyst additives affect selectivity and synergism?

2.1 Photocatalysts

Photocatalysts are usually semi-conductor materials that enhance the photocatalytic reaction by lowering the required activation energy of the reaction due to the special electronic band structure they possess. A wide range of semi-conductors have been tested for photocatalytic processes such as: TiO_2, ZnO, Fe_2O_3, WO_3, CdS, and ZnS. However, the desirable properties of TiO_2 in terms of catalytic activity, chemical stability, non toxicity, cheapness and availability made it the photocatalyst of choice.

Photocatalysts, and more specifically the most popular one TiO_2, possesses a special electronic band structure. As a semi-conductor, it contains equally spaced energy levels with electrons termed "valence band". In addition, there is another set of equally spaced energy levels, at a higher state, which are electron deficient called the "conduction band". The separation between these two bands is termed the "band gap". When a photocatalyst undergoes illumination by a light source emitting radiation at a specific wavelength with an energy equal to or greater than that of the band gap, it absorbs the energy promoting an electron excitation from the valence band, to the conduction band. This leaves a fraction of the surface with electron deficiency forming a hole denoted as h^+. This process is illustrated in Figure 2.1 as well as in the following equation:

$$TiO_2 + h\nu \longrightarrow h^+ + e^- \qquad (2.1)$$

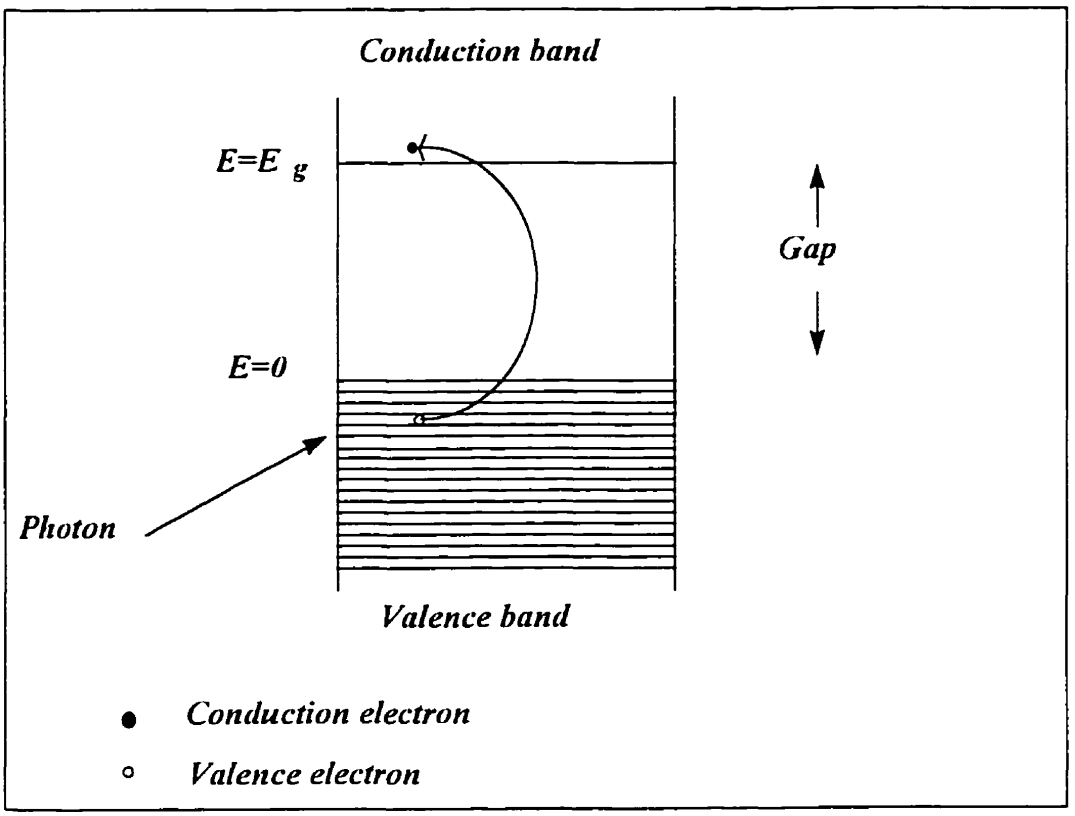

Figure 2.1: The electronic structure of an excited TiO_2 atom.

Ref.: Van Vlack, (1982), pg. 277.

The above described step lowers the activation energy of the oxidation reaction of pollutants with oxygen. The final products of this oxidation reaction are eventually, in most cases, carbon dioxide, water and several other mineral salts.

Once the step described by eq. (2.1) is completed, a number of chemical reactions are thought to proceed, as will be described later on in this chapter (Reaction Mechanism Section).

Titanium dioxide is a semi-conductor with a chemical formula of TiO_2. It does not dissolve in water, which makes it a very good candidate for water treatment processes.

However, it dissolves in many alcohol and organic solvents such as methanol and acetone. TiO_2 powder is white in color, has no smell and it crystallizes in two forms: anatase and rutile. TiO_2, under the rutile crystallographic form, is usually used as a pigment in white paints and as a base in cosmetic products.

Light absorption of TiO_2 is suitable at the band gap light energy between 230-390 nm. This region falls in the near ultraviolet spectrum. The anatase form has demonstrated great efficiency in terms of photocatalytic activity much more than the rutile phase. The band gap of the anatase crystal is 3.2 eV [Bolton *et al.*, (1995)], and this indicates that only photons that have a 290-390 nm wavelength may be absorbed by the crystals.

2.2 Photoreactor Design

Several laboratory scale reactors have been built to test and to develop the UV/TiO_2 technology. On the other hand, few units were built at a large scale, and this is due to the relative high cost of lamp powering, lamp replacement, catalyst separation and catalyst regeneration. However, novel concepts taking advantage of the use of solar energy can also have significant future impact such as the Almeria unit in Spain [Muriel *et al.*, (1996)]. In general, it is our view that new designs with high efficiency promoting total pollutant mineralization should be encouraged [Serrano and de Lasa, (1997)].

In order to achieve this, careful consideration of the following factors is required: selection of UV source, reactor configuration, special arrangement for lamp placement, catalyst type, size, distribution and impregnation and efficient interaction between the light, the catalyst and the reacting fluid.

2.2.1 Reactor Configuration

Regarding possible reactor configurations, there are a significant number of studies dealing with different designs, different classes of pollutants, pollutants concentrations, and operating under different conditions. These different conditions involve temperature, relative humidity, pressure , space time and irradiation time.

For the specific application of gaseous streams containing organic pollutants solid-gas reactors are considered. The TiO_2 particles, constituting the solid phase, are held on a solid surface in many different ways including:

a) A thin film of TiO_2 coated on the inner surface of the reactor wall [Jacoby *et al.*, (1996)].

b) TiO_2 supported onto a porous fibrous mesh [Peral and Ollis (1992),)], or monolith [Blanco *et al.*, (1996), Obee *et al.*, (1995)], Honeycomb[Suzuki, (1993)].

c) TiO_2 entrapped in supporting particles [Dibble *et al.*, (1992), Yamazaki-Nishida *et al.*, (1993), Yamazaki-Nishida *et al.*, (1994), and Anderson *et al.*, (1993)]

d) TiO_2 coated on an optical fiber bundle. Optical fibers have the advantage of direct fiber-photocatalyst radiation transfer and high activated surface area to reactor volume. Care has to be taken given the potential catalyst deactivation due to heat build up in the fiber optic bundle array [Peill *et al.*, (1995), and Peill *et al.*, (1996)].

Regarding the above mentioned options, most of the work developed in the past used either option a) or b). The above mentioned supports for TiO_2 can be configured in reactors of different geometry such as: fluidized beds, fixed powder layer reactors, annular reactors, and monolith reactors.

A bench scale, flat plate fluidized bed was utilized by Dibble *et al.*, (1992) to study the photocatalytic oxidation of TCE, produced during the air stripping of contaminated ground water. TiO_2 was supported on silica gel beads, that were 250-450 μm in diameter, inside the reactor cavity that was 10mm wide, 60mm high and 4 mm thick. A 4 W lamp was used to emit light with maximum intensity near 390nm. This design of fluidized bed is suited for isothermal operation, large scale, improved heat transfer and reduced mass transfer conditions. Catalyst regeneration is also relatively easy to implement. However, gas bypass, attrition of the photocatalyst and non-uniform residence time for the solids are potential problems of fluidized bed reactors [Ollis, (1993)].

In this respect, Formenti *et al.*, (1976) proposed a reactor with the TiO_2 supported on a metallic support to study the photo-oxidation of alkanes. Peral and Ollis (1992) employed a reactor with TiO_2 supported on a fritted glass plate for the oxidation of various aromatics in air. It is argued that powder layer fixed beds are more suited for compact systems having little extent of gas backmixing. In these systems, there is, however, limited light distribution and only relatively small air flow rates can be treated [Ollis, (1993)].

The annular photoreactor is another possible design configuration. The inner surface is coated with a thin layer of TiO_2 with the UV light source placed in the center of

the cylindrical reactor. Jacoby *et al.*, (1996) made use of this geometry to control the VOCs in indoor air. This method has, however, the disadvantage of low area to volume ratio.

Finally, another alternative design uses a coated TiO_2 monolith. In this respect, toluene oxidation was achieved by Blanco *et al.* (1996) in a coated monolith. Air streams at 150-450°C were contacted with the catalyst in the presence of UV light provided by a Xenon lamp. In this respect, commercially available monoliths can be operated under low pressure with narrow distributions of gas residence times. However, given side illumination in these devices, illumination of the photocatalyst is limited and non-uniform [Ollis ,(1993)].

2.2.3 Light Absorption and Sources

Regarding the light absorbed, it is assumed that the light is absorbed by the photocatalyst ($I_{abs,cat}$) with no light absorbed by fluid or substrate molecules [Childs and Ollis, (1980)]. $I_{abs,cat}$, is influenced by many factors including: reactor geometry, wavelength, inhomogeneity of reaction mixture, absorption coefficients and light source.

The intensity profile of a light source in an absorbing medium can be related to the incident light intensity as follows:

$$\mathbf{Log(I_0/I)=\mu x= Absorbance} \qquad \mathbf{(2.2)}$$

with μ being the absorbance coefficient of powdered solids, x the penetration depth into TiO_2 layer, and I_o the incident intensity.

A typical value of UV light penetration into a TiO_2 powder is about 2 μm [Childs and Ollis, (1980)]. Thus, the range of light penetration for a particle (100 μm) may be limited to the 1-2 μm of the TiO_2 particle outer shell. Anderson *et al.* (1993) reports that : in a packed bed, UV light is completely absorbed in the first 10-15 μm of the TiO_2 pellets. In summary, the use of particles bigger than 10 microns is largely unwarranted.

There are many different photoreactor types and light sources which are used for the purpose of illuminating the photocatalyst. Besides the solar energy, artificial lamps of different kinds can be used. Bolton *et al.* (1995) classifies and characterizes the various UV sources as follows:

a) Low pressure mercury lamps. They have the characteristic of having long life (~5000 hr), and approximately 80% of the emission is in the 254 nm range.

b) Medium pressure mercury lamps. This kind of UV lamp is known to have a moderate life (~2000 hr) and broad spectral output, not much below 250 nm.

c) Advanced proprietary medium pressure mercury lamps. These lamps provide a strong output below 250 nm, and have long life (~3000 hr).

The estimation of light absorption may be done by actinometry [Valladares, (1995), Matthews, (1988)]. The actinometry technique is based on the photochemical conversion of Fe (III) to Fe (II) ion. However, sometimes special procedures are required to measure the photon flux in the reactor. A good methodology for assessing the light emitted and the light absorbed by a catalyst mesh is the one proposed by Serrano and de Lasa (1997) and also described further in this thesis.

Anderson *et al.*, (1993) reported that reaction rates showed a first order with respect to light intensities. They also anticipated that the linearity in the relationship indicate that mass transfer is not limiting the TCE conversion rate. In their analysis the absorbed light intensity was the amount absorbed by the catalyst particles and not by the fluid molecules.

2.3 Reaction Kinetics

2.3.1 Reaction Pathway and the Limiting Step

The photocatalytic reaction involves a number of physical and chemical processes that take place before the formation of the end products (CO_2 and H_2O). In this respect, Jacoby *et al.*, (1996) has done some work to identify these steps proposing the following steps:

(1) Bulk mass transport of the reactants from the gas phase to the surface of the catalyst particle.

(2) Mass transport of the reactants within the catalyst particles "intraparticle diffusion".

(3) Adsorption of the reactants onto the catalyst surface.

(4) Surface chemical reaction.

Following the surface chemical reaction, two other steps, product desorption and mass transport from the catalyst surface to the bulk flowing stream, take place. Among these steps the slowest one in the whole process is the limiting or the controlling step.

The mass transfer coefficient for the external resistance, which covers the transfer of substrate from the mixing gas stream in the bulk to the exterior surface of the catalyst pellet (0.3-1.6 mm) in a packed bed, was estimated by Yamazaki *et al.*, (1993) and Anderson et al., (1993) using the Petrovic-Thodos correlation and Chilton-Colburn factor. Results indicated that the calculated values for the mass transfer coefficient were several orders of magnitude higher than the corresponding pseudo-order rate constant. Therefore, they concluded that external mass transfer is not controlling the photocatalytic reaction rate.

Another set of experiments was carried by Yamazaki *et al.*, (1993) to investigate the effects of the internal film resistance using TiO_2 particles supported on 0.3-1.6 mm pellets. The experiments were conducted by changing the photocatalyst pellet size (0.3-1.6 mm) for a given catalyst weight. Results revealed no effect on the rate of TCE degradation. However, Anderson argued that "theoretical calculations " showed that the internal diffusion was in the Kundsen regime and its influence on the reaction rate could be important if all the internal pellet surface was considered to be active. Given UV light is completely absorbed on the 10-15 μm pellet outer region, it is concluded that intraparticle diffusion effects are not significant.

In another report, Jacoby *et al.*, (1996) developed additional research with TiO_2 to investigate the relative influence of the different steps and to determine the limiting step. They performed a comprehensive study of the adsorption process to decide if adsorption was limiting. Adsorption was examined by conducting experiments using benzene as a model pollutant. Experiments were performed by feeding benzene, water vapor, and air to

an annular photocatalytic reactor with TiO_2 coated on the inner surface of the outer cylinder under various parameters and operating conditions. The different cases studies are summarized in Table 2.1 and the results of each case are illustrated in Figure 2.2.

Table 2.1: Mass transport/adsorption experiments using benzene in air as model pollutant as reported by Jacoby *et al.* (1996).

Case	Light	Catalyst	Air/N_2	Water Vapor (mtorr)
I	No	No	Air	500
ii	Yes	No	Air	500
iii	No	Yes	Air	500
iv	Yes	Yes	N_2	500
v	Yes	Yes	N_2	Dry
vi	Yes	Yes	Air	500

Figure 2.2 suggests that the interaction between both the UV light and the TiO_2 particles is important in the adsorption process. In case i), total absence of both UV radiation and catalyst, little benzene was adsorbed on the Pyrex tube. However, this amount increased when the UV was turned "on" (case ii), and it almost tripled in the presence of a thin TiO_2 film (case iii). Furthermore, when the catalyst layer was illuminated by UV, it led to a large increase in the amount of benzene adsorbed (Cases iv, v, and vi). However, the highest increase was achieved with dry air (Case v) which confirms that water does affect the adsorption of aromatics on the surface of the photocatalyst [Jacoby *et al.*, (1996)]. In addition these authors found that the

photoreaction occurs at rates much slower than the adsorption process, hence they concluded that the surface chemical reaction is the controlling step.

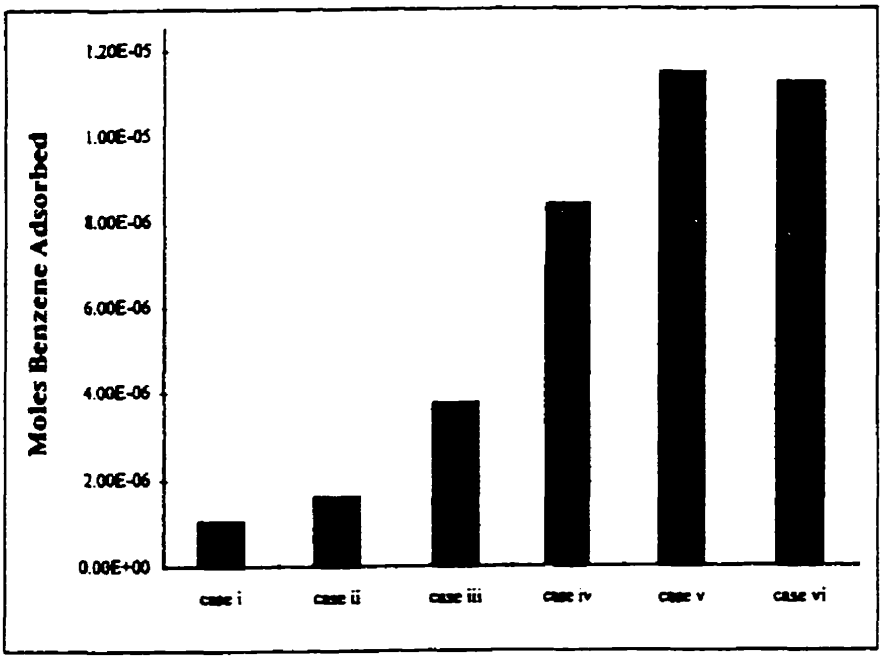

Figure 2.2: Amount of benzene adsorbed as a function of presence or absence of catalyst and near UV irradiation; cases shown in Table 2.1.

Ref.: Jacoby *et al.*, (1996).

2.3.2 Kinetics of the Adsorption Reaction

The adsorption of an organic substrate onto the surface of the photocatalyst can be predicted by a Langmuir-Hinshelwood type model. Fox and Dulay (1993) have incorporated the following assumptions in their adsorption model:

(1) At adsorption equilibrium, the number of surface adsorption sites is fixed.

(2) Only one substrate may bind at each surface site.

(3) The heat of adsorption by the substrate is identical for each site and is independent of surface coverage.

(4) There is no interaction between adjacent adsorbed molecules.

(5) The rate of surface adsorption of the substrate is greater than the rate of any subsequent chemical reactions.

(6) No irreversible adsorption of active sites occurs.

Thus, at adsorption equilibrium the following Langmuir adsorption isotherm equation results:

$$\theta = K_{(ads)}C/(1+K_{(ads)}C) \qquad (2.3)$$

with θ being the surface coverage of the reactant, $K_{(ads)}$ the adsorption equilibrium constant which can be measured at the solid-gas interface, and C the initial concentration of the reactant.

Once the fraction of the adsorbed reactant is determined, one can search for evidence of transient formation of the reduction-oxidation intermediates. According to Fox (1988) kinetic modeling should allow a distinction between a Langmuir-Hinshelwood mechanism, where the primary redox intermediates undergo subsequent thermal reactions before desorbing from the surface, and an Eley-Rideal model, where the redox intermediate desorbs before undergoing secondary reactions. After Fox(1988) it is also possible to kinetically distinguish a Langmuir model where the surface is considered to be smooth so that adsorption is not dependent on surface coverage and a Freundlich model wherein adsorption on a rough surface depends on pre-adsorption of the substrate or co-adsorbates.

It was suggested by Fox, (1988) that a modification of the derived rate equation based on the Langmuir-Hishelwood form is required to accommodate the competitive adsorption between more than one species. Under these conditions the modified rate equation takes the following form:

$$r_{LH}=kK_{(ads)}C/(1+K_{(ads)}C+\sum K_{(ads)i}C_i) \qquad (2.4)$$

with i referring to the competitively adsorbed chemical species.

2.3.3 Kinetics of Surface Reaction

Studies concerning kinetics of photocatalytic reactions are usually done on fixed bed reactors. For good kinetics calculations, designs have been carefully developed to be free of mass transfer or diffusional limitations [Ollis (1993)].

Pearl *et al.*, (1992), propose the following pseudo homogeneous model equation for a packed bed reactor assuming complete and uniform light absorption. These authors utilized a 12.5 cm^3 flow reactor with a fritted glass plate to support the catalyst and a 200 W high pressure Hg-Xe lamp or a 100 W black light placed outside shinning through quartz window covering the top of the reactor. A pollutant mass balance yields the following:

$$-vdC/dz=k(I)\ f(C) \qquad (2.5)$$

with v being a gas superficial velocity, C a gas phase reactant concentration, k(I) an intensity dependent apparent rate constant, z the axial distance through the TiO_2 layer, and f(C) a concentration dependent function.

Note that the k parameter is a function of the light intensity as shown in eq. (2.6) below with Ω being in the range of $0.5<\Omega<1$. The Ω value of 0.5 indicates a high intensity, while $\Omega=1.0$ corresponds to a low intensity. In addition, Beer's law provides a relationship between the variation of intensity with distance, hence the k parameter can be written in the following form:

$$k(I)=k_o(I/I_o)^{\Omega}= k_o e^{(-\Omega\beta z)} \qquad (2.6)$$

with Ω being a constant, z the axial distance through the TiO_2 layer, and β the effective extinction coefficient of the photocatalyst which in the case of TiO_2 is equal to $10211 cm^{-1}$ [Luo and Ollis, (1996)].

Note that f(C) is the reactant concentration dependent function that can take various mathematical forms. As an example, one can postulate a Langmuir-Hinshelwood form for f(C):

$$f(C)=KC/(1+KC) \qquad (2.7)$$

Substituting eqs. (2.6) and (2.7) into eq. (2.5), it results:

$$v(dC/dz)=-k_o e^{(-\Omega\beta z)}[KC/(1+KC)] \qquad (2.8)$$

Integrating this equation over the complete length of the TiO_2 layer from $z=0$ to $z=L$ where L is the depth of the TiO_2 layer, the integral of equation(2.8) yields:

$$[\ln(C_L/C_o)]+K(C_L-C_o)=-k_oK(1- e^{(-\Omega\beta L)}/(\Omega\beta v) \qquad (2.9)$$

According to Formenti *et al.*, (1971), when L>15μm all light radiation is adsorbed in the catalyst layer, as a result the term $e^{(-\Omega\beta z)}$ approaches the value of zero. Then equation (2.9) is simplified to:

$$[\ln (C_L/C_o)]/(C_L-C_o)=-k_oK/(\Omega\beta v\,(C_L-C_o))-K \qquad (2.10)$$

Thus, if the proposed approximation is correct, when $[\ln(C_L/C_o)]/(C_L-C_o)$ is plotted against $(1/(C_L-C_o))$ a straight line should result with $k_oK/(\Omega\beta v)$ being the slope and -K the intercept. Experimental values of the slope and the intercept allow the determination of k_o and K. These parameters were actually determined by Peral and Ollis (1992), for some pollutants including acetone, 1-butanol, and m-xylene. Values are summarized in Table 2.2. Parameters estimation was also performed by Luo and Ollis (1996) for toluene. When comparing the values reported, it appears that acetone, toluene and m-xylene have the same order of magnitude of the photo-oxidation rate constant and adsorption constant, whereas the 1-butanol has a greater reaction constant indicating a higher potential for reactivity.

Table 2.2: Kinetics constants for selected pollutants as reported in Peral and Ollis (1992)

Pollutant	k_o (g/L.min)	K (m^3/mg)	Reference
Acetone	7.75	.00644	Peral and Ollis (1992)
1-Butanol	49.2	.00109	Peral and Ollis (1992)
Toluene	3.14	.0046	Luo and Ollis (1996)
m-Xylene	1.3	.00659	Peral and Ollis (1992)

Ollis (1993), also reported that for lower UV intensities or slower rates ($\Delta C<5\%$), equation(2.10) can be approximated by the following finite difference equation:

$$-\Delta C/C_o=-k_oK/(\Omega\beta v)+ K\Delta C \qquad (2.11)$$

where ΔC represents the $C_L - C_o$ difference.

In this case the values of k_o and K are evaluated by plotting $\Delta C/C_o$ versus ΔC. Note that the Ω value was determined on the basis of eq. (2.6) by plotting the logarithm of the reaction rate versus the logarithm of the incident irradiation. A straight line was obtained with Ω as a slope. Peral and Ollis (1992) found that this slope was 0.7 which was an intermediate value between the two extremes 0.5 and 1.

Another example of a suitable reaction rate equation is the one developed for toluene oxidation by Luo and Ollis (1996). It was found that below 160 mg/m^3 the reaction rate can be approximated with a first order expression, while in the range of 160-

550 mg/m^3 the reaction falls between zero and first order. Consistent with this, the following rate equation was proposed:

$$\textbf{Rate} = 3162\ C_{tol}/(1+0.00463\ C_{tol}) \qquad (2.12)$$

2.3.4 Reaction Mechanism

The detailed mechanism of semi-conductor assisted photoreactions is still not fully understood. A suggested mechanism representing initial reaction steps is the one proposed by Peral and Ollis (1992):

$$TiO_2 + h\nu \longrightarrow h^+ + e^- \qquad (2.13)$$

$$h^+ + OH^- \longrightarrow OH \qquad (2.14)$$

$$Ti^{4+} + e^- \longrightarrow Ti^{3+} \qquad (2.15)$$

and

$$Ti^{3+} + O_{2ads} \longrightarrow Ti^{4+} + O_{2ads}^- \qquad (2.16)$$

or

$$O_{2ads} \longrightarrow 2O_{ads} \qquad (2.17)$$

$$Ti^{3+} + O_{ads} \longrightarrow Ti^{4+} + O_{ads}^- \qquad (2.18)$$

Thus, once the process is initiated by the promotion of electrons in the TiO_2 catalyst by the near UV light to a higher energy band (conduction band), holes are left behind (eq. 2.13). Electrons are trapped by Ti^{-4} (eq. 2.15) or adsorb oxygen molecule

(O_{2ads}) yielding either two adsorbed oxygen ions O_{ads}^- (eqs. 2.17 and 2.18) or an adsorbed oxygen molecular ion O_{2ads}^- (eq. 2.16). On the other hand, the generated holes adsorb hydroxyl ions (OH^-)or water molecules creating hydroxyl radicals ($^{\cdot}OH$) which react with an adsorbed pollutant molecules initiating the degradation process.

As it was described above, the main products of the TiO_2 conduction band electrons are adsorbed O^-_{2ads} or O^-_{ads}, and/or adsorbed hydroxyl radicals from the generated holes in the valence band. Anderson *et al.* (1993) were able to show that O^-_{2ads} radicals contributed to additional $^{\cdot}OH$ radical formation through the following reaction sequence:

$$TiO_2 + h\nu \longrightarrow h^+ + e^- \quad (2.19)$$

$$O_{2ads} + e^- \longrightarrow O_{2ads}^- \quad (2.20)$$

$$O_{2ads}^- + H^+_{ads} \longrightarrow HO_{2ads} \quad (2.21)$$

$$2HO_{2ads} \longrightarrow H_2O_{2ads} + O_{2ads} \quad (2.22)$$

$$H_2O_{2ads} + e^- \longrightarrow {}^{\cdot}OH_{ads} + OH_{ads}^- + O_{2ads} \quad (2.23)$$

Note that these extra $^{\cdot}OH$ radicals can also be involved in the photoconversion reaction.

2.3.5 Influence of Water Vapor on Kinetics

Water vapor content has different effects on contaminant degradation rates and this depends on its concentration and the pollutant's structure. It was found that water

vapor strongly inhibits the oxidation of iso-propanol [Bickley *et al.*, (1973)], TCE at high concentration [Dibble *et al.*, (1992), Bickley *et al.*, (1973)] and acetone [Peral and Ollis (1992)]. Water vapor enhances however, toluene oxidation [Peral and Ollis, (1992)], has no effect on 1-butanol oxidation and increases m-xylene oxidation rate up to 1500 mg/m^3 and decreases the rate thereafter [Peral and Ollis, (1992)]. Furthermore, for a low TCE inlet concentration (6 ppm) the reaction rate was not influenced by the water concentration [Dibble *et al.*, (1992)].

These differences due to water content were explained by Peral and Ollis (1992) as due to relative "adsorption competition". These authors stated that acetone appeared to be less strongly adsorbed into the TiO_2 than 1-butanol. Thus, water could displace surface-adsorbed acetone but not the latter. As a result, the variable role of water in m-xylene photo-oxidation may follow that of TCE, where traces of water are required for activity, but excess water is inhibitory [Peral and Ollis (1992), p563].

Muradov *et al.*, (1996) disagreed, however, with the above results and stated that water vapor in the inlet air stream increases the oxidation yields of acetone and ethanol by 5.6% and 13.3%, respectively. This was explained arguing that an increased water vapor enhances hydroxyl radical formation and this outweighs the inhibiting effects caused by water adsorption on the available active sites on the TiO_2 surface.

Moreover, in a recent study by Luo and Ollis (1996) it was found that toluene oxidation rate was higher in the presence of water up to 23-40 % relative humidity(2000-3000 mg/m^3). Inhibition was significant at 60% relative humidity (6100mg/m^3). These authors postulated a formula applicable for water contaminants below 6000mg/m^3. This

formula relates the surface photochemical reaction rate of toluene with water concentration as follows:

$$r=710.7[C_{H2O}]/[1+5.325*10^{-4}\ [C_{H2O}]+1.9241*10^{-7}([C_{H2O}])^2] \qquad (2.24)$$

where $[C_{H2O}]$ is in mg/m^3 and r is in $mg/(m^3.min)$.

It has to be mentioned that Luo and Ollis's results (1996) are consistent with Ibusuki and Takeuchi (1986), who studied the photo-oxidation of toluene and found that the relative humidity in an air stream increases toluene photo-oxidation. Their findings were explained by the following sequence of steps as proposed by Bickley *et al.*, (1973):

$$TiO_2 \longrightarrow h^+ + e^- \qquad (2.25)$$

$$OH^- + h^+ \longrightarrow {}^{\cdot}OH_{ads} \qquad (2.26)$$

$$O_2 + e^- \longrightarrow {}^{\cdot}O^-_{2ads} \qquad (2.27)$$

As it has been pointed out earlier in this thesis, the excitation of a TiO_2 molecule by UV light produces a hole and an electron. Once the hole is trapped with OH^-_{ads}, the electron promotes O_2 adsorption on the TiO_2 surface. The more water molecules available, the more OH^-_{ads} will be available, allowing even further adsorption of oxygen molecules. Since both ${}^{\cdot}OH_{ads}$ and ${}^{\cdot}O_2^-{}_{ads}$ have the potential to oxidize the intermediate products resulting from the oxidation of toluene, it is postulated that higher rates of oxidation are achieved with little or no intermediates being detected.

2.3.6 The Influence of Temperature on the Kinetics of the Reaction

Temperature is a significant parameter that often influences reaction rates. In general, temperature was found to have a minimal effect on the photo-oxidation process. However, temperature had some influence on the oxidation of ethanol, acetone and nitroglycerine [Muradov *et al.*, (1996)]. In this case, as temperature was increased, the rate of photodegradation was decreased. It has to be mentioned that the observed temperature effect was mainly due to the adsorption-desorption dynamic process. Pollutant adsorption is an exothermic process overall. Thus, increasing the temperature shifts the overall adsorption process towards a dominant desorption . In the case of acetone, the reduction of the photodegradation rate was clear since acetone was less adsorbed on TiO_2 surface than the other compounds.

Anderson *et al.*, (1993) found that when increasing the temperature between 23°C and 62°C, the reaction rate for TCE degradation remained essentially constant meaning that there was no significant energy barrier for the initial reaction steps to take place.

Thus, photocatalytic reactions are not dramatically influenced by temperature. Fox *et al.*, (1993) and Fox *et al.*, (1988) argued that this results because the excitation energy is generally much larger than the energy required to overcome ground state activation energy barriers.

2.4 Review of the Previous Toluene Studies

Reports in the technical literature address many aspects related to the engineering of the photocatalytic process, kinetic constant determination and problems associated with cost, scale up and commercialization. Several patents and increasing numbers of papers are being published dealing with different reactor configurations and model pollutants.

TCE photo-oxidation has been broadly evaluated [Wang *et al.*, (1993); (Dibble *et al.*, 1990); and Yamazaki *et al.*, (1994)], because of its high photocatalytic quantum yield [Luo and Ollis (1996)]. Toluene is frequently used, given it is a typical pollutant from several chemical industries and the largest constituent of aromatic hydrocarbon anthropogenic emissions [Lonneman *et al.*, (1974)]and [Heuss *et al.*, (1974)]. Toluene oxidation has been studied as a single pollutant and in mixtures to determine the selectivity behavior of the photocatalytic reaction.

Blanco *et al.* (1996), investigated the oxidation of toluene (3000-6000ppm) on monolithic catalysts. These monoliths were based on titania dispersed on a fibrous silicate and irradiated with a 4000W Xenon lamp (average flux reaching the surface=8W/cm^2) at temperatures of 130-450 °C. Runs below 130 °C were avoided due to potential toluene condensation, as well as runs above 500°C due to catalyst properties changes. Reactions with 96% conversion rates were achieved. It is worth noting that this set-up did not have a very efficient lamp, since 0.2 % of the actual supplied power reached the catalyst surface.

Initially Suzuki *et al.* (1991) studied the photo-oxidation deodorization of air with low pollutant concentration including toluene (80 ppm) in a 8 x 6 x 2 cm^3 box with a 500 W UV lamp. These authors proposed a pseudo-first order reaction for all compounds including toluene which degraded in 60 min achieving a 90% conversion with a rate constant of 0.059 min^{-1}. Based on this experimental work, Suzuki (1993) developed a 70 % efficient purifier that can fit new and existing cars.

Luo and Ollis (1996) studied the kinetics and the time-dependent catalyst activity for both individual and in-mixture oxidation of toluene and TCE. Toluene oxidation in the range of 80-550 mg/m^3 and relative humidity of 20% was tested in a bed flow reactor designed by Peral and Ollis. This study revealed Langmuir-Hinshelwood rates with 20-8% conversion for 80 mg/m^3 and 550 mg/m^3 respectively, no intermediate products detection and a reaction rate constant and an adsorption constant of k=3.14 g/L.min and K_{ads}=0.00463 m^3/mg, respectively.

Another interesting study of toluene was conducted by Obee *et al.*, (1995) who proposed a Langmuir-Hinshelwood reaction rate for a bimolecular surface reaction of the following form:

$$r=k_o F_p F_w \tag{2.28}$$

$$F_p=K_1 C_p/(1+K_1 C_p+K_2 C_w) \tag{2.29}$$

$$F_w=K_4 C_w/(1+K_3 C_p+K_4 C_w) \tag{2.30}$$

where r is the oxidation rate ($\mu mol.cm^{-2}h^{-1}$), k_o is the constant of proportionality ($\mu mol.\ cm^{-2}\ h^{-1}$), K_1, K_2, K_3, and K_4 are the Langmuir adsorption equilibrium constants ($ppmv^{-1}$),

C_p, C_w are the gas phase concentrations of the pollutant and water vapor, respectively, and F_p and F_w are the competitive adsorption for the pollutant and the water on the same active sites. Experiments were conducted at room temperature and 40 % relative humidity. Values for the Langmuir adsorption equilibrium constants and the rate constant were found to be: K_1=2.02, K_2=.000727, K_3=2.02, K_4=.000727, and k_o=3.84. These authors explain that in the case of high toluene concentration (>60 ppm), the L-H rate equation will be first order in water concentration.

Studies of toluene in mixtures were also conducted by several researchers. Akimoto *et al.*, (1978) investigated the photo-oxidation of toluene-NO_2-N_2 and /or O_2 as a function of reactant concentrations and they proposed mechanisms and possible pathways for the reaction. Atkinson et al., (1980) tested similar systems involving toluene/NO_x/air, toluene/benzaldehyde/NO_x/air and cresol/NO_x/air. Besemer *et al.*, (1982) describes the products resulting from the photochemical oxidation of toluene and toluene/ ^{14}C in a smog chamber. Shepson *et al.* (1984) reviewed the photo-oxidation of toluene and o-xylene in the CH_3ONO/NO/air system and extensively explained the mechanisms involved for product formation.

2.5 Conclusions

This chapter reports progress on the understanding of the fundamental aspects of photocatalysis with TiO_2. This includes mechanistic insights as well as kinetic modeling of airborne pollutant photo-oxidation. There is also a review of the influence of the important parameters such as irradiation intensity, temperature, model pollutant

concentration and water concentration. Finally, a review of current photoreactors for air treatment is provided with the goal of advancement through design improvements, as proposed in Photo-CREC-Air.

CHAPTER 3

SCOPE OF THE RESEARCH

The primary objectives of the present research were:

1. to design, build and operate a novel photoreactor, Photo-CREC-Air, for air purification utilizing TiO_2/UV photo-oxidation technology. This reactor includes with special features in terms of geometric configuration, TiO_2 catalyst loading, and light distribution to yield optimal reactor configuration and high quantum yields. For achieving this a novel design is considered accounting for various physico-chemical reactions and engineering aspects of the technology.
2. to evaluate the performance of the prototype developed in the course of this research. Performance evaluation also involves qualitative and quantitative analysis of intermediate species and end products.
3. to examine the effects of water vapor content, temperature, pollutant concentration on the photocatalytic oxidation rate and use these data to establish a photodegradation rate model.

It is worth mentioning that the medium term goal for this research is to establish a laboratory scale photocatalytic unit for testing the photodegradation of airborne contaminants. This entails the construction of a unit with special features such as high catalyst loading, uniform air flow, good reactor illumination, high quantum and chemical yields.

The long term intents of this work are to provide results that can be the basis for scaling up and the transfer of the technology to an industrial/residential site.

CHAPTER 4

PHOTO-CREC-AIR DESIGN

There is a lack of proper design procedures and technical data for photocatalytic reactors. The newly proposed reactor, Photo-CREC-Air, [de Lasa, (1997), de Lasa and Ibrahim, (1998)] is designed for optimal operation taking into account the need to fulfill the requirements of good mixing, high mass and heat transfer, high quantum efficiency and optimum operation. Other factors that influence reactor performance and model pollutant conversion rate include intensity of the light source, air mixing and flow patterns, interaction between phases, choice of the material of construction, choice of photocatalyst, choice of photocatalyst support, choice of photocatalyst immobilization or impregnation method, and illumination arrangement. This chapter summarizes the main Photo-CREC-Air geometrical features and its associated internal components.

4.1 Photo-CREC-Air General Design

Photo-CREC-Air was designed with special features to achieve high quantum efficiency, quantum yield and chemical yield. As part of this research a first prototype Photo-CREC-Air was designed, manufactured, and assembled at the CREC-UWO laboratories. A schematic flow sheet of the batch circulating photoreactor with its main components is shown in Figure 4.1. A more detailed representation of the Venturi section, where the lamps are placed, will be shown later on in this chapter.

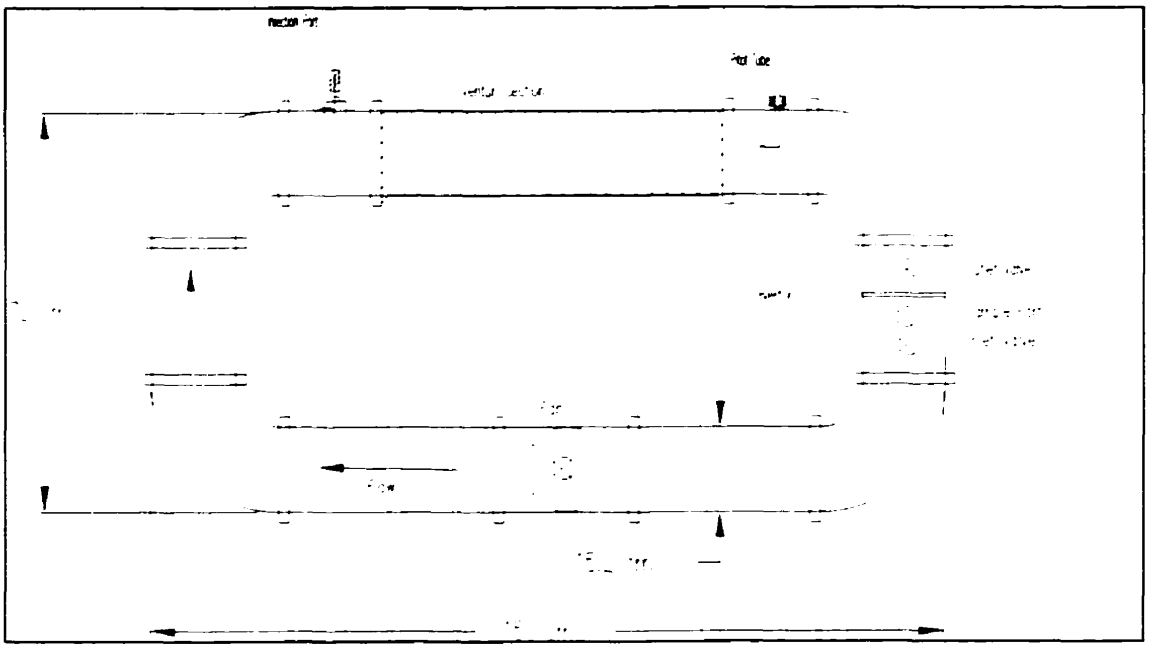

Figure 4.1: Schematic representation of Photo-CREC-Air and its associated internal components.

The Photo-CREC-Air developed, in the context of this study, has a capacity of 0.065 m^3. This unit was constructed to handle an air flow of 0.066 m^3/s (at room temperature and a static pressure of 1 inch of water), and a maximum gauge pressure of 44.4 kPa. Changes in the reactor cross section were calculated to provide air velocities of 18 m/s at the throat and 3.6 m/s elsewhere.

Air was introduced to the system through the inlet port and its recirculation was driven by a 0.152 m diameter in-line fan supplied by Slade-Eng. Systems Limited (Cambridge, Ont.). As the gaseous stream reached the Venturi, its velocity was increased to a maximum at the throat. Then it decreased progressively through the divergent section, where the mesh was illuminated by two Pen Ray® UV lamps. It was at this

divergent section where most of the pressure drop was recovered. At the exit of the Venturi , air passed through a perforated heated plate, before it was recirculated in the loop of the reacting vessel.

The reactor was illuminated externally through the plexiglass windows. Rubber gaskets were used between flanges and were very effective in preventing air leakage to the surroundings. The desired amount of pollutants was injected through the injection port which was a heated block with a septum. Organic compounds were introduced to the system by means of a syringe. In terms of safety, the reactor was totally contained in a plywood enclosure with a fan in the upper section to achieve good ventilation.

The following special characteristics were incorporated in the design of Photo-CREC-Air as to fulfill the criteria required:

a) Venturi section.

b) Windows with focused illumination.

c) Mesh section.

d) Heating plate.

While these features along with others are reviewed in more detail in the following sections, the main achievements with Photo-CREC-Air are to provide: uniform gas distribution while in contact with the mesh, good TiO_2-light interaction, firm attachment of TiO_2 on the fibrous mesh with high loading.

4.2 Construction Materials

The main body of Photo-CREC-Air was made of straight exhaust pipe 0.152 m in diameter connected by four zinc plated elbows. This choice was made so as to provide a material which would be able to withstand the operating conditions in terms of temperature and pressure. At the same time, construction materials for the reactor were selected to have a good resistance to corrosion to prevent rust particle formation.

The Venturi section was constructed out of stainless steel tubing given it is easier to weld and it has better thermal resistance than the exhaust tubing. The windows in the divergent section of the Venturi were made of plexiglass. The edges and the different parts of the photoreactor were sealed using welds and white silicone closed cell sponge gaskets. Clear transparent Silicone sealant was also used to properly seal the fan and some other sections of the reactors.

4.3 Catalyst and Catalyst Support

For the proposed Photo-CREC-Air, the TiO_2 used was "TiO_2 P25" manufactured and supplied by Degussa Corporation (Ridgefield, NJ.). The TiO_2 batch used had a BET surface area of 35-65 m^2/g , average primary particle size 21 nm, and a specific gravity of 3.7.

In order to test which support would more efficiently and tightly hold the TiO_2 particles, three different supports were tested in this project: a) Filtrete ™, b) 3M Blue Pleated Filter, and c) Bionaire Filter. The 3M Blue Pleated Filter mesh was found to be a

good candidate for this type of application due to its cheapness, light weight, convenience of handling, transparency to light in the desired range, inertness to gases, possession of a fibrous porous structure and sufficient thermal resistance. The porous structure of the 3M Blue Pleated Filter was desirable since it minimized pressure drop, provided high surface area, good light transmittance, did not plug, and allowed maximum catalyst loading.

4.4 Venturi Section

A Venturi section was incorporated into the Photo-CREC-Air design to provide good mass transfer without excessive pressure drop and to establish a "self-cleansing" system. Air flow pattern at the Venturi throat showed, as expected, the lowest measured pressure in the reactor and the highest velocity. This was good to prevent the particles from sticking to the windows which might affect light transmission to the targeted filter. The use of the Venturi also eliminated the need for windows cleaning. As the air stream was approaching the throat of the Venturi, it increased its velocity reducing the pressure and smoothly changing its flow direction, with minimum flow disturbance. The stream exiting the Venturi impinged on the mesh with the high velocity required for the high mass transfer condition. The incorporation of the Venturi section allowed the lamps to be placed in such an orientation that close to 100% illumination of the TiO_2 loaded in the mesh was achieved. Dimensions of the Venturi section were chosen as to meet specific pressure drops, thus allowing for good gas-mesh contacting (Figure 4.2).

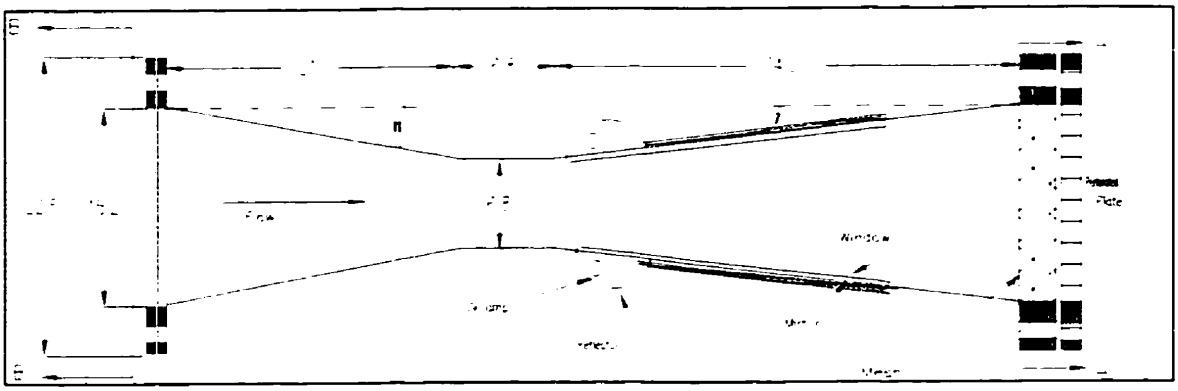

Figure 4.2: Schematic representation of the Venturi section (dimensions in cm).

In order to optimize the main design parameters, a Fortran program (Appendix A) was written to help in relating the length of the Venturi, the diameter of the throat and the pressure drop through it.

Figure 4.2 illustrates the dimensions of the constructed Venturi section. Figures 4.3 and 4.4 show different sections of the Venturi for visualization assistance. The Venturi was 62 cm in length and was made up of three parts: convergent section (21cm), straight section (6.8cm), and divergent section (34.2cm). The upstream cone angle was 11° and the downstream cone angle was 7°. The latter was constructed out of four flat surfaces to assist in placing the windows, through which the UV radiation illuminated the mesh. Note that the windows' construction will be discussed in more detail in the coming section.

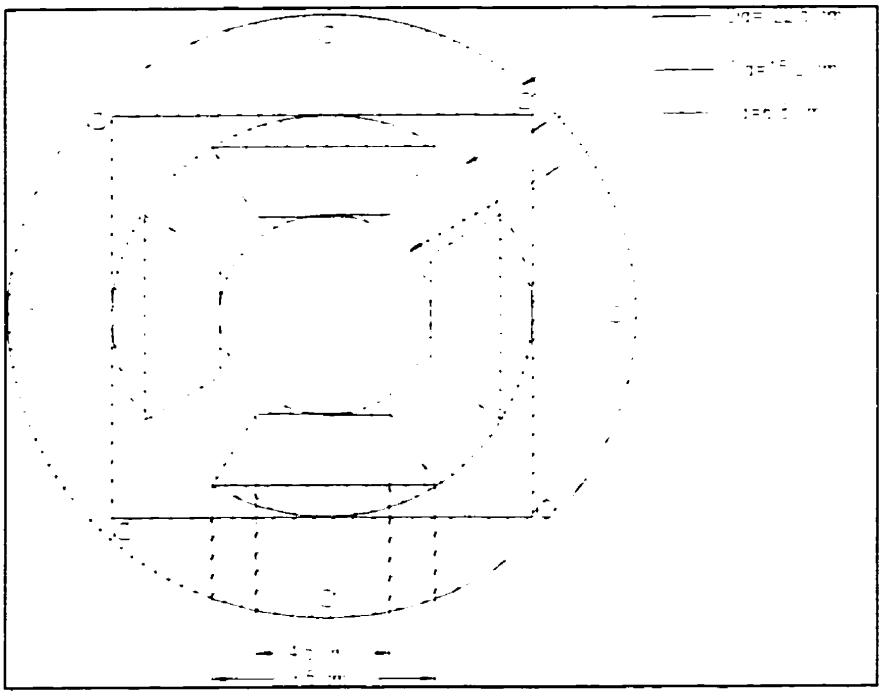

Figure 4.3: Cross section of the Venturi, section A-A.

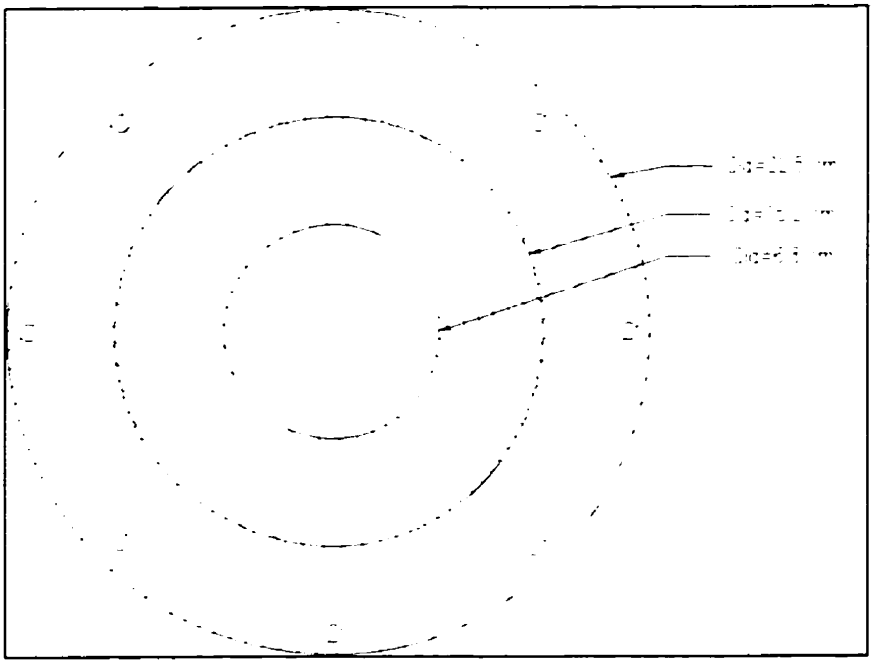

Figure 4.4:Cross section of the Venturi, section B-B.

The pressure drop across the Venturi was calculated using the following equation as noted in McCabe *et al.*, (1993):

$$V_2 = C_v Y \sqrt{\frac{2g_c(p_1 - p_2)}{\rho_1(1-\beta^4)}} \tag{4.1}$$

where:

V_2: average fluid velocity at the throat of the Venturi (m/s).

C_v: Venturi coefficient which is empirically determined and is about 0.98 for a well designed Venturi of pipe diameter 2-8 inches (-).

Y: dimensionless expansion factor, for the flow of compressible fluid (-).

g_c: dimensional constant (32.17 lb ft/lb$_f$ s^2). If SI units are used then g_c=1.

p_1: fluid pressure under upstream conditions (Pa).

p_2: fluid pressure at the throat conditions (Pa).

ρ_1: density of the fluid under upstream conditions (kg/m^3).

β: ratio of diameter of the Venturi throat to diameter of pipe (-).

Note that the dimensionless factor, Y is equal to unity for non-compressible fluid flow and it can be evaluated for a compressible fluid by eq. (4.2), [Perry's *et al.*, 1984]:

$$Y = \sqrt{r^{\frac{2}{k}}\left(\frac{k}{k-1}\right)\left(\frac{1-r^{\frac{k-1}{k}}}{1-r}\right)\left(\frac{1-\beta^4}{1-\beta^4 r^{\frac{2}{k}}}\right)} \tag{4.2}$$

with k parameter being the specific heat ratio C_p/C_v and r the ratio of the pressure at the throat to the inlet pressure. Values of Y were calculated and presented in a form of a

graph in Perry *et al.*, 1984 pg 5-13. Note that, in the Photo-CREC-Air case, calculations showed that Y is approximately 0.99.

4.5 Windows

Windows can to be cut of any chemically stable transparent solid media. Different types of glass could have been used including: plexiglass, quartz glass, Pyrex glass or stove glass. With an increasing cost as well as light transmission efficiency, they were ranked as follow: stove glass provided 40%, plexiglass 50%, Pyrex© 80%, and quartz 90 %. In the present study, windows were manufactured from plexiglass.

Moreover, the shape of the windows conformed, to the shape of the metallic frame of the reactor to provide uniform illumination of the coated filter placed transverse to the flow. It is planned in future designs to cut windows from Pyrex© glass having an absorption of 20 % of the incident radiation instead of 50 % for the plexiglass.

Window sealing represented a significant challenge. First window sealing was attempted using Silicone (a clear, transparent adhesive material) with windows being glued to the metallic frame of the reactor from the outside. However, this did not prevent air leakage. As an alternative solution, windows were fixed from the inside of the unit so air was pushed against the frame. While this provided extra sealing, it only worked for several runs. Finally, and to have an acceptable sealing, windows were fixed from the outside of the reactor frame using studs which formed a mesh with studs spaced about 1.5 cm from each other all around the window.

Selected plexiglass windows were 5 mm thick and had a trapezoidal shape with the parallel sides being of 4.5 and 8.5 cm in length (Figure 4.5).

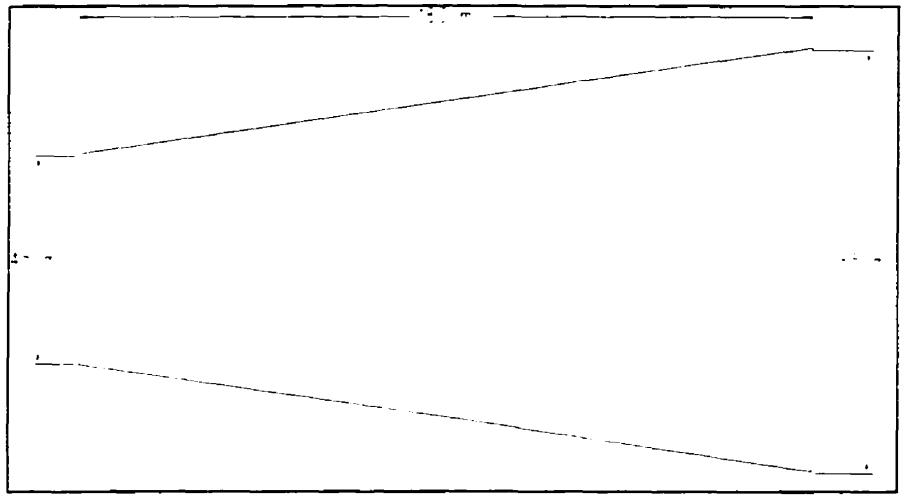

Figure 4.5: Photo-CREC-Air windows' dimensions.

Initially, four plexiglass windows were used, but to minimize light losses and maximize its transmission two of them were replaced by mirrors of the same shape and size to directly focus the incident and scattered light rays on the impregnated mesh (the target).

4.6 Light Sources

UV sources for the unit can in principle be any conventional lamp as long as it provides the required energy for the photoconversion reaction . Different types of UV light sources exist including: low pressure mercury lamp, medium pressure mercury lamp and advanced proprietary medium pressure mercury lamp. Each of them has specific characteristics and features suitable for the different applications (refer to section 2.2.3).

These lamps differ in terms of energy density, emission range, life and electrical to photon energy efficiency.

Irradiation specifications including: wavelength, intensity and operating life are crucial factors in the photocatalytic processes. These factors depend mainly on the catalyst used, concentration of the pollutants, and lamp employed. As far as TiO_2 is concerned, ultraviolet light with wavelength ≥350nm [Sauer and Ollis, (1994)] and <385nm [Sczechowski *et al.*, (1995)] and [Zhang *et al.*, (1994)], is necessary to provide the band gap energy required to yield an electron-hole combination for the initiation of the photoconversion process.

As for the light intensity, this is a major factor that influences the photoconversion rate (refer to section 2.2.3). In the Photo-CREC-Air two ultraviolet lamps with an output in the range of 365 nm and an electrical output of 4W/lamp were used. These lamps were supplied by UVP (Upland, CA.) and they were termed the Pen-Ray® lamps.

These portable miniature Pen-Ray® were utilized due to their small size that can be fitted in the Photo-CREC-Air reflectors. According to the specifications provided by UVP, manufacturer and supplier, these low pressure, mercury gaseous discharge lamps were constructed of double bore quartz with a tubular filter. These lamps were designed for stable, low noise operation, and had a rated lamp life of 5000 h with an exponential intensity decay of 20% in the first 1000 h and another 20% over the following 1000 operational hours. A decay curve was prepared (Figure 4.6) to estimate the lamp power decay with time of utilization. Corrections were introduced to the calculated kinetic

constants and apparent quantum yields according to this decay curve (Sections 7.2.5 and 7.2.6).

The Pen Ray Field lamps were supplied with DC power supplies (9V battery) and were 12.07cm in length , with a lighted length of 5.72 cm and an outside tube diameter of 0.95 cm. Their peak emission was at 365 nm.

The intensity of the UV light was measured using a UVX radiometer manufactured and supplied by UVP (Upland, CA.). The UVX radiometer was a digital radiometer that works in conjunction with a specific sensor that measure the wavelength in the desired range up to 20 mW/cm^2 with an accuracy of ± 5% (UVP). The radiometer is calibrated using standards of the National Institute of Standards and Technology (NIST) and UVP 's published standards. The radiometer provided three ranges of readings: 0-200 $\mu W/cm^2$, 0-2000 $\mu W/cm^2$, and 0-20 mW/cm^2.

The treated filter mesh was illuminated externally from outside the windows. Note that lamps in Photo-CREC-Air were not immersed into the fluid to avoid particle deposition and flow disturbance.

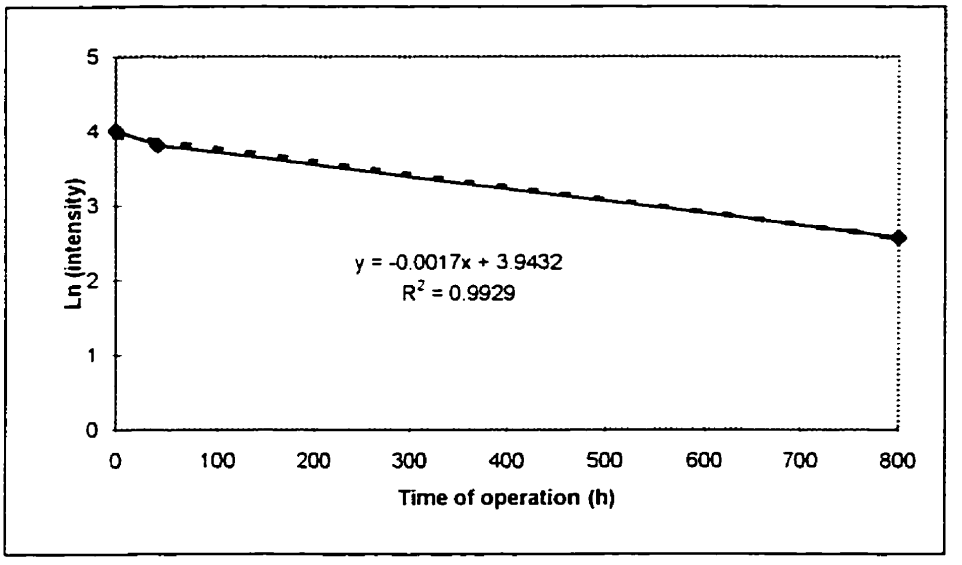

Figure 4.6: Intensity decay curve for the UV lamps used.

4.7 Reflectors

Photo-CREC-Air reflectors were designed to optimize the utilization of the emitted light. The reflectors (Figure 4.7) were parabolic in shape with an elliptical cross section with the following design equation:

$$\frac{x^2}{25} + \frac{y^2}{9} = 1 \qquad \textbf{(4.3)}$$

These reflectors were manufactured from aluminum in the UWO-Machine Shop with the following dimensions: length of 7.7 cm, width: 7.2 cm from the bottom and 5.5 cm from top. Reflectors were equipped with side slots to hold the UV lamps. The Photo-CREC-Air reflector function was complemented with mirrors, covering the section of the windows not covered by the reflector, and helped focus most of the light on the target mesh.

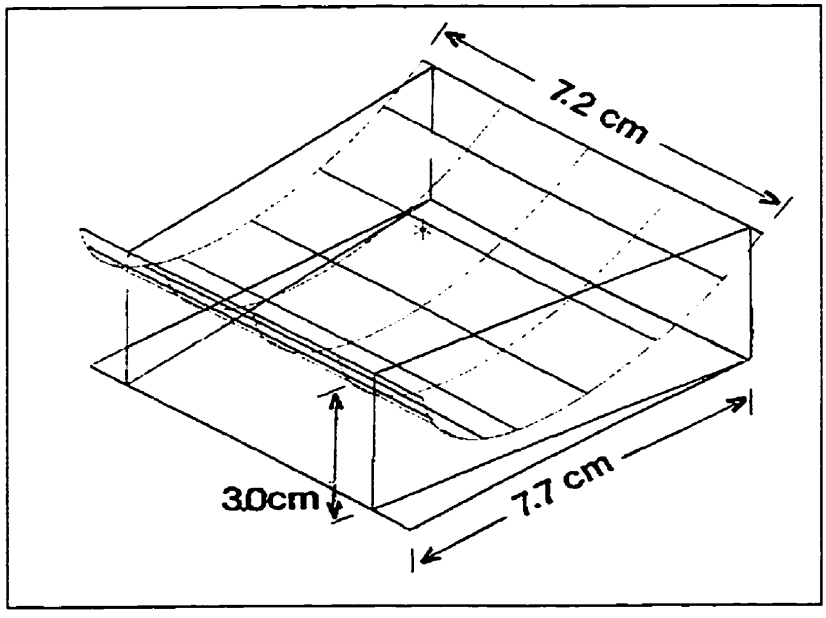

Figure 4.7: Details of Photo-CREC-Air reflector.

4.8 Perforated Plate

A perforated plate was incorporated in the design as an extra support for the impregnated mesh and also to secure uniform distribution of fluid when in contact with the mesh. The plate was heated to ensure that the mesh was free of water, since it has been reported that water has a potential effect on the photoreaction rate.

The perforated plate was made of stainless steel to prevent any rust particles from entering the gas stream. The plate had a 22 cm diameter and a 0.83 cm thickness with 144 holes, each having a 0.83 cm diameter (Figure 4.8). Four 150 W cartridge heaters were symmetrically inserted in the plate and connected to a variable voltage power supply. This supplied the required energy to maintain the plate at the desired temperature. The heaters were 3.8 cm in length and 0.9 cm in diameter.

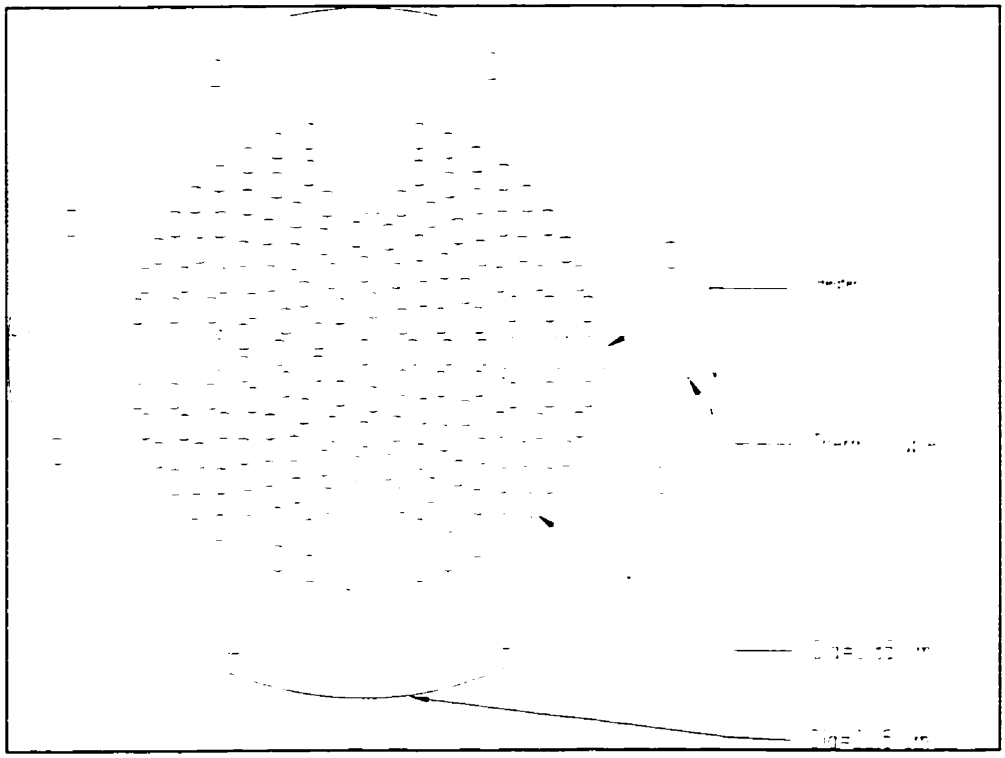

Figure 4.8: Mechanical drawing of the perforated plate.

Temperatures were measured by type K thermocouples connected to digital thermometers supplied by Omega Engineering (Stamford, CT.). The thermocouples were 15.5 cm in length and 1.5 mm in diameter. The thermocouples were also supplied by Omega Engineering.

Pressure drop across the plate was considered as a major aspect in its design, since proper values should ensure uniform contacting between the gas stream and the supported mesh. The pressure drop across the perforated plate was approximated using Van Winkle's equation , [Perry *et al.*, (1984)]. This equation applies for the flow of gases through perforated plates with square-edged holes on an equilateral triangular spacing for hole Reynolds number range of 400-20,000 and hole pitch/hole diameter ratio of 2-5:

$$W = C_o A_f Y \sqrt{\frac{2 g_c \rho_1 \Delta p}{1 - \frac{A_f}{A_p}}} \qquad (4.4)$$

with W being the mass flow rate, C_o the orifice coefficient, A_f the total free area of holes, A_p the total sectional area of the perforated plate, Y dimensionless expansion factor for the flow of a compressible fluid, g_c a gravity dimensional constant, ρ_1 the fluid density at the upstream conditions, and Δp the pressure drop across the plate.

It has to be mentioned that the pressure drop calculated using this equation is just an approximation since the perforated plate holes in Photo-CREC-Air were not on an equilateral triangle pitch. In addition, the perforated plate had rounded punched holes. Thus expected C_o coefficients should be slightly larger than the ones for the square-edged holes [Perry *et al.*, pg5-37, (1984)]. C_o was approximated from Figure 5-41 in Perry *et al.*, 1984, (Figure 4.9). This figure provides the perforated plate orifice coefficient as a function of the hole Reynolds number and the physical characteristics of the plate.

Y was approximated using the following correlation:

$$Y = 1 - \left(\frac{1 - r}{k}\right)\left(.041 + .35\beta^4\right) \qquad (4.5)$$

Y was found to be approximately equal to unity. This is expected since the pressure drop through the plate is moderate (124 Pa) and still adequate to secure uniform flow distribution.

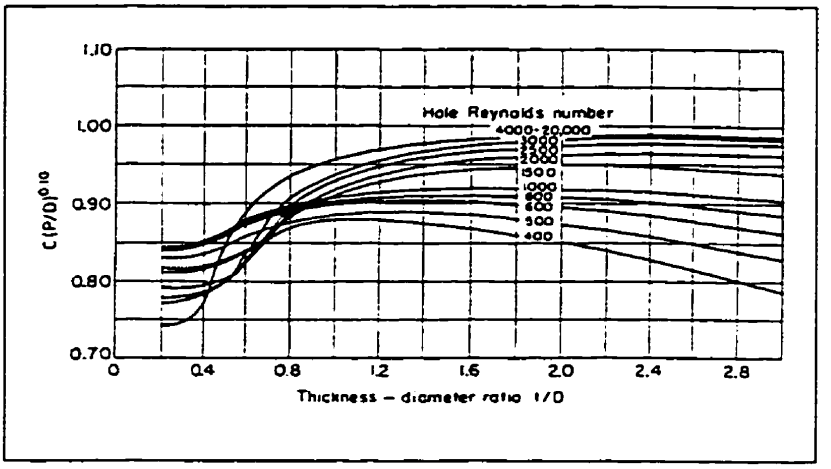

Figure 4.9: Perforated plate orifice coefficient versus hole Reynolds number and physical characteristics of plate.

Ref.: Perry *et al.*, (1984), pg.5-37.

4.9 Injection Port

The injection port was made from a stainless steel block. A cartridge heater of 120 W power was inserted into the block to raise the temperature and keep it at around 120 °C. Under this condition the model pollutant (e.g. toluene) was injected and evaporated in the air stream.

The heater was 3.8 cm in length and 0.6 cm in diameter. A thermocouple was introduced in injector block to monitor the temperature. This thermocouple was 15.5 cm in length and 1.5 mm in diameter and was connected to a digital thermometer supplied by Omega Engineering.

The injection port was equipped with a septum through which the desired amount of toluene, supplied by Caledon Laboratories Ltd. (Georgetown, Ont.), was fed to the

reacting vessel. To prevent septum damage or back flow of the injected sample out of the system, an on-off valve was used.

4.10 Mode of Operation

The determination of the Photo-CREC-Air performance is a crucial aspect of the present study. While different modes of operation may include batch, semi batch or continuous system, the current testing was developed in a batch system with high gas recirculation given various safety issues. Moreover, this mode of operation may simulate the treatment of a confined volume of gas (building, painting shop) being continuously treated in a Photo-CREC-Air reactor.

4.11 Conclusions

The special geometrical features of the designed Photo-CREC-Air was demonstrated in this section of the study. Thus, it is expected that Photo-CREC-Air configuration will allow and lead to optimal photocatalytic performance and high photoconversion yields.

CHAPTER 5

FILTER IMPREGNATION AND CHARACTERIZATION

The objective of the mesh impregnation with TiO_2 is to achieve high loading of TiO_2 on the fibrous mesh, firm attachment of the particles and efficient operation during the experimental runs. Ideally, the impregnation process must keep the TiO_2 crystals in their original crystalline form without any deformation, thermal shocks or changes. In addition, strong bonding and attachment of the TiO_2 crystals to the mesh is required in order to prevent any crystal washout or crystal detachment during operation. Crystal detachment can result in TiO_2 losses either in the air stream or inside the reactor. Finally, uniform distribution of the catalyst particles across the surface area of the mesh is necessary to allow equal contacting between the phases and to allow uniform catalyst irradiation by UV.

5.1 Catalyst Support

Several types of filters were tested to find an efficient support where particles can bond firmly in order to minimize losses of any appreciable quantities inside the reactor or in the air stream. Filters were tested as well for their ability to provide good light transmittance and high thermal resistance in the operating condition range.

With this goal, three filters were tested in the present study for compatibility with Photo-CREC-Air including:

a) Filtrete™ Filter. This is a white pleated fiber with a supporting metallic mesh made and supplied by 3M (London, Ont.). Filtrete™ air filter is constituted by

electrostatically-charged fibers. These fibers attract and retain micro particles strongly.

b) 3M Blue Pleated Filter. This poly-olefin based filter has a similar structure to the Filtrete™ ; however it is not electrostatically charged. This filter develops, however, charges with air flow. This filter was made and supplied by 3M (London, Ont.).

c) Bionaire Electrostatically Charged Filter. This filter has a flat construction and is designed of fibrous material covered by a thin layer of another fibrous material.

While only some bulk properties are available for these filters, they were tested in this study to reveal their overall performance in terms of: catalyst loading (the TiO_2 amount that the filter can hold on a mass basis), light transmittance before and after impregnation, thermal resistance, and water desorption. Details of the tests performed are discussed in the following sections. Table 5.1 summarizes the main findings.

Table 5.1: Properties of the different filters tested.

Test	Filtrete™	3M Blue Pleated Filter	Bionaire
catalyst loading	high(50%)	high(50%)	low (weak attachment)
light transmittance	high	high	low
Thermal resistance	low	high	moderate
Water desorption	good	good	good

Results revealed that the Blue Pleated Filter was the one with the best combination of the required properties of high catalyst loading, high light transmittance, high thermal resistance and good water desorption. Consequently this was the filter selected for further utilization.

5.2 Photocatalyst Impregnation Techniques

A number of different impregnation methods were developed to compare the results in terms of attachment strength and catalyst loading. None of the considered methods required treatment of the mesh prior to the TiO_2 loading process. These methods can be classified as wet, in which a suspension of 21 nm TiO_2 particles is prepared, and dry, in which the catalyst is utilized as a dry powder.

A first method (Method 1) involved preparing a suspension of TiO_2 in a water-methanol mixture. It is worth noting that the mixture contained 30% methanol to 70% water and 5 g per liter of TiO_2. Methanol addition was found to enhance the attachment of TiO_2 particles to the filter as reported in Valladares (1995). A piece of filter was fixed by a hose clamp, to prevent its movement, on a specially designed plexiglass ring with four openings from the bottom, to allow the circulation of the water (Figure 5.1).

The solution was placed in a glass container along with a stirrer that provided adequate mixing to keep the TiO_2 particles in suspension. Mixing was allowed for 5 min before inserting the plexiglass ring with the filter, and the suspension was forced through the mesh for about 20 min. Unfortunately, low and non-uniform TiO_2 loading was achieved.

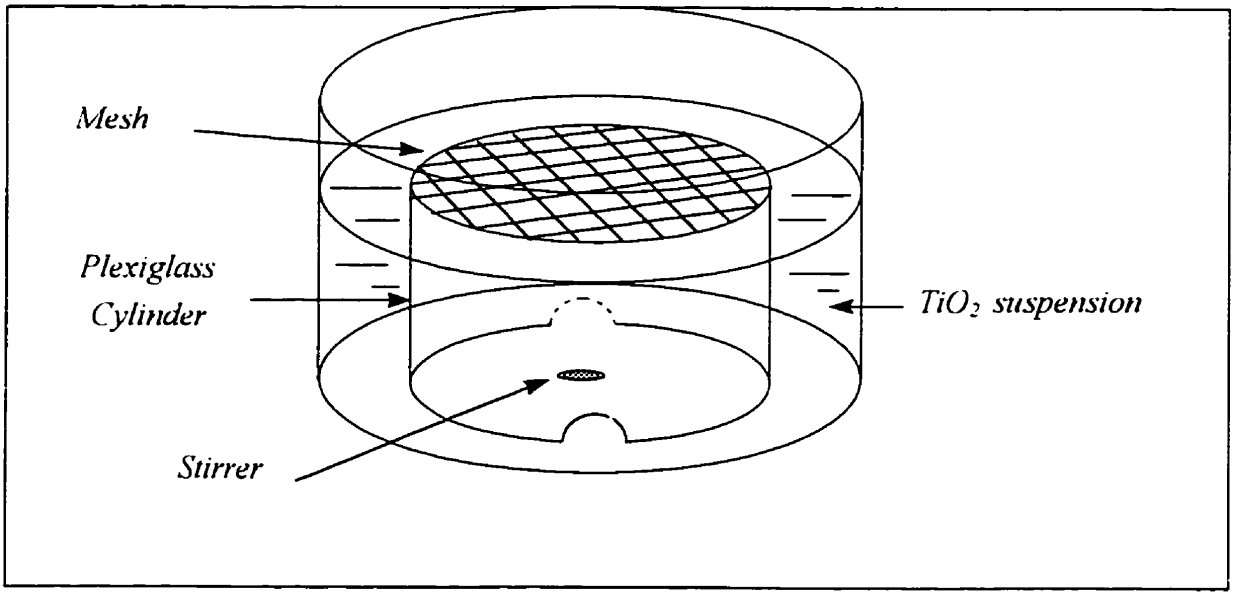

Figure 5.1: Impregnation system in which the mesh was fixed on a plexiglass ring, inserted in a methanol-water-TiO_2 mixture.

A second impregnation technique (Method 2) utilized an methanol-water solution of the same composition as in Method 1 and a special unit, (Figure 5.2), made mainly of plexiglass and a stainless steel mesh supporting the filter. A submerged pump was used to pump the TiO_2 suspension from one end to the other. In a typical experimental run, the solution was pumped through the mesh for about 40 min. This technique gave a quite non-uniform distribution of TiO_2 particles on the mesh. Particles tended to settle and concentrate on the center while there were few particles on the filter sides (edges).

Another approach (Method 3) considered supporting the filter by a hose clamp on a metallic ring, spraying the top surface with an methanol-water solution of the same composition as in Method 1 and leave it to dry for 30 min before spraying a second coating. Analysis did not show any significant TiO_2 loading.

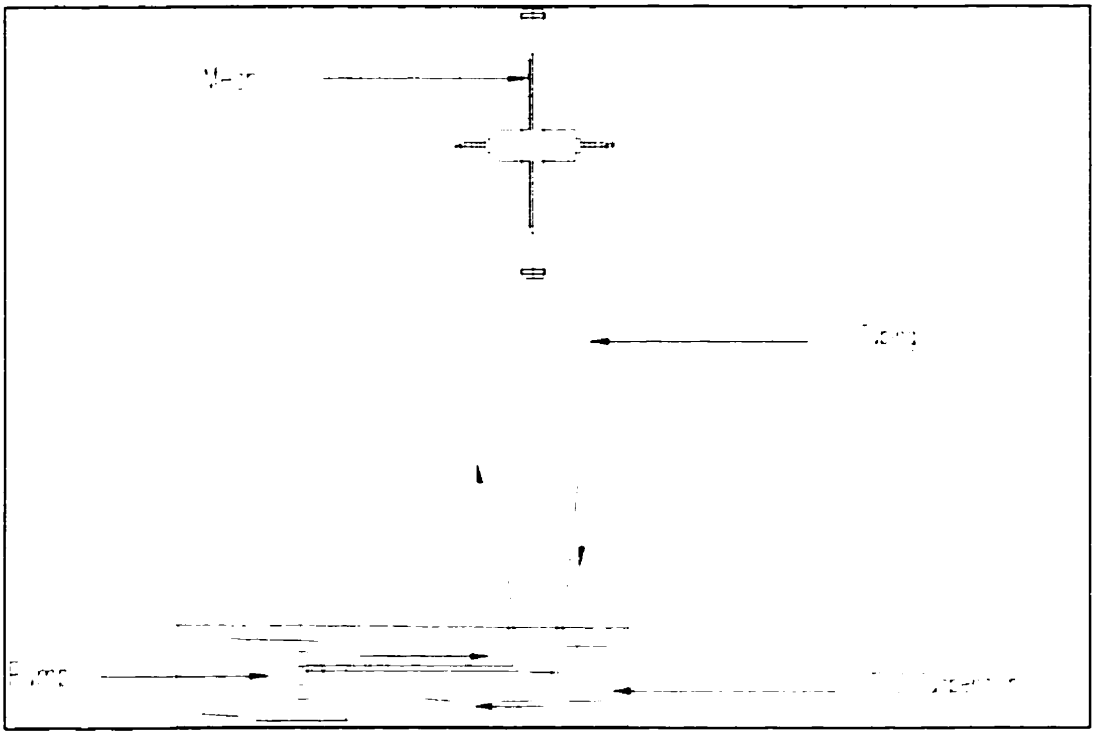

Figure 5.2: Filter impregnation system that involved pumping a methanol-water-TiO_2 mixture to a plexiglass unit supporting the mesh.

The next attempt (Method 4) was a dry method using a small fluidized bed. TiO_2 was poured into the bed and the filter was fixed in the upper section. Air was introduced from the bottom allowing the TiO_2 to fluidize and reach the surface of the filter. Unfortunately, the TiO_2 powder (being very fine) did not fluidize very well and particles tended to fly through the porous structure of the filter.

Finally, a process (Method 5) which involved applying a pre-weighted amount of TiO_2 powder, 2-2.5g, on a pre-weighted mesh, 6-8.5g, using a soft painting brush, was practiced and adopted. Care was taken to proceed gently in order not to affect the filter surface structure. Acetone was sprayed to attach the particles to the upper surface and

transport them into the fibrous mesh. The impregnation procedure is illustrated in Figure 5.3. About five coatings were performed before the desired TiO_2 amount was loaded on the mesh. This exercise gave loadings on the filter of up to 50% (g of catalyst/g of fibrous mesh.

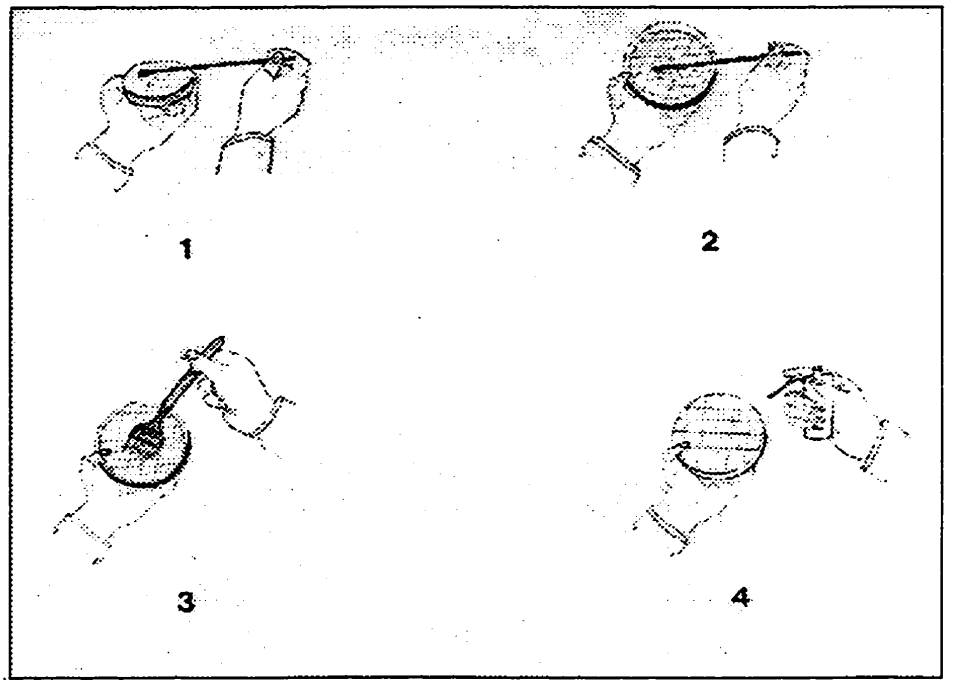

Figure 5.3: Steps followed in the adopted impregnation technique (Method 5):

(1) Weigh 2-2.5 g of the catalyst in a glass plate;

(2) Apply some of the catalyst on the mesh surface;

(3) Gently spread the catalyst with a soft painting brush;

(4) Spray acetone on the surface and leave to dry for 25 min and;

(5) Repeat the steps until catalyst is all on surface.

5.3 Light Transmittance Measurement

Light transmittance through the filter before and after treatment is a very important property of the mesh to ensure efficient light penetration throughout the filter layer. Light transmittance of the specific wavelength (365 nm) was measured using a PU 8625 UV/VIS Spectrophotometer supplied by Philips.

In a typical measurement, a small piece of the filter was cut and placed in a specially designed cell made of plexiglass. This cell was inserted in the spectrophotometer after re-zeroing it with respect to the bare untreated filter. A reading was taken which corresponded to the optical or the decadic density. Then the fraction of focused light beam that made its way through the filter piece was approximated as:

$$\textbf{Optical density} = \log (I_o/I) = \log (1/T) \qquad (5.1)$$

with T being the fraction of light transmitted through the filter piece.

Analysis revealed that light transmittance of the Filtrete™ and 3M Blue Pleated Filter were approximately (1-4)% and (1-2.5)%, respectively after treatment with TiO_2 and acetone. The readings for the bare untreated filters were (12 %) and (1.3-2.8)% for the Filtrete™ and 3M Blue Pleated Filter, respectively. Thus, it was concluded that the addition of TiO_2 in the 3M Blue Pleated Filter did not affect the desired near UV light (365 nm) transmission properties.

5.4 Temperature Programmed Desorption (TPD)

This analysis was performed in order to estimate the temperature at which the filter will be essentially water free. Temperature programmed desorption was performed in a Micromeritics TPD/TPR 2900 machine. A small wet piece of the filter was inserted into a U tube and was treated continuously with helium as a carrier gas. Programmed desorption began by raising the temperature linearly with time to 140° C with a rate of 15°C/min while a constant stream of helium was passing over the sample. At a certain temperature(102 °C), the heat overcame the activation energy, therefore the bond between the adsorbate and adsorbent broke. The desorbed water molecules entered the stream of the inert carrier gas and were swept to the detector. A typical TPD for the filter is illustrated in Figure 5.4.

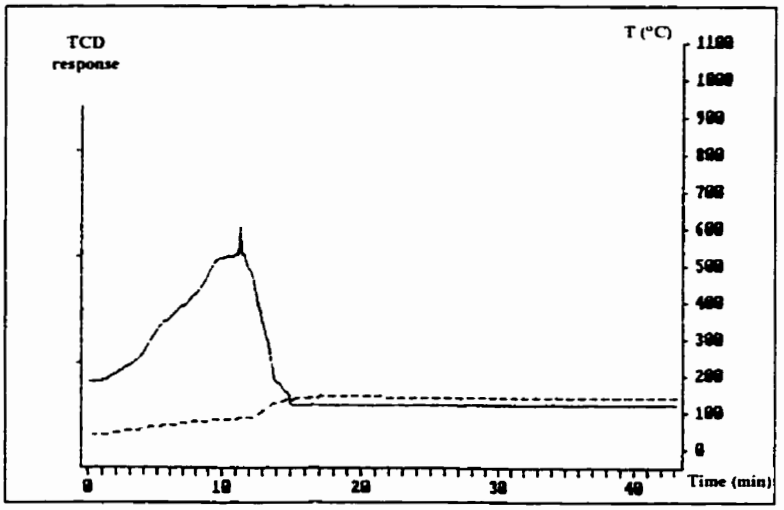

Figure 5.4: TPD of the 3M Blue Pleated Filter. The full line represents the water desorption from the mesh. The dashed line is the adopted temperature program.

According to the results, all three filters had good water desorption properties, with the water being fully desorbed from the filter at around 100 °C, the temperature at which a peak was observed. Hence, the temperature of the plate was raised as high as 100 °C during the experiments to ensure that the filter operated free of water.

5.5 Particle Attachment to the Filter

TiO_2 loaded filters were studied under Scanning Electron Microscopy (SEM) (Figures 5.5 and 5.6). This helped in the assessment of TiO_2 distribution and it also proved that the particles were actually attached to the fibrous strands and not loosely held in the spaces of the porous structure. SEM photos of different regions revealed that 3M Blue Pleated Filter is good in retaining the TiO_2 particles. Samples of the analysis are shown below in Figures 5.5and 5.6. SEM photos show, however, the presence of multiple uniformly distributed aggregates of well anchored TiO_2 throughout the mesh fibers. Figure 5.6 shows the mesh fibers (having typically 15 μm diameter) holding particle aggregates of about 2 μm.

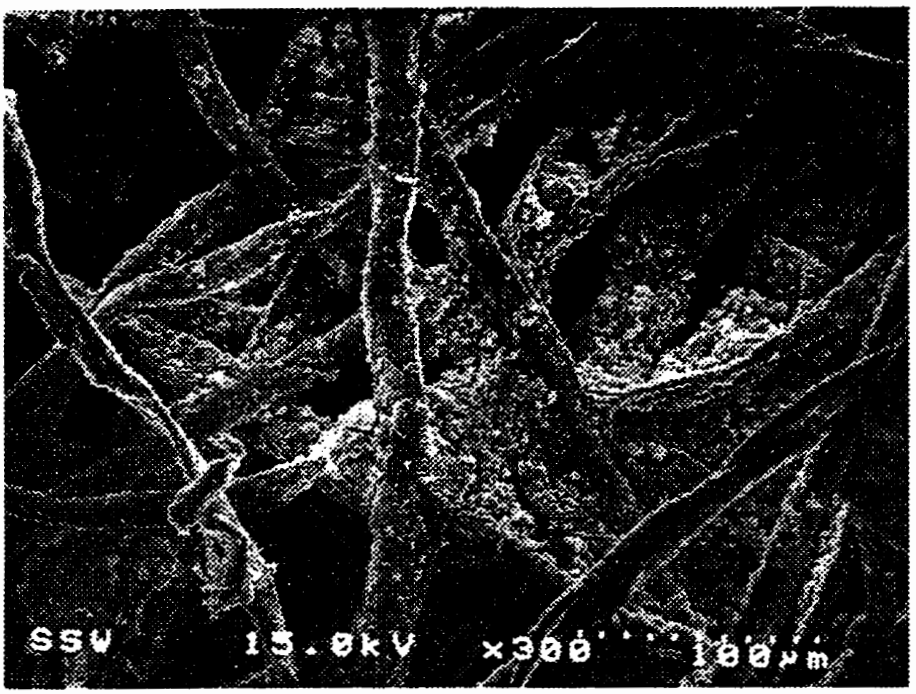

Figure 5.5: SEM photo of a treated 3M Blue Pleated Filter.

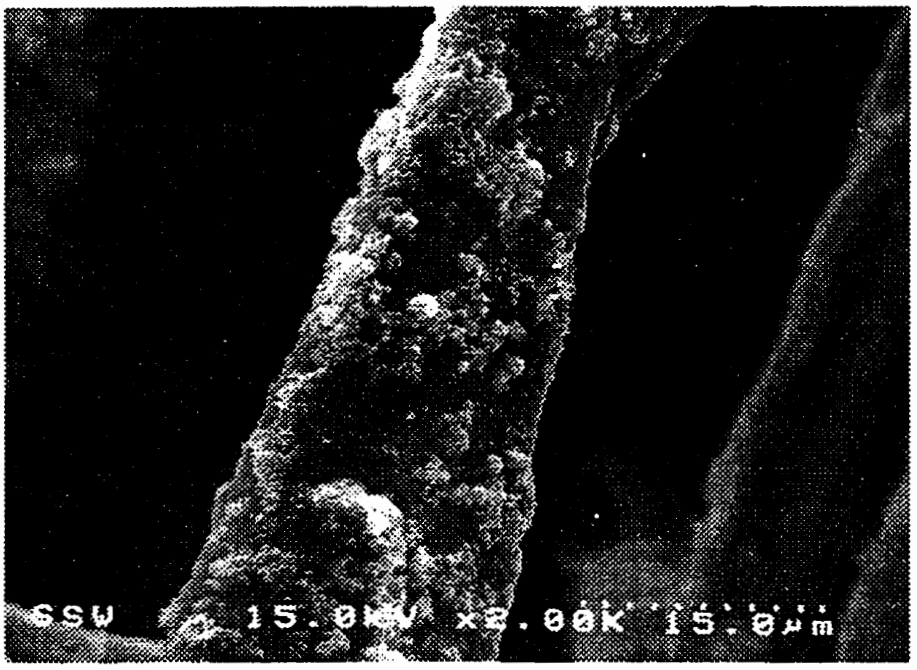

Figure 5.6: Close up picture of Figure 5.5 showing a single treated strand and TiO_2 attached to it firmly.

5.6 Electrostatic Charges

The bonding of the TiO_2 particles to the surface of the fibrous mesh is influenced to a significant degree by electrostatic forces. Electrostatic filters have inherent electrostatic charges generated by the "electret" fibers from which they are made. As a stream of fluid is circulating through the filter, the amount of charges increases and holds the particles more firmly and strongly. This property was used to assess the strength of particles bonding to the fibrous mesh.

The electrostatic charges induced or found on the different tested supports were measured using a Faraday Pail provided by the Applied Electrostatic Research Center (AERC) at UWO. This test was carried out to measure the strength of bonding between the catalyst particles and the mesh. A Faraday Pail consists of two pails placed one inside the other and connected by a wire to an electrometer. A sketch of the system is shown below in Figure 5.7.

Using this technique it was possible to show that both Filtrete™ and the Bionaire filters were electrostatically charged compared to the neutral 3M Blue Pleated Filter. Measurements revealed that the white Filtrete™ possessed negative charges, about one order of magnitude larger than that of the 3M Blue Pleated Filter. Unfortunately, the utilized set-up from AERC provided measurements with a large uncertainty of roughly fifty percent. Thus, measurements with the Faraday Pail were only good for relative charge readings but not absolute values.

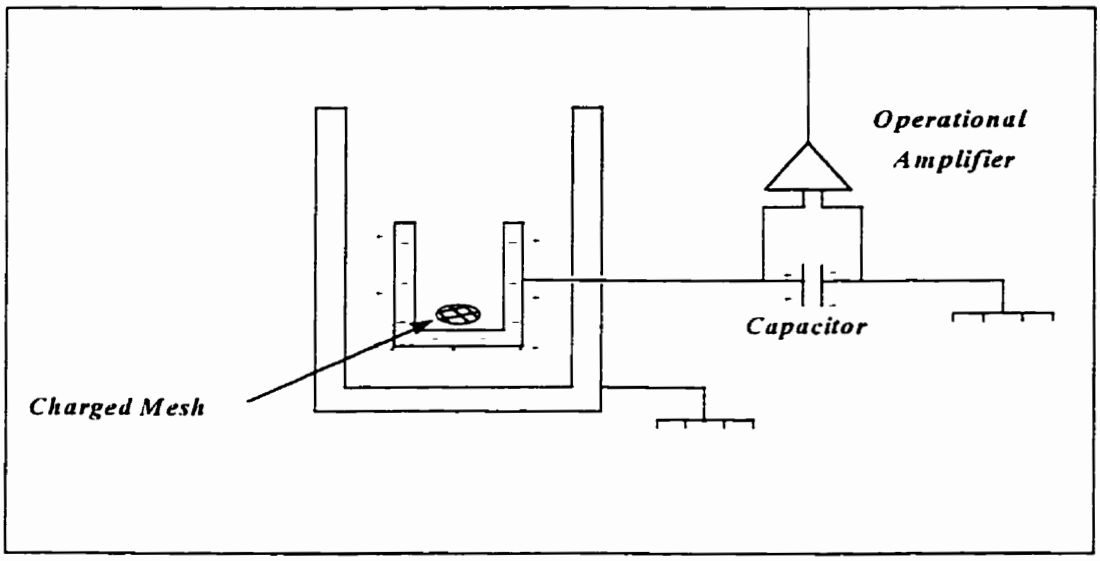

Figure 5.7: Schematic representation of Faraday Pail.

5.7 Conclusions

In summary, the final selection of the filter involved several factors including: a)catalyst loading, c) thermal resistance, c) water desoprtion, d) light transmittance and, e) electrostatic charges, and f) strength of particles attachment. These various analytical techniques revealed that 3M Blue Pleated Filter was the best choice for the application in Photo-CREC Air.

CHAPTER 6

EXPERIMENTAL METHODS

Once the Photo-CREC-Air unit was debugged, the filter impregnation technique was established and the preliminary characterization of the system was accomplished, an experimental program was initiated to test the performance of the unit. The main goal was to study the influence of the different operational parameters on the initial photo-oxidation rate of toluene. This chapter summarizes the analytical techniques employed during the course of experimentation.

6.1 Analysis of Reactor Samples

Gaseous samples containing unreacted chemicals along with the end products and intermediates were analyzed quantitatively and qualitatively using 5890 Hewlett Packard gas chromatograph (GC). This unit is equipped with a Hewlett Packard 3393A integrator which allows the reporting of the different peaks along with their retention times and integrated areas. The peak for a given compound is propotional to the number of moles of that compound passing through the detector. The relationship between the number of moles of each species (CO_2, toluene and water) was determined by making a series of calibration injections (Refer to Appendix B).

To complete the various analytical tasks, two GCs were used. One was equipped with a Porapak Q packing column 1.83 m long and 0.318 cm in diameter in conjunction with a thermal conductivity detector (TCD). The other one was operated with a 25m-0.33 μm HP-1 capillary column associated with a flame ionization detector (FID). Both

GCs used helium as the carrier gas. In the case of the packed column, a 2.5 mL sample was injected at an oven temperature of 30°C and was held there for about 0.5 min before its temperature was raised to 200°C at a rate of 45°C/min and remained there for 8 min. This allowed good separation and identification of the collected mixture components. The temperature program is shown in Figure 6.1.

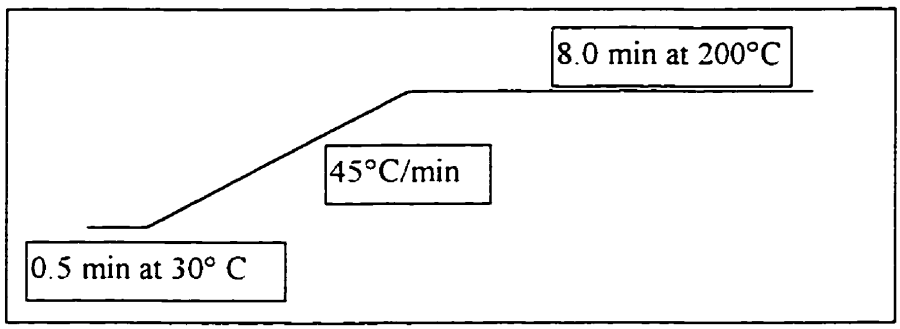

Figure 6.1: Temperature program adopted for the Poropak Q packed column.

Identification of intermediate products was carried out by injecting a 2.5 mL sample into the capillary column at 30°C. Temperature was held at 30° C for 3 min, ramped up to 90°C at a rate of 15°C/min and held there for 2 min before it was brought back to 30°C. This temperature program is illustrated in Figure 6.2.

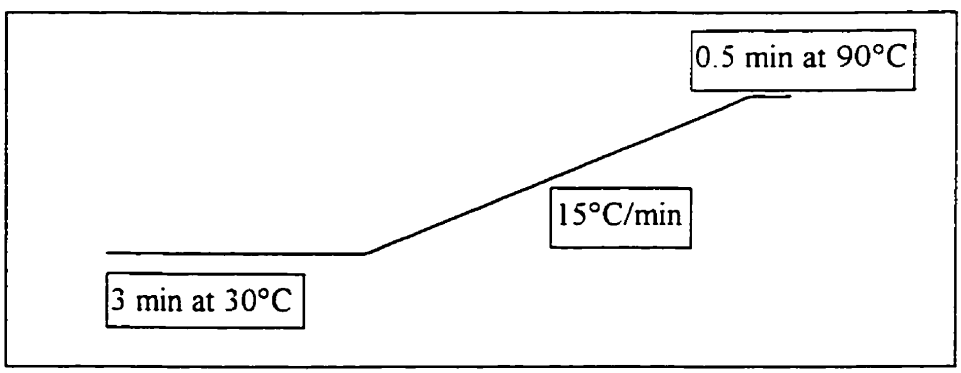

Figure 6.2: Temperature program adopted for the capillary column.

6.2 Photo-CREC-Air

Experiments were carried out in the Photo-CREC-Air reactor. The geometry and the internal components of this unit were reviewed in Chapter 4.

6.3 Experimental Procedure

Dry air gas supplied from BOC (Toronto, Ont.), was used during the experimental program. The reactor was filled with air bringing the final gauge pressure up to 13.78 kPa. This over-pressure provided an adequate internal pressure as for taking enough samples over the experimental time. Following this, the heaters were turned "on" until the desired temperature (50-100° C) was attained. At the same time the heater of the injection port was turned "on" to reach ≈120°C, a temperature high enough to completely vaporize the toluene sample. The reactor contents were allowed to circulate and were recycled for about half an hour before any samples were taken. In the case of high humidity level experiments, water was also injected into the reactor about half an hour before the toluene injection.

Note that during the first four hours the UV light was not turned on, allowing the toluene to be adsorbed onto the TiO_2 particles. After that, light was turned on for 20-22 h. Samples were taken every 0.5-1 h. Note also that samples were not injected on-line in the GC.

Reaction samples were collected in a vinyl tubing from the sampling port to a 1L Tedlar bag. Later on, gas samples were injected manually into the GC using a 2.5mL syringe. Figure 6.3 provides a detailed drawing of the Tedlar sampling bag port. After the experimental time was elapsed, the system was purged with air for an hour. Eventually, a new mesh was set before a new experiment was initiated.

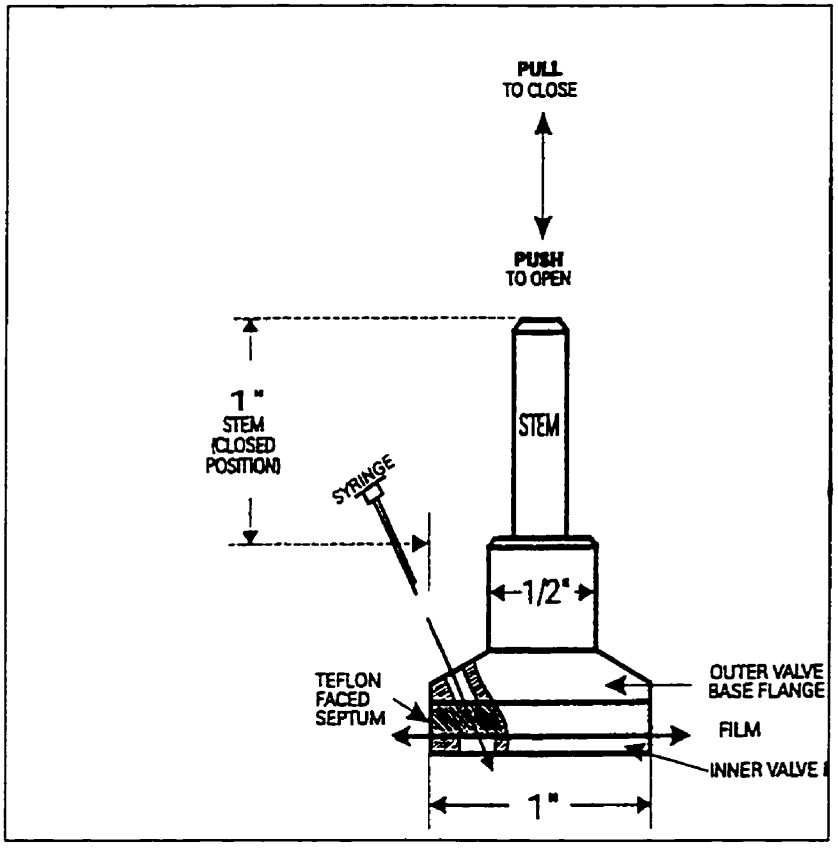

Figure 6.3: Detailed drawing of the Tedlar sampling bag port.

Toluene concentrations of 5.2-13 $\mu g/cm^3$ were used during the testing. These concentrations were achieved by injecting samples of 0.4 -1.0 mL of toluene into the reactor volume. In addition, four temperatures over the range of 20-100 °C were used in the heating plate supporting the mesh. The investigation also included two humidity

levels: high and low. The low concentration level corresponded to the one with no water addition and the high water concentration level was equivalent to 32 $\mu g/cm^3$.

6.4 Internal Standard Procedure

An internal standard procedure was implemented in this study and this to reduce the uncertainty related to variable gas samples injected into the GC. Given air was essentially unaffected by the photoconversion, oxygen consumption was negligible, hence the air peak was taken as a reference value. Thus, the ratio of toluene/air was used to monitor the rate of toluene disappearance with time on-stream and this to account for the potential combined effects of leaking, adsorption, condensation and reaction. To illustrate the internal standard procedure Figure 6.4 provides a typical reporting on the evolution of the toluene/air fraction during a run.

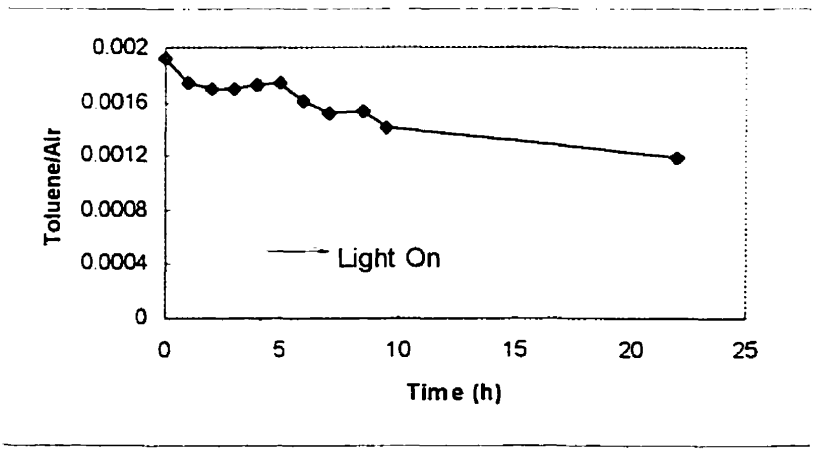

Figure 6.4: Toluene/air ratio versus time, the internal standard used in the experimental run.

6.5 Mass Balances

Regarding mass balances, they were performed using both carbon and hydrogen. Results are shown in Appendix C. The actual amounts of the various components were determined from the GC calibration curves (Appendix B) prepared for carbon dioxide, water and toluene, shown in Figures B1, B2, and B3 respectively. The elemental balance for hydrogen closed within ±13%. On the other hand the elemental balance for carbon was always below 100%, the worst closure being 57%.

A possible explanation for this is the characteristic of the mechanism involved. Water is a product that is being formed during the different steps of the reaction, whereas carbon dioxide is an end reaction product. As a result, the hydrogen balances, strongly relying on water formed, should close much better than the carbon balances significantly affected by carbon dioxide. Moreover, carbon may also exist in the form of oxidized intermediate species. However, given that the level of these species cannot be detected individually, closing of the carbon balance involves intrinsic inaccuracies and this is particularly true for conversions in the low level. It is also worth noting that the color of the TiO_2 changed from white to yellow after experimentation. This is an indicator of adsorbed intermediates or toluene at the surface of the TiO_2 mesh a possible cause of the lack of closing of the carbon balance. Note that this change in the catalyst color was also observed by Ibusuki and Takeuchi (1986).

Note that hydrogen mass balances for runs at low temperatures (20-75°C) did not close as well as for runs at 100°C. This problem was assigned to some water condensation at the lower temperatures.

6.6 Reproducibility of the Results

Several runs (5) were carried out for each experimental condition to ensure the reproducibility of the data. In addition to this, repeats were also carried with the same catalyst to record potential catalyst deactivation and to be able to predict the eventual influence of the catalyst deactivation on the reaction rate. It is noteworthy that each experimental point on the results graph is actually the average of two or three readings (injections) of the same sample.

6.7 Conclusions

This chapter describes the different analytical techniques that were used in the present study in the areas of collecting and analyzing samples, setting an analytical method based on an internal standard and developing mass balances. While both hydrogen and carbon balances were attempted, the hydrogen balances appeared to provide satisfactory results at 100° C.

CHAPTER 7

RESULTS AND DISCUSSION

7.1 System Characterization

Testing of the Photo-CREC-Air system performance was developed in terms of pressure profiles, velocity profiles at both room and elevated temperatures, UV intensity profiles across the filter surface at several positions, and UV intensity decay profiles.

7.1.1 Pressure Profile

Pressure was measured at several points along the reactor length using a water manometer. The position of the seven pressure taps are shown in Figure7.1.

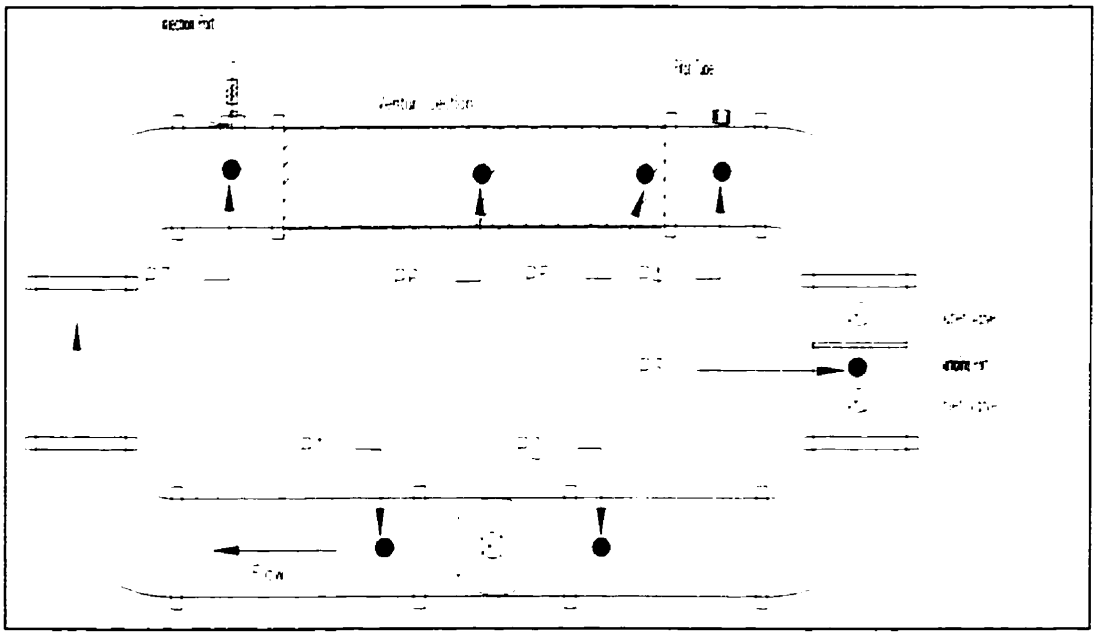

Figure 7.1: Schematic of the pressure taps locations:P1, P2, P3, P4, P5, P6, and P7.

Figure 7.2 provides detail of a typical pressure profile along Photo-CREC-Air. Positive gauge pressure was only observed after the fan (tap1). It is worth noting that this profile was taken with the fan running at room temperature and with the system sealed and at 0 gauge pressure. Another interesting observation was given by the fact that the lowest pressure in the system was observed at P6 which corresponds to the neck of the Venturi and this was expected given the Venturi fluid-dynamics where velocity increases considerably and pressure is reduced at this particular section.

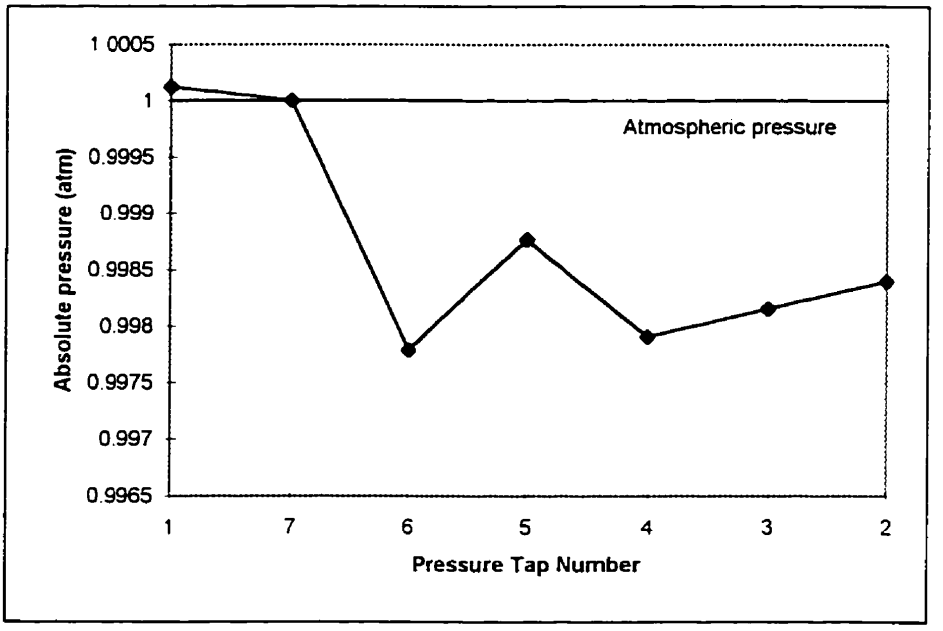

Figure 7.2: Typical pressure profile of Photo-CREC-Air.

7.1.2 Velocity Profile

Velocity profiles in Photo-CREC-Air were measured immediately after the perforated plate (P4). Measurements were made using a Pitot tube supported with a holder allowing measurements at different radial positions. The two profiles were

recorded (Figures 7.3 and 7.4) when the heating plate was at room and elevated temperatures (97°C), respectively.

From this data, it is apparent that there is a sharp velocity change in the outer area of the mesh (r>6 and r<-6) with velocity changes becoming less pronounced in the core of the stream(-6<r<6). While this trend of relatively uniform gas velocity was observed at both room temperature and 97° C, in the case of the higher temperature, the gas velocities were more uniform and provided a more symmetric velocity profile.

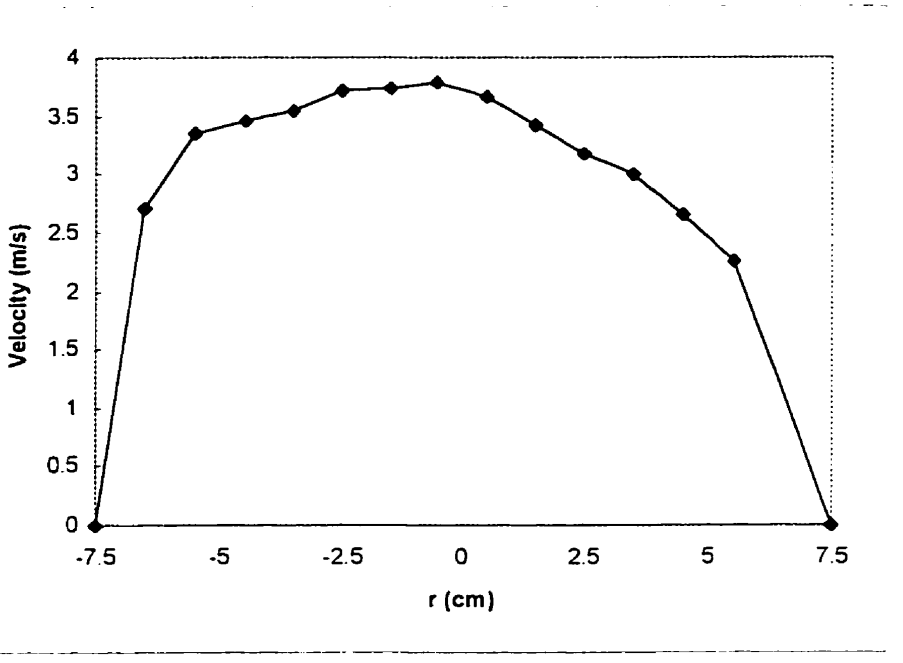

Figure 7.3: Velocity profile at 25 °C. Average superficial velocity 2.83 m/s.

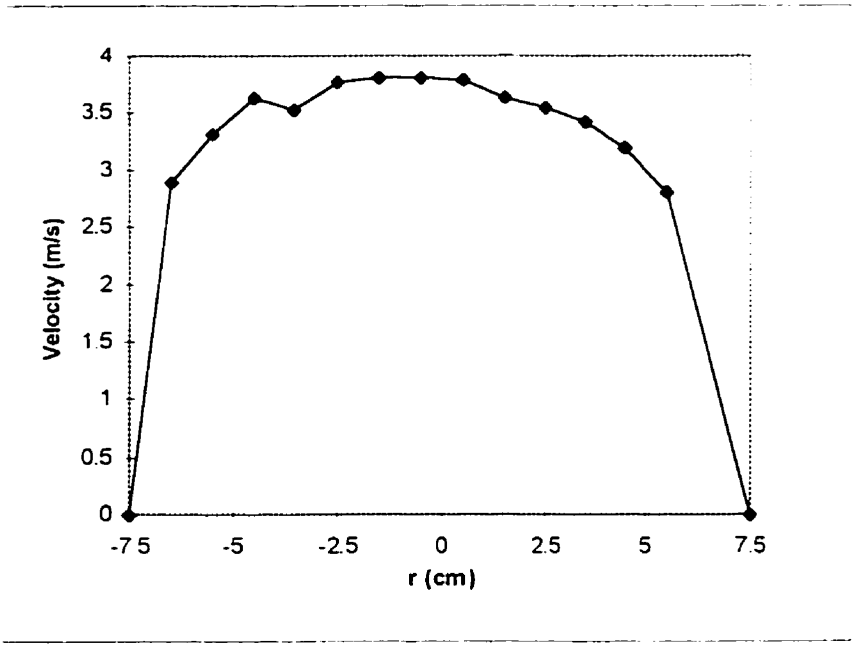

Figure 7.4: Average velocity profile at 97°C. Average superficial gas velocity 3.0= m/s.

7.1.3 UV Intensity Profile

The intensity of the ultraviolet light was measured at the location where the impregnated supported mesh was placed. As well, UV intensity was measured at different circumferential positions: 0 degrees, 45 degrees, 90 degrees, and 135 degrees (the various positions are shown in Figure 7.5). Light flux entering the reactor and reaching the filter area was measured with the radiometer. The observed irradiated profile was almost symmetric in shape, flat at the middle bending somewhat at the edges. Average radiation received was 40 $\mu W/cm^2$. While received radiation tended to change across the filter

surface, most of the filter was illuminated (Refer to Figure 7.5) with close to 55 $\mu w/cm^2$. There was a relatively small outer annulus with radiation levels below 50 $\mu w/cm^2$.

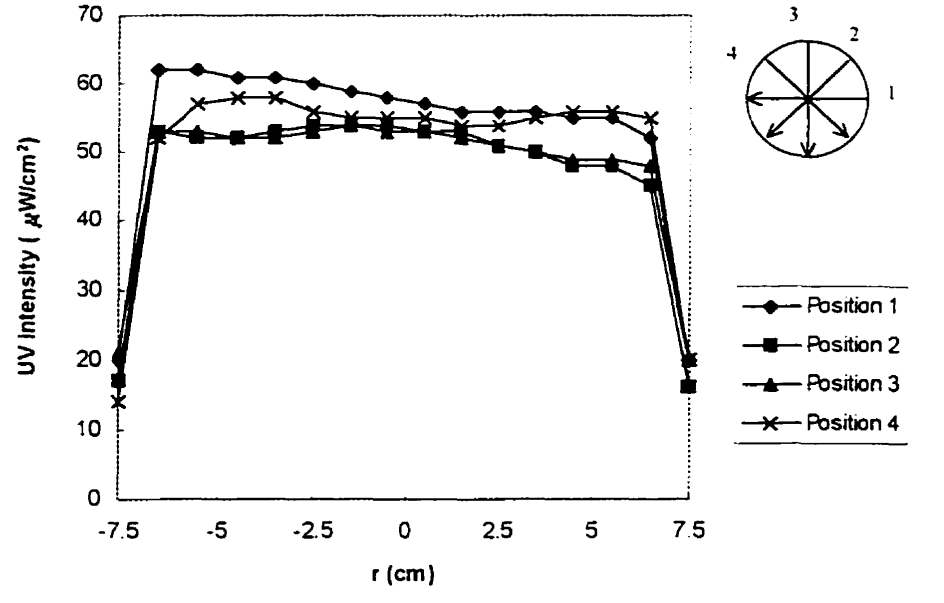

Figure 7.5: UV intensity profile across the filter sectional area with r=0 representing the center of the filter. Position 1: 0 degrees, Position 2: 45 degrees, Position 3 :90 degrees, Position 4: 135 degrees.

A radiometer equipped with a 365nm sensor, which was moved in the direction of the arrows indicated in the figure, was used with a specially designed rotating plate, that allowed the UV intensity measurement at the different positions.

The UV lamp power decay with time of utilization was estimated by measuring the intensity profile at the mesh location along position 1 indicated in Figure 7.5 for 3 h. It was observed that there was a consistent power decay (Figure 7.6). For instance after 190 min at the radial position of 5 cm the irradiation observed was 42.4$\mu W/cm^2$ instead of

44.4μW/cm^2 representing 5% decay in about 3 h. Note that this decay in the intensity was calculated (Figure 4.6) and its effect was included in the kinetic constants calculations performed later on in this thesis.

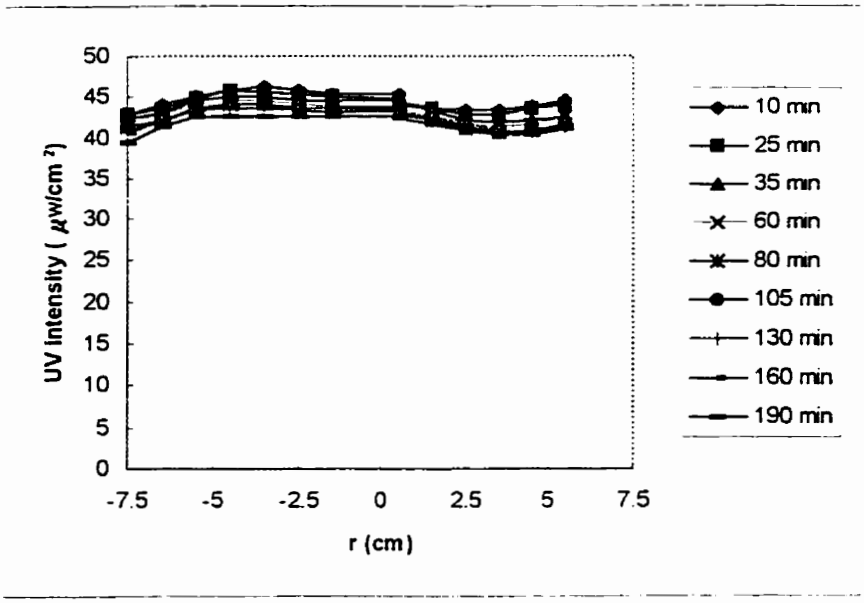

Figure 7.6: Radial UV intensity decay profile across the mesh with r=0 representing the center of the mesh.

7.2 Photocatalytic Conversion Experiments

Photocatalytic degradation of pollutants carried in a gas stream involves three main components: catalyst, radiation and oxygen. In order to assess the various effects in addition to the actual reaction runs, blank runs were developed. Results of both the blank runs and the reaction experiments are presented in this section. This section also reviews the values of the kinetic constant as well as the apparent quantum yields obtained.

Toluene was chosen as the model pollutant for several reasons: (a) it is a compound that can be used safely given its relatively high safety threshold concentration value (50 ppm). This is particularly relevant when comparing the toluene threshold value with the ones for other chemical species such as benzene (0.5 ppm), (b) toluene has been studied already by other researchers which provides a useful basis for comparison, and (c) toluene photo-oxidation does not reveal formation of any significant amount of harmful intermediates (e.g. phosgene is a typical intermediate of the photo-oxidation of chlorinated compounds).

7.2.1 Blank runs

As stated above, blank runs are important to establish the potential effect of the various factors outside the photocatalytic reaction. Two types of blank experiments were conducted: type 1 runs were performed with no UV illumination and with no TiO_2 catalyst particles or mesh at two temperatures: 20° C and 100° C; type 2 runs were carried out in the presence of the TiO_2 mesh at high temperature (100°C). Results of the first type of blank runs at the low (20°C) and the high (100°C) temperatures are illustrated in Figures 7.7 and 7.8, respectively. Figure 7.7 shows that at low temperature, there is about 22% concentration drop with respect to the initial toluene concentration over a period of 9 h. This toluene gas phase concentration drop was similar to the one observed during a reaction run (UV lamp on and TiO_2 particles in mesh) for the same reactor time-on-stream. This showed that no or very little toluene photo-oxidation took place at 20°C. Therefore, given the above mentioned uncertainty, reaction runs at 20°C were not considered further when assessing kinetic constants and apparent quantum yields.

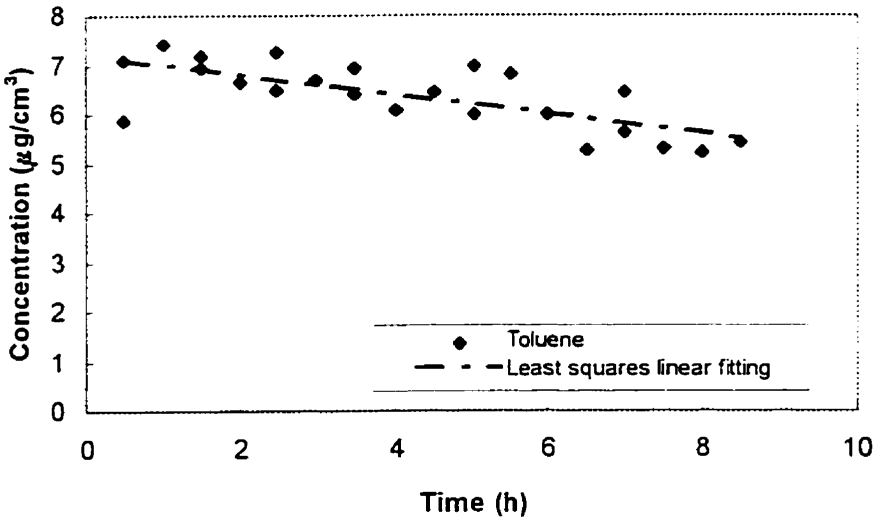

Figure 7.7: Results of the blank runs in Photo-CREC-Air without TiO_2 mesh and with no UV irradiation at 20°C.

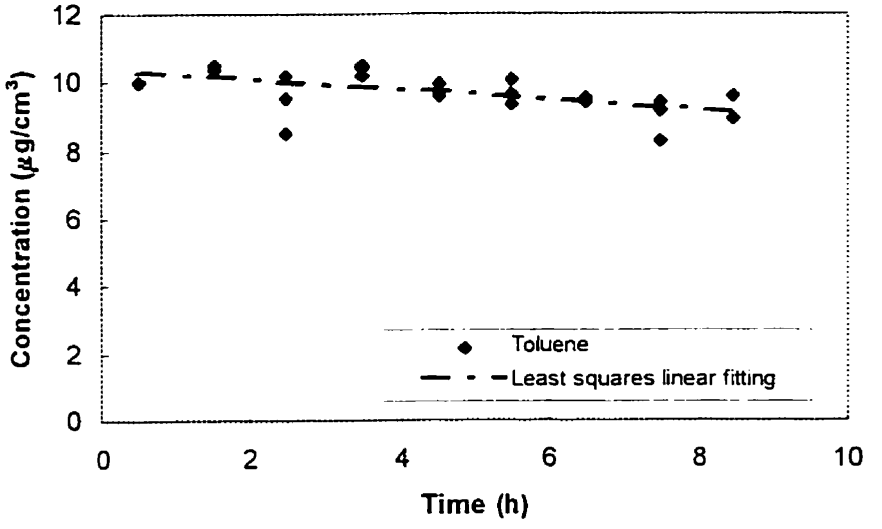

Figure 7.8: Results of the blank runs in Photo-CREC-Air without TiO_2 mesh and with no UV irradiation at 100°C.

Regarding toluene concentration changes at 20°C, these toluene concentration drops were assigned to condensation. Even if initial calculations using HYSIM thermodynamic package suggest no toluene condensation at the concentrations and temperatures under study, condensation appears to take place at 20°C. Condensation is a phenomenon also reported for concentrations in the same range by Blanco *et al.* (1996).

Regarding the potential influence of toluene condensation at higher temperatures, it can be stated that condensation was steadily reduced while increasing the temperature of the heating plate supporting the mesh from 20°C to 100°C. Given that a 9% drop (blank runs) is relatively a smaller concentration drop versus the toluene drop (25-50%) observed at 100°C under reaction conditions, it was concluded that at higher temperatures the photocatalytic oxidation was the dominant phenomenon. Therefore, these data were the ones considered to have relevance for kinetic parameter estimation.

In order to confirm that toluene drops during the " non-reaction period" were limited, extended blank runs with TiO_2 mesh and no UV light were also conducted at high temperature(100° C) and for about 16 h. These experiments revealed that after 4-6 h of operation, there was an insignificant change in the toluene concentration (3% extra) and no change in the carbon dioxide level (Figure 7.9). This Figure also depicts the photocatalytic effect one would expect under the same conditions of operation. Therefore, it was concluded that steady state was reached in the unit after 4-6 h and subsequent concentration changes with the lamp "on" could only be explained as a result of the photocatalytic reaction. Note that adsorption does not seem to occur to any

significant degree, since ~3% extra toluene concentration drop was observed in the case where a TiO_2 mesh was used compared to a run without the TiO_2 mesh.

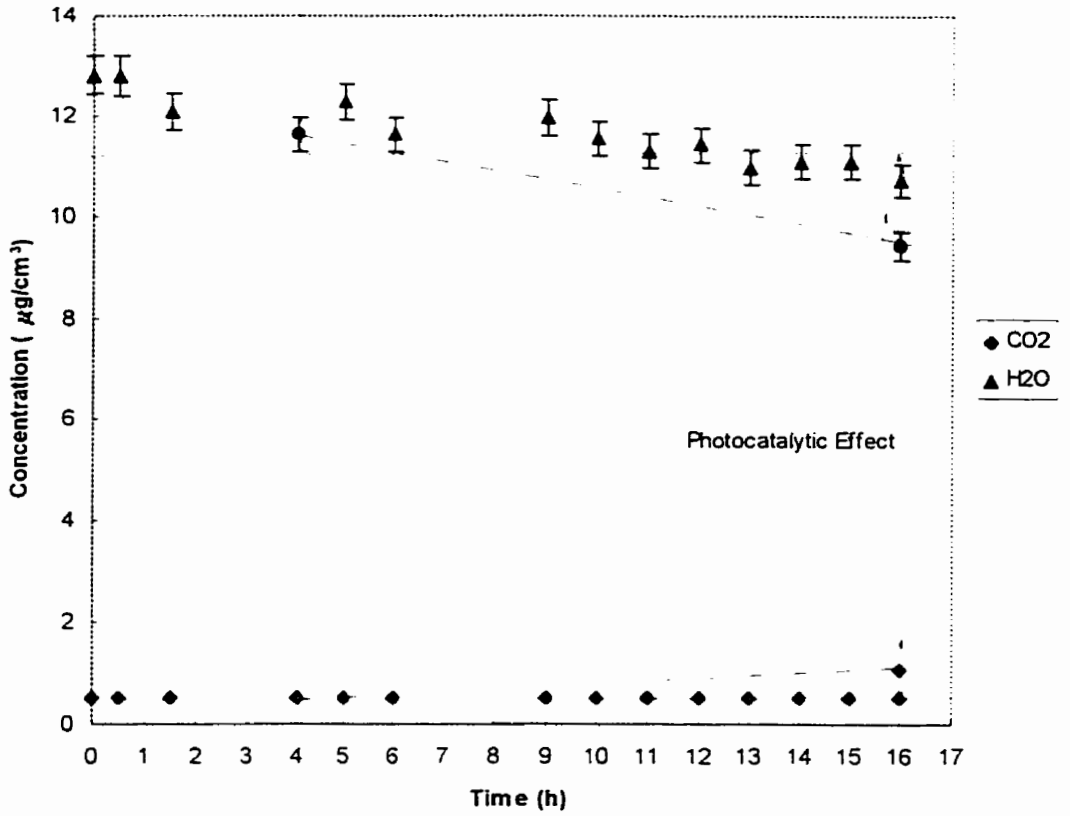

Figure 7.9: Concentration changes of both carbon dioxide and toluene during an extended blank run in the presence of TiO_2 mesh and UV lamp turned off (maximum deviations ~ 4% and 2% for toluene and carbon dioxide, respectively).

7.2.2 Typical Experimental Run

Following the blank runs, a number of reaction runs were developed. Figure 7.10 reports a typical plot of the observed changes of model pollutant and product

concentration as a function of time-on-stream and with the mesh temperature held at 100°C.

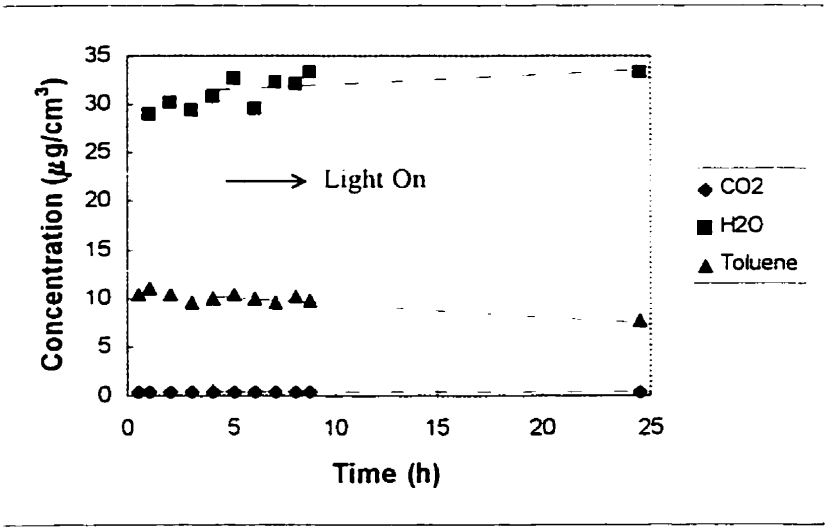

Figure 7.10: Typical experimental curves showing changes of reactant and product concentration as a function of time-on-stream with toluene concentration being 10.4 μg/cm³ and heating plate at T=100°C.

This figure shows a consistent toluene concentration decrease and a simultaneous water and carbon dioxide increase. An interesting observation was given by the fact that change in toluene as well as carbon dioxide concentrations were quite regular while there was some higher dispersion of the water concentrations measured. This higher dispersion on water concentration measurements was linked to the higher inaccuracies related to water measurements.

Regarding these experimental results, it should be stated that at 100 °C the toluene concentration drop during the first four hours (light off) was very mild and this was a potential indication of condensation and/or adsorption. However, given that condensation

was already estimated as 9 %(refer to section 7.2.1), it was concluded that adsorption in the context of Photo-CREC-Air reaction runs was not significant. Thus on this basis, the potential applicability of a pseudo-homogeneous model (no adsorption of pollutants on the TiO_2 mesh) for kinetics modeling should be strongly considered.

It has to be stressed that experiments were performed with the light source "off" during the first period of the experiment (< 4 h). This first period of the experiment allowed the determination of the condensed/adsorbed amount of toluene on the TiO_2 mesh surface. Following this, the lamp was turned on. Typical runs lasted 22-24 h having the mesh-TiO_2 about 18-20 h under UV radiation.

Figures 7.11 and 7.12 depict typical chromatograms of injected samples for both the TCD and the FID, respectively. Examination of these figures along with Figure 7.10 reveal the following:

1. Main products from toluene photo-oxidation are water and carbon dioxide,
2. No intermediate products are observed,
3. There is a substantial increase in both carbon dioxide and water while the run is progressing.

It has to be pointed out that the first observation was consistent throughout all the experiments carried out. While both detectors (FID and TCD) were used for product quantification, the FID detector was used specifically to help identifying potential intermediate species.

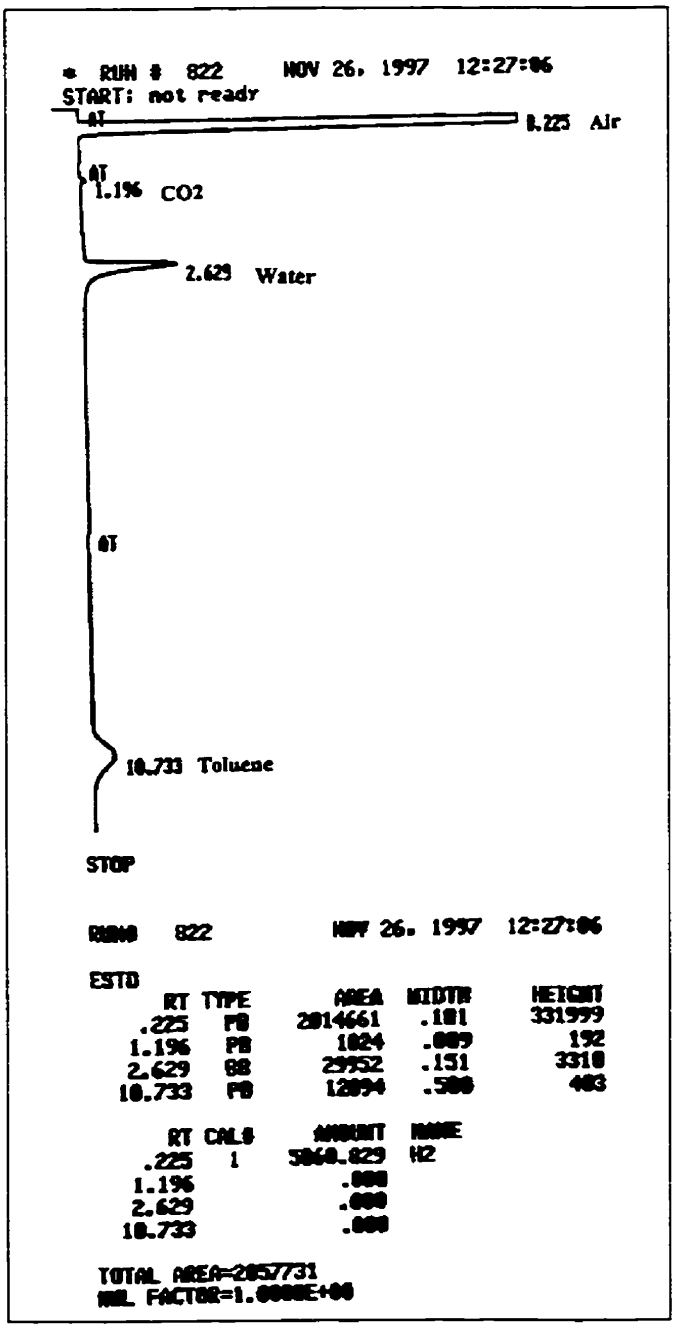

Figure 7.11: TCD chromatogram of an injected sample. Different compounds forming the sample mixture are shown: (a) air, (b)carbon dioxide, (c) water, (d) toluene.

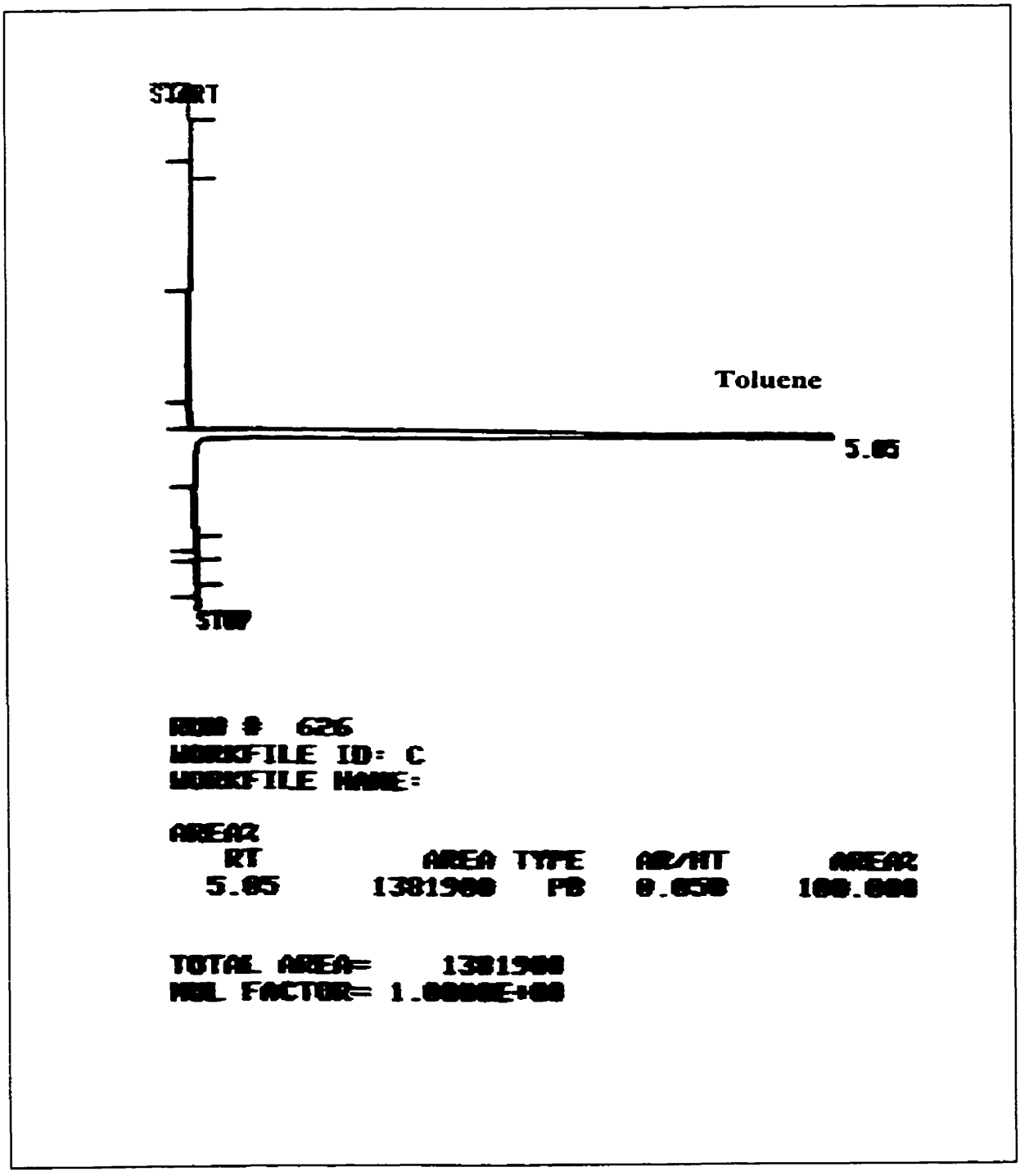

Figure 7.12: FID chromatogram of an injected sample indicating the presence of toluene as the only hydrocarbon without any intermediate species.

Results suggest that there are no chemical species other than water and carbon dioxide formed or at least if individual intermediate species exist in the gas phase they are in negligible amounts (below the detectable limits). This observation is a very important one given intermediate species can represent a potential hazard in some cases with toxicity larger than the original pollutant.

Note that this experimental observation of a negligible amount of intermediate species was consistent throughout all the experimental runs. This was also supported by the findings of Luo and Ollis (1996) and Ibusuki and Takeuchi., (1986). These authors reported very low levels of benzaldehyde (<2ppm) besides carbon dioxide during toluene photocatalytic oxidation.

7.2.3 Kinetic Parameters Estimation

One of the goals of the present study was to establish the kinetics of toluene photo-oxidation under UV illumination. With this end, initial photo-oxidation rates were measured and values obtained were in the 0.005-0.05 μmole/(gcat.s).

While several kinetic models have been proposed in the literature[Luo and Ollis, (1996), Obee *et al.* (1995)], an attempt was undertaken to model the experimental data with a first order pseudo-homogeneous model. This approach was chosen given the negligible adsorption effect observed (refer to Section 7.2.1). Adsorption effects normally translate in the need for a Hinshelwood-Langmuir model with an overall order between 0 and 1.

Given the condition of negligible adsorption and the assumption of uniform concentration in Photo-CREC-Air as a result of the intense air recirculation, the following balance equation applies for toluene:

$$V\, dC_T/dt = W\, r_T \qquad (7.1)$$

with V being the total gas hold up, W the weight of the catalyst utilized, C_T toluene concentration at time t, and r_T is the rate of toluene photo-oxidation. The latter can be formulated using the following first order equation:

$$r_T = -k_s C_T \qquad (7.2)$$

with k_s is the intrinsic rate constant. Substituting eq. (7.2) into eq. (7.1),

$$V\, dC_T/dt = W\, k_s C_T \qquad (7.3)$$

An integral form of eq. (7.3) yields the following:

$$\ln(C_T/C_{To}) = -(k_s W/V)t \qquad (7.4)$$

or

$$\ln(C_T/C_{To}) = -kt \qquad (7.5)$$

Kinetic constants (k) were evaluated in a two step process. In the first step, ln C_T/C_{To} was plotted versus time for each individual run to produce a straight line with a slope equal in value to the kinetic constant k (eq. 7.5). Kinetic constants obtained were found to be in the range of 0.009-0.027 (h^{-1}). Results are reported in Table 7.1. Once the k values were established, they were corrected for the decay of the UV lamp intensity

using the correlation suggested by Ollis (1993), Luo and Ollis (1996) and Peral and Ollis (1992):

$$k = k_o (I/I_o)^{\Omega} \quad (7.6)$$

with Ω=1.0 for the low light intensity used in Photo-CREC-Air.

Table7.1: Summary of the calculated parameters of the different experimental runs.

Experiment	[T]		k	$k_{corrected}$	Apparent Quantum	Conversion	r_{To}
#	mL	kg/cm^3	(h^{-1})		Yield (%)	(%)	(μmole/gcat.s)
1	0.4	5.19E-09	0.011	0.011	44	31	0.005
2	0.4	5.19E-09	0.010	0.012	46	19	0.006
3	0.4	5.19E-09	0.011	0.013	50	19	0.006
4	0.4	5.19E-09	0.009	0.015	59	16	0.007
5	0.6	7.79E-09	0.020	0.024	139	28	0.017
6	0.6	7.79E-09	0.020	0.025	148	29	0.018
7	0.6	7.79E-09	0.038	0.051	299	41	0.036
8	0.6	7.79E-09	0.014	0.047	276	16	0.034
9	0.8	1.04E-08	0.022	0.031	238	30	0.029
10	0.8	1.04E-08	0.020	0.029	224	30	0.027
11	0.8	1.04E-08	0.019	0.028	220	26	0.027
12	0.8	1.04E-08	0.010	0.029	229	8	0.028
13	1	1.3E-08	0.015	0.022	218	25	0.027
14	1	1.3E-08	0.030	0.049	478	38	0.058
15	1	1.3E-08	0.023	0.039	379	32	0.046
16	1	1.3E-08	0.020	0.047	457	41	0.056
29	0.8	1.04E-08	0.012	0.04	292	15	0.036
30	0.8	1.04E-08	0.015	0.05	369	16	0.045
31	0.8	1.04E-08	0.015	0.05	374	21	0.045
32	0.8	1.04E-08	0.016	0.05	425	18	0.052

Corrected k values are reported in Table 7.1. With the only exception of the runs at the lower toluene initial concentration (5.2 $\mu g/cm^3$), the k value is found to equal 0.033 ± 0.014 h^{-1}(Figure 7.13) Kinetic constants at the high humidity level (32 $\mu g/cm^3$) were also in the same range.

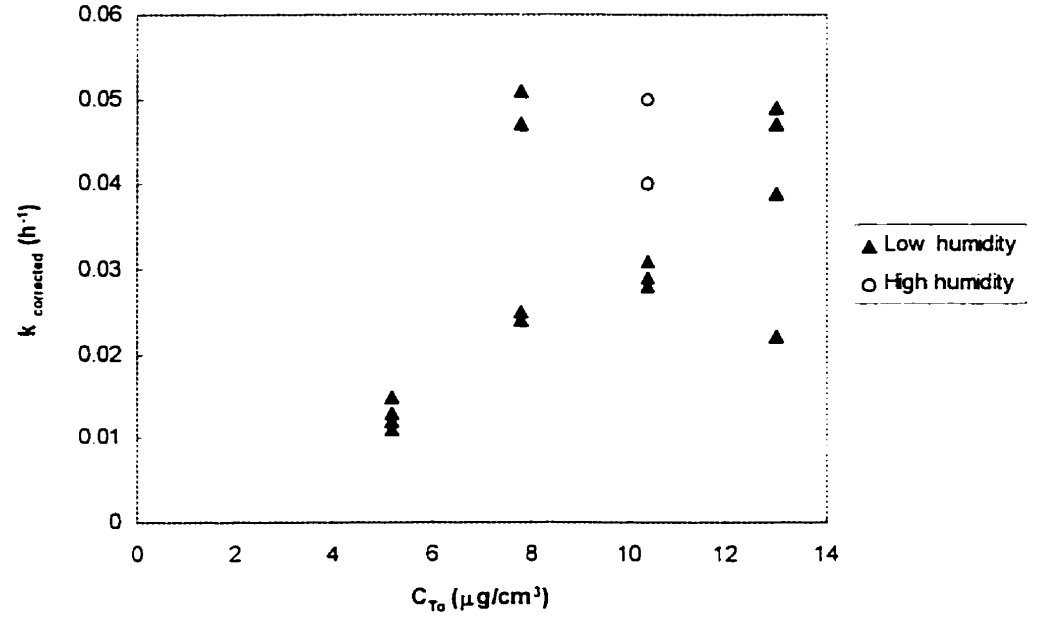

Figure 7.13: Kinetics constants for the different initial toluene concentration.

On this basis, the following can be postulated: a) the first order is adequate for the reaction of toluene photoconversion and this is consistent with the applicability of a pseudo-homogeneous model at 100° C, b) the humidity level does not appear to influence either positively or negatively the performance of Photo-CREC-Air and this is in agreement with the designed conditions of the unit: a heating plate preventing water adsorption on the mesh.

7.2.4 Influence of the Different Parameters

In order to clarify the influence of the different operating parameters, an experimental program was developed with systematic changes of toluene concentrations, temperatures, and humidity levels. The different experimental conditions are given in Table 7.2.

Table7.2: Summary of the different experimental conditions.

Experiment #	mL	C_{to} $\mu g/cm^3$	Plate Temp. (°C)	Humidity $\mu g/cm^3$	Mesh #	Experimental Time (h)
1	0.4	5.2	100	<25	14	24
2	0.4	5.2	100	<25	15	23
3	0.4	5.2	100	<25	16	22
4	0.4	5.2	100	<25	21	24
5	0.6	7.78	100	<25	12	24
6	0.6	7.78	100	<25	13	21
7	0.6	7.78	100	<25	19	22
8	0.6	7.78	100	<25	31	23.5
9	0.8	10.4	100	<25	26	21
10	0.8	10.4	100	<25	20	24
11	0.8	10.4	100	<25	25	23
12	0.8	10.4	100	<25	30	22.5
13	1	13	100	<25	24	27
14	1	13	100	<25	23	24
15	1	13	100	<25	22	22
16	1	13	100	<25	32	26
17	0.8	10.4	75	<25	27	23
18	0.8	10.4	75	<25	27	24
19	0.8	10.4	75	<25	27	23
20	0.8	10.4	75	<25	27	23
21	0.8	10.4	50	<25	28	22
22	0.8	10.4	50	<25	28	24
23	0.8	10.4	50	<25	28	24
24	0.8	10.4	50	<25	28	23
25	0.8	10.4	20	<25	29	22
26	0.8	10.4	20	<25	29	25
27	0.8	10.4	20	<25	29	24
28	0.8	10.4	20	<25	29	23
29	0.8	10.4	100	>30	30	22.5
30	0.8	10.4	100	>30	30	22
31	0.8	10.4	100	>30	30	24.5
32	0.8	10.4	100	>30	30	22.5

7.2.4.1 Effect of Toluene Concentration

Experiments with four different concentrations ranging between 5.2 $\mu g/cm^3$-13 $\mu g/cm^3$ were carried out. Model pollutant concentrations were obtained by injecting different amounts of toluene of a volume between 0.4 and 1.0 mL into the reactor vessel. The order of experiments was randomized to eliminate any source of systematic errors related to the order of the runs.

Figures 7.14-7.21 depict the increase in the carbon dioxide level, as well as the natural logarithm of the dimensionless toluene concentration, [ln (C_T/C_{To})] at various t^* [$t^* = t(I/I_o)$] for four repeat runs for each of the four concentrations examined.

Note that figures of ln (C_T/C_{To}) versus the corrected time correct for the decay in the lamp intensity by bringing replicates to the same condition of lamp time of utilization (t^* =40 h with an estimated light power of 50 $\mu W/cm^2$ reaching the mesh):

$$\mathbf{ln(C_T/C_{To})=-k_o\,(I/I_o)\,t} \qquad \mathbf{(7.7)}$$

or

$$\mathbf{ln(C_T/C_{To})=-k_o\,t^*} \qquad \mathbf{(7.8)}$$

with t being the time elapsed from the instant the lamp was turned on.

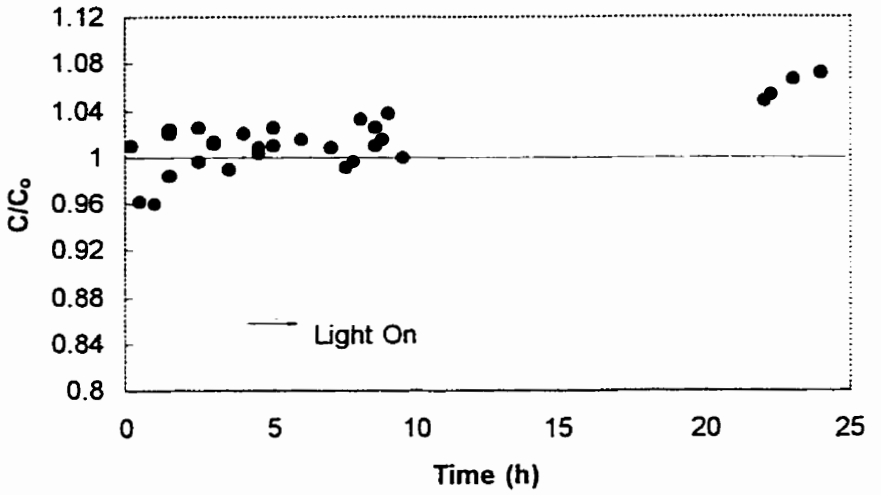

Figure 7.14: Carbon dioxide level during experimental runs with Photo-CREC-Air: initial toluene concentration=5.2 μg/cm^3, temperature=100 °C, water level below 25 μg/cm^3.

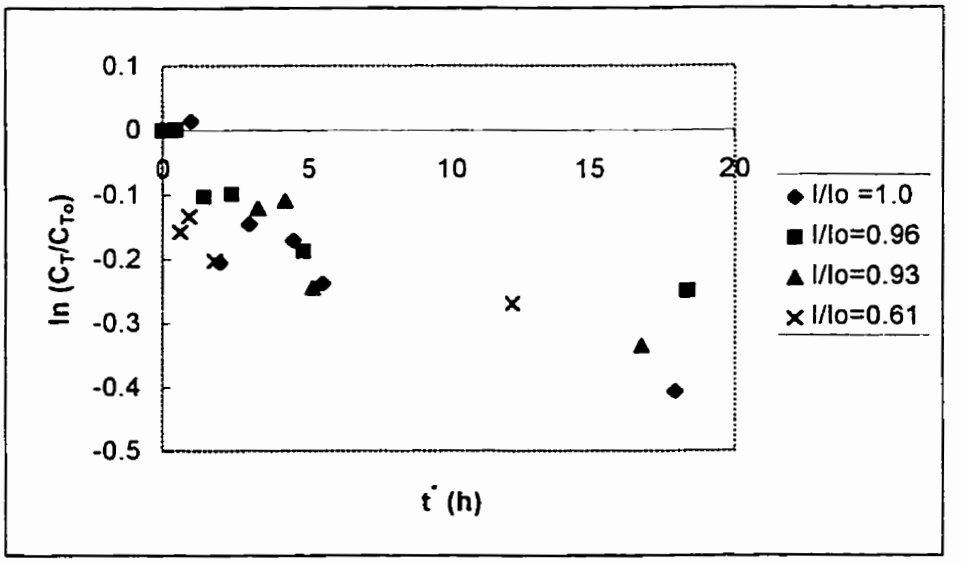

Figure 7.15: Ln (C_T/C_{To}) versus the corrected time ($t^{\cdot}=I/I_o\ t$) during experimental runs with Photo-CREC-Air: initial toluene concentration=5.2 μg/cm^3, temperature=100 °C, water level below 25 μg/cm^3.

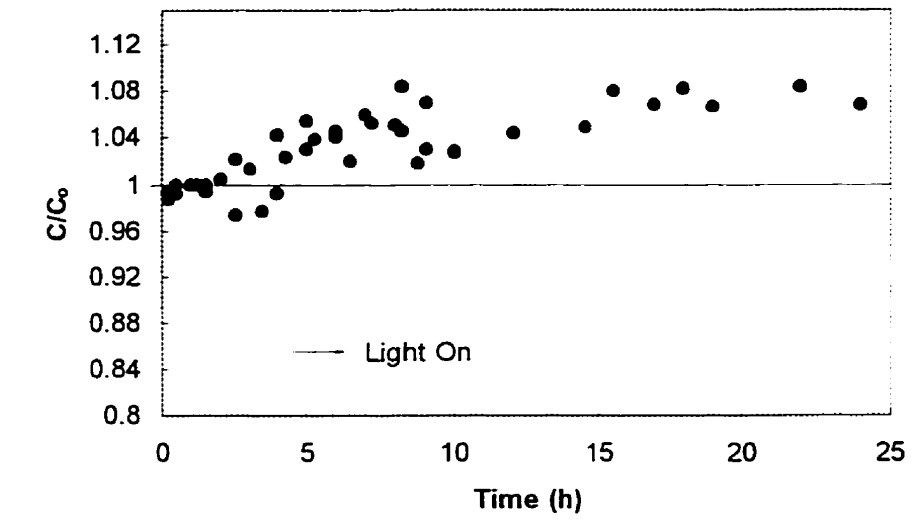

Figure 7.16: Carbon dioxide level during experimental runs with Photo-CREC-Air: initial toluene concentration=7.8 μg/cm^3, temperature=100 °C, water level below 25 μg/cm^3.

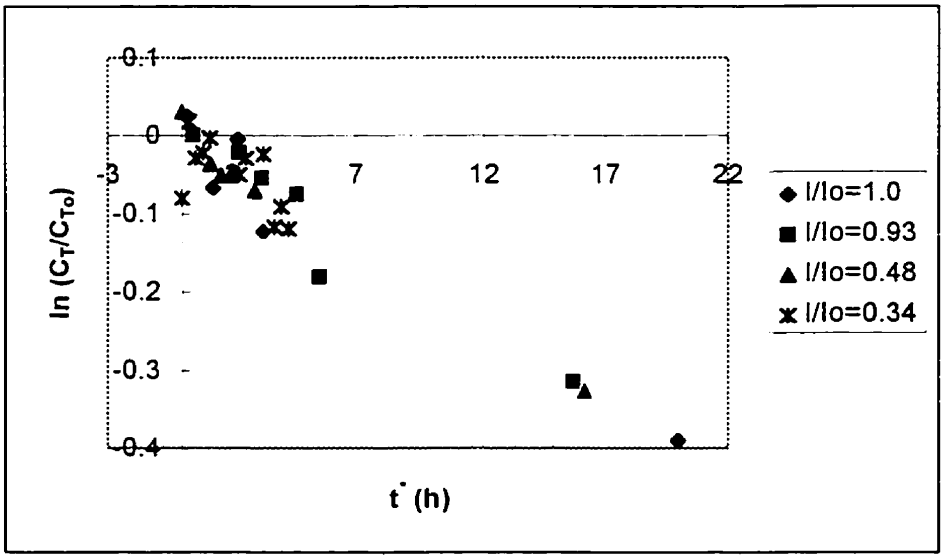

Figure 7.17: Ln (C_T/C_{To}) versus the corrected time ($t^*=I/I_o\ t$) during experimental runs with Photo-CREC-Air: initial toluene concentration=7.8 μg/cm^3, temperature=100 °C, water level below 25 μg/cm^3.

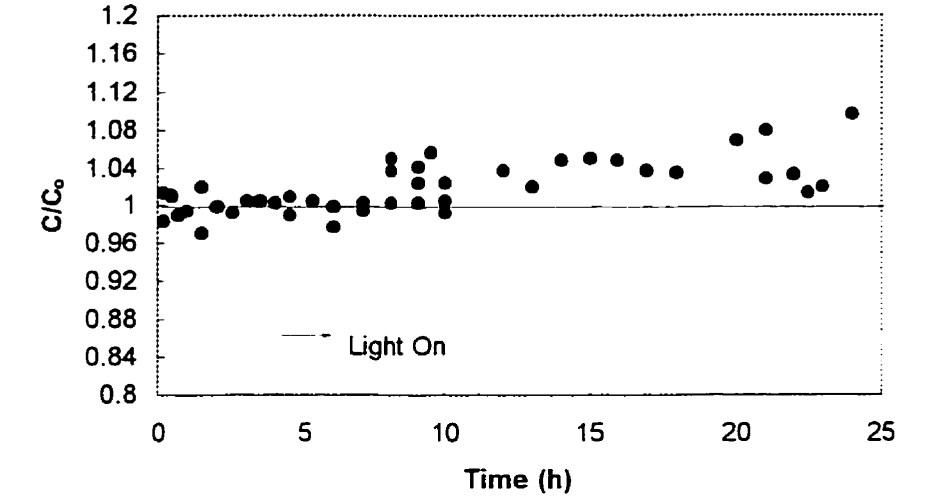

Figure 7.18: Carbon dioxide level during experimental runs with Photo-CREC-Air: initial toluene concentration=10.4 μg/cm^3, temperature=100 °C, water level below 25 μg/cm^3.

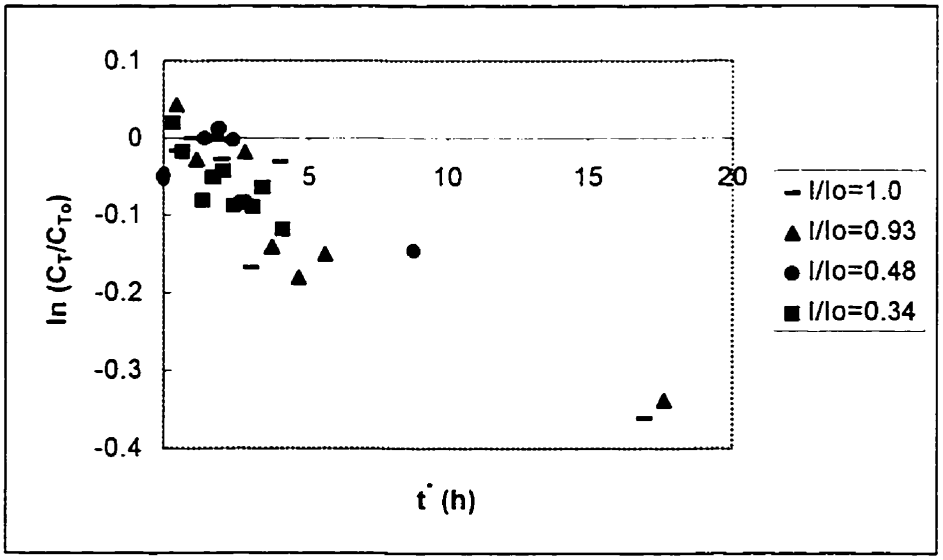

Figure 7.19: Ln (C_T/C_{To}) versus the corrected time ($t^*=I/I_o\ t$) during experimental runs with Photo-CREC-Air: initial toluene concentration=10.4 μg/cm^3, temperature=100 °C, water level below 25 μg/cm^3.

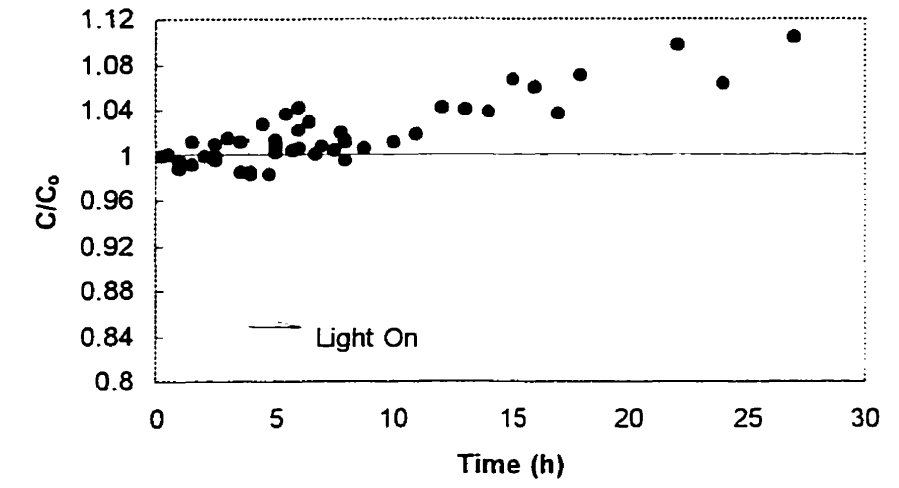

Figure 7.20: Carbon dioxide level during experimental runs with Photo-CREC-Air: initial toluene concentration=13 μg/cm^3, temperature=100 °C, water level below 25 μg/cm^3.

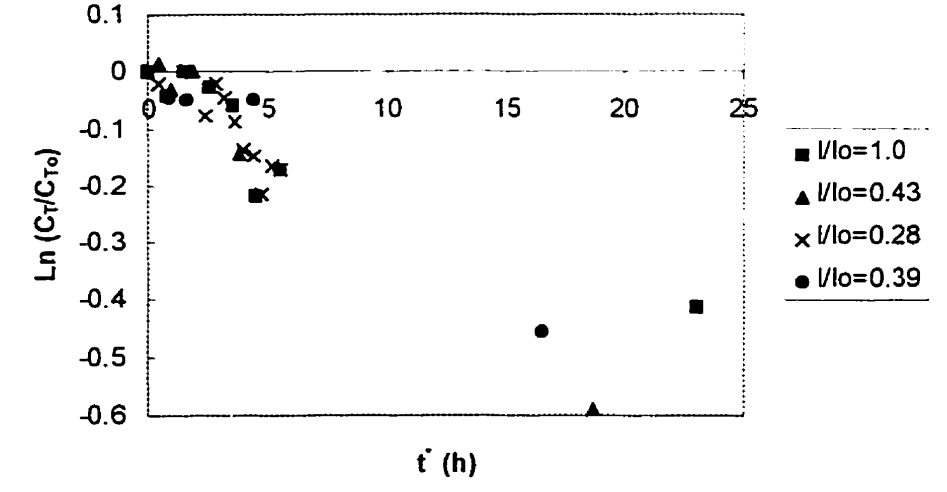

Figure 7.21: Ln (C_T/C_{To}) versus the corrected time ($t^*=I/I_o\ t$) during experimental runs with Photo-CREC-Air: initial toluene concentration=13 μg/cm^3, temperature=100 °C, water level below 25 μg/cm^3.

It can be observed in Figures 4.14, 7.16, 7.18, 7.20, that throughout the runs at different concentrations, a consistent increase in the carbon dioxide level provides support that there is a photocatalytic effect during the period where TiO_2 was illuminated. Furthermore, the reporting of the ln C_T/C_{T_o} versus t^* demonstrated that once the power of the lamp was corrected for power decay, the various repeat runs fall all in a single straight line and this is a strong indication of the first order kinetics and of the reproducibility of the data obtained.

7.2.4.2 Influence of Temperature

Temperature effect on the operation of Photo-CREC-Air over the 20-100°C range was investigated as part of the present study. Initially, it appeared that increasing the temperature was not going to bring a significant enhancement of toluene photo-oxidation. However, once the problem of toluene condensation on the reactor walls was well established, it was realized that a detailed analysis of the effect of temperature was of particular importance. Therefore, runs with the heating plate at 20°, 50°, 75°, and 100° C were conducted. It was observed that only the runs at 100° C provided adequate conditions to minimize toluene condensation and were appropriate for kinetic constant calculations.

In summary, the experiments developed with the heating plate at 100° C provided conditions of minimum toluene condensation as well as good removal of adsorbed water from the mesh surface.

7.2.4.3 Effect of Water Content

When similar experiments were repeated in the presence of higher water contents (32 μg/cm^3), the value of the kinetic constant calculated were found to be slightly higher than the ones for the runs at low water concentration. This indicates the importance of the heating plate in removing the water off the TiO_2 mesh surface and hence reducing its effect on the photocatalytic reaction. Data of carbon dioxide increase and toluene decrease are summarized in Figures 7.22 and 7.23.

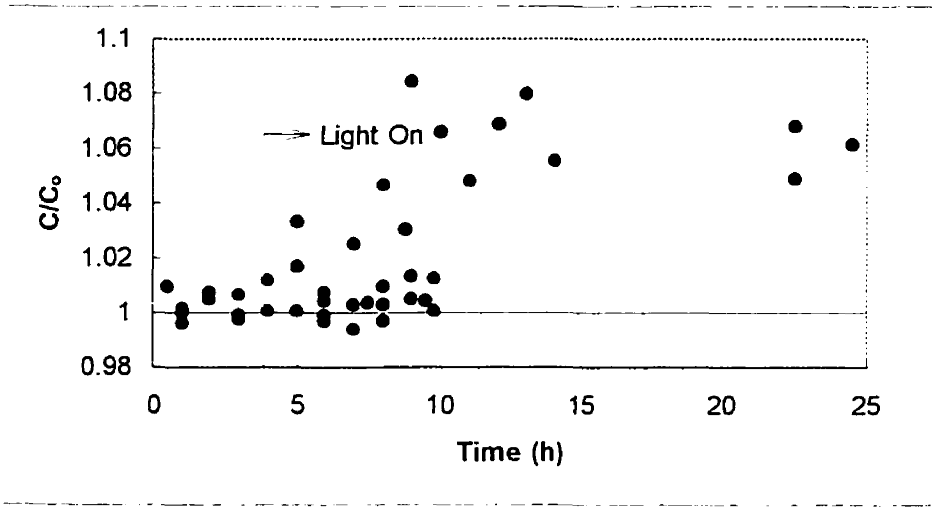

Figure 7.22: Carbon dioxide level during experimental runs with Photo-CREC-Air: initial toluene concentration=10.4 μg/cm^3, temperature=100 °C, water about 32 μg/cm^3.

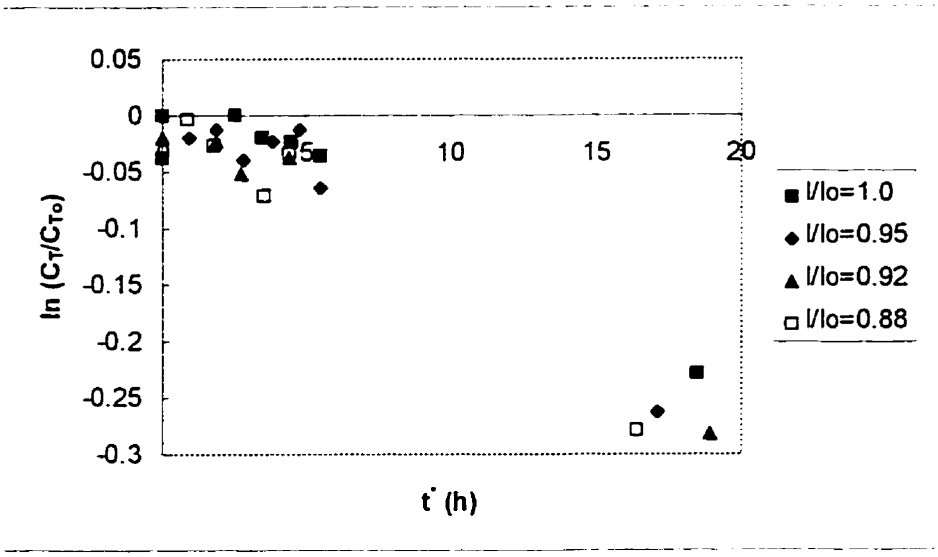

Figure 7.23: Ln (C_T/C_{T_0}) versus the corrected time ($t^*=I/I_0\ t$) during experimental runs with Photo-CREC-Air: initial toluene concentration=5.2 $\mu g/cm^3$, temperature=100 °C, water level 32 $\mu g/cm^3$.

Concerning the important effect of water, it is our view that this has to be investigated further. A wider humidity level range is strongly advised. This type of experimentation would allow a more careful analysis of postulations such as the ones of Luo and Ollis (1996), Ibusuki and Takeuchi (1986) who reported that no reaction proceed in the total absence of water. Thus, while some water has to be provided to allow the photo-oxidation reaction to take place, on the other hand too much water can turn as detrimental blocking catalyst sites.

7.2.5 Conversion

After 18-20 h of UV irradiation, typical conversions achieved were in the 8-40 % range. Conversion values are summarized in Table 7.1. It should be noted that these values do not include the 9% decrease in the toluene level that resulted from condensation

during the first four hours. It has to be mentioned also that pollutant concentrations used in the present study (5.2-13 $\mu g/cm^3$) were one order of magnitude larger than typical levels in indoor air pollution or considered by other researchers [Luo and Ollis (1996), (Obee *et al.*, (1995) and Ibusuki and Takeuchi (1986)]. For example, Luo and Ollis (1996) obtained conversions of 8-20% for 0.550-0.080 $\mu g/cm^3$ toluene concentration, respectively.

While reviewing the toluene conversions and the performance achieved in Photo-CREC-Air, one has to consider the light power and the rate of photoconversion achieved. As it will be shown in the next section, Photo- CREC-Air shows very good prospects in all these respects given the high apparent quantum yields obtained.

7.2.6 Apparent Quantum Yield

The quantum yield is a parameter that needs to be determined in photocatalytic reactions to establish the overall photon utilization efficiency. The apparent quantum yield is frequently defined as the number of moles of pollutant degraded per photon being provided to the system. In the present study, it was preferred to define the apparent quantum yield on the basis of photons absorbed by the TiO_2 on the mesh. Thus, the following equation was employed for the apparent quantum yield (φ) calculation:

$$\varphi=[r_{mp,o}]_{max} V N_A h C/[\lambda Q_{m,abs}] \qquad (7.9)$$

where:

$[r_{mp,o}]_{max}$: rate of model pollutant destruction based on the corrected kinetic constants and gas phase toluene concentration light was turned on.

V: total gas hold up.

N_A: Avogadro number (6.023 x 10^{23} molecules/mole).

h: Plank's constant (6.62 x 10^{-34} J.s).

C: speed of light in vacuum (2.997 x 10^{10}cm/s).

λ: wavelength (nm).

$Q_{m,abs}$: rate of light energy absorbed by the TiO_2 mesh in the photocatalytic reactor (J.s) at 40 h of lamp operation (50 μW/cm^2).

As presented in Table 7.1, the apparent quantum yields obtained were in the range of the 60-450 % range. Figure 7.24 depicts the increase in the apparent quantum yield with the initial toluene concentration. It should be noted that when calculating the apparent quantum yields corrections were introduced for the UV intensity decay and the average $k_{corrected}$ value was also used in this calculation.

Apparent quantum yields obtained were consistently, except to the lowest toluene concentration, bigger than 100%, and this confirms the special character of the photocatalytic oxidation reaction of air pollutants where one photon appears to be involved in more than one photocatalytic event suggesting a chain mechanism in the decomposition path. This finding is consistent with Luo and Ollis (1996) who quoted quantum yields as high as 4 (400%) and Berman and Dong (1994) who reported photoefficiencies of 590% for TCE, 220% for perchloroethylene, 920 % for methanol and 190% for ethanol. Note that Jacoby *et al.*, (1995) mentioned the possibility of quantum yields up to 4000 % again with a chain reaction mechanism. The high levels of apparent

quantum yields obtained in Photo-CREC-Air point towards the good performance of Photo-CREC-Air under the conditions selected for its design and operation.

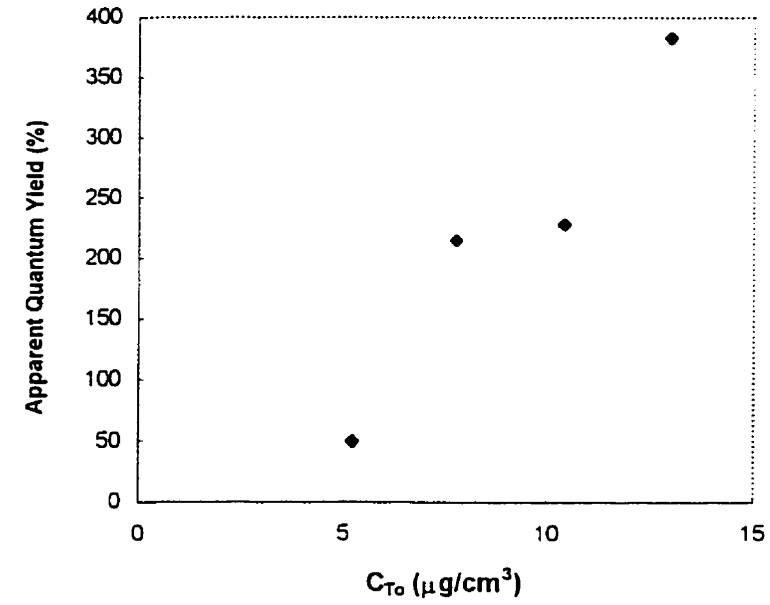

Figure7.24: Apparent quantum yields assessed for the different toluene initial concentrations studied.

7.2.7 Kinetic Modeling-Reaction Mechanism

Kinetics modeling and the insights on the reaction mechanisms was another important aspect of the present study. The basis of the analysis is a series reaction mechanism where toluene is oxidized to intermediates (oxidized species) and these intermediates species are later on converted to carbon dioxide and water:

$$\text{Toluene} \xrightarrow{k1} \text{Oxidized Intermediates} \xrightarrow{k2} CO_2 + H_2O \qquad (7.10)$$

Given that intermediates could not be detected(i.e. were below detectable limits) a possible quantification of the phenomena was achieved by increasing the kinetic constant k_2, and leaving the kinetic constant k_1 unchanged for the following reaction network:

$$dC_T/dt=-k_1C_T \quad (7.11)$$

$$dC_{OI}/dt=k_1C_T-k_2C_{OI} \quad (7.12)$$

$$dC_{CO2}/dt=k_2C_{OI} \quad (7.13)$$

Details about the Fortran program used are given in Appendix D. For example, it is shown in Figure 7.25 that having k_1 of a similar order of magnitude as k_2 yields oxidized intermediates concentrations above the detectable limits. Thus, in order that the oxidized intermediates be just at detectable limits k_2 has to be increased to about 7 times k_1 (Figure 7.26). Therefore, under these conditions it can be estimated that the first step is the slowest step controlling the photo-oxidation process. Given that the in actual experiments intermediates were not detectable (refer to Section7.2.2) it is likely that $k_1<<k_2$ and that the first oxidation step is the controlling one for the complete photo-oxidation process.

It is also worth noting that in the case where one desires to achieve a faster photoconversion, a higher Q_{abs} (absorbed light power) should be provided. For instance, with 10 times bigger Q_{abs} (Figure 7.27), 60% conversion is achieved in 3 h only. It is assumed, in this calculation, that both constants k_1 and k_2 are equally affected by the light power increase. As well, this calculation assumes that the increase of the kinetic constants is directly proportional to the power increase (Section 2.3.3).

Note that this Q_{abs} increase can be achieved in Photo-CREC-Air by increasing the number of UV lamps used, the power of each lamp, using Pyrex glass to maximize light transmittance through windows, or by a concurrent change of the factors mentioned.

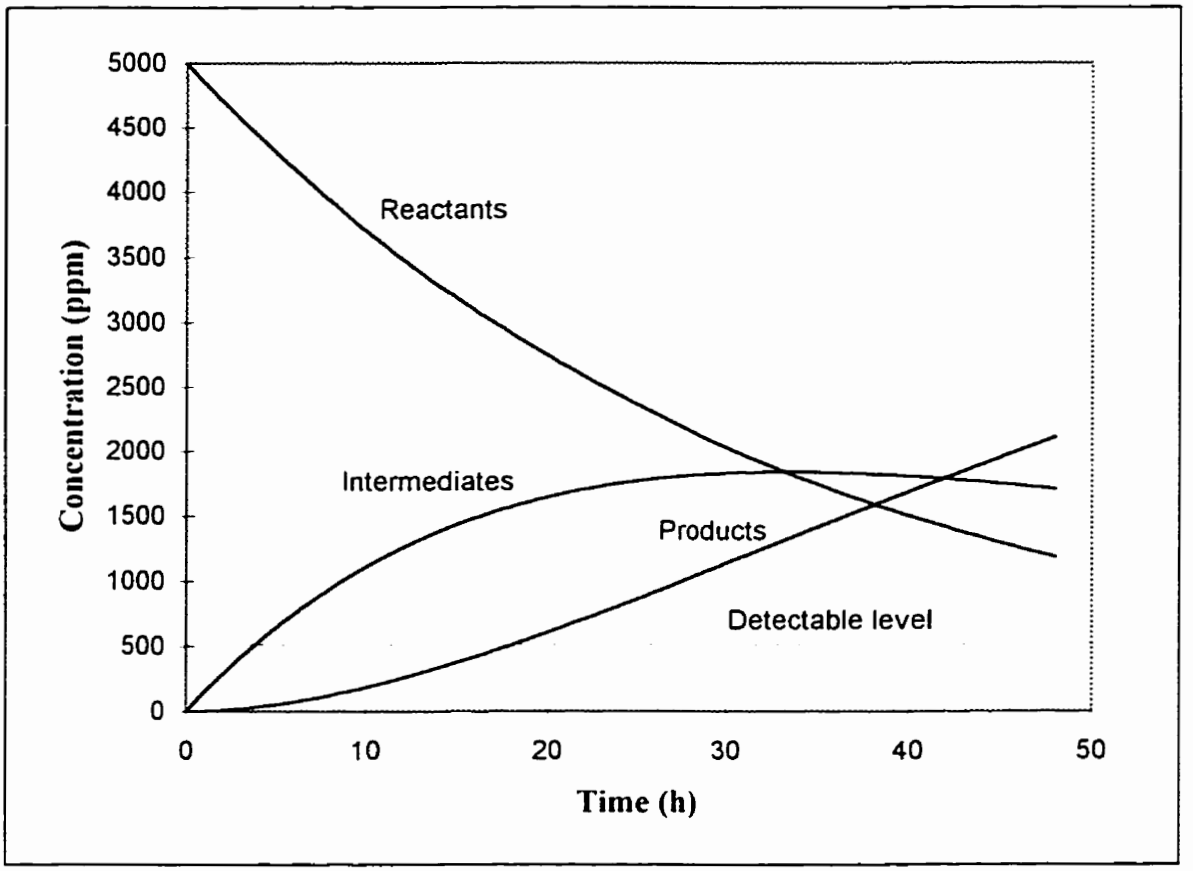

Figure 7.25: Simulated chemical species distribution for the following set of constants and operating conditions: k_1=0.03(h^{-1}), k_2=0.03(h^{-1}), and C_o=18 μg/cm^3 (5000ppm).

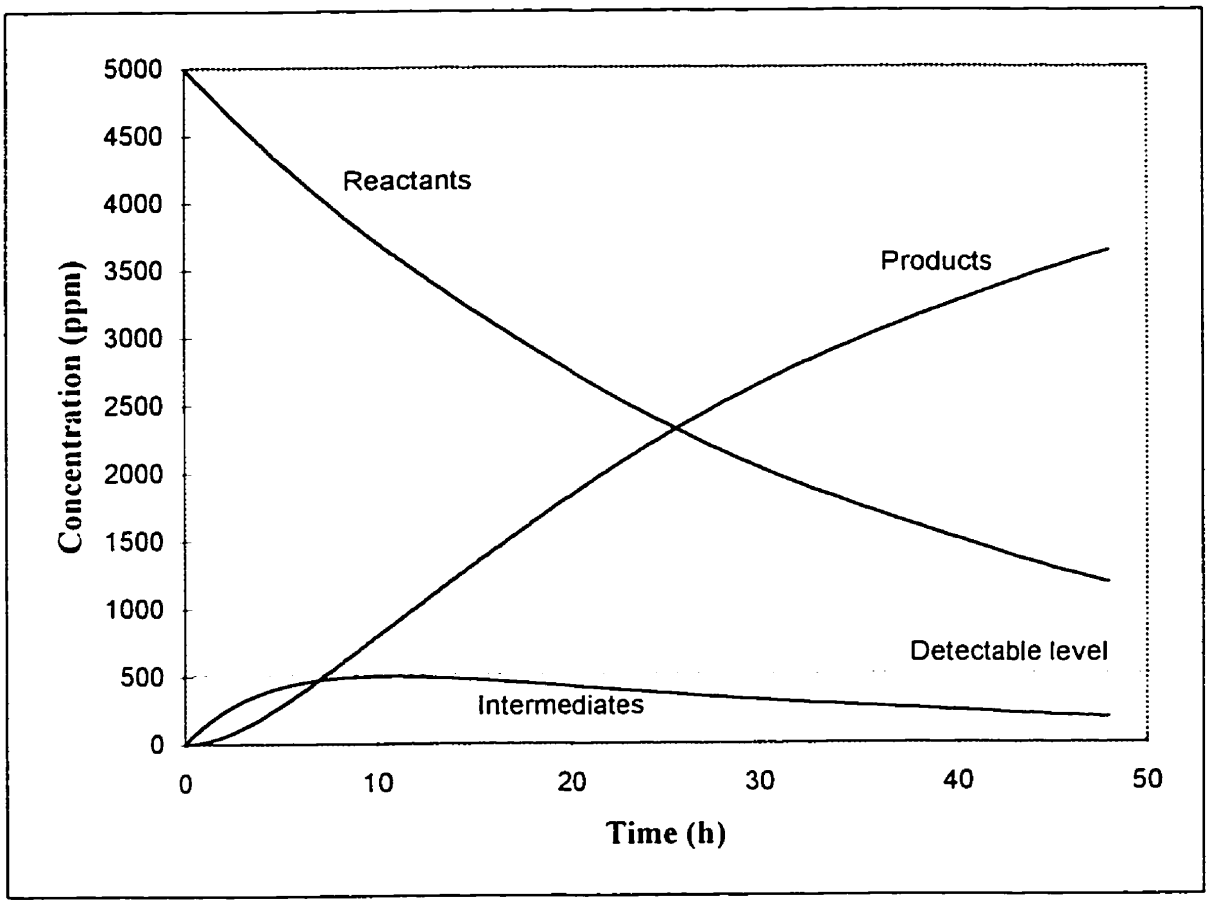

Figure 7.26: Simulated chemical species distribution for the following set of constants and operating conditions: k_1=0.03 (h^{-1}), k_2=0.22 (h^{-1}), and C_o= 18μg/cm^3(5000ppm).

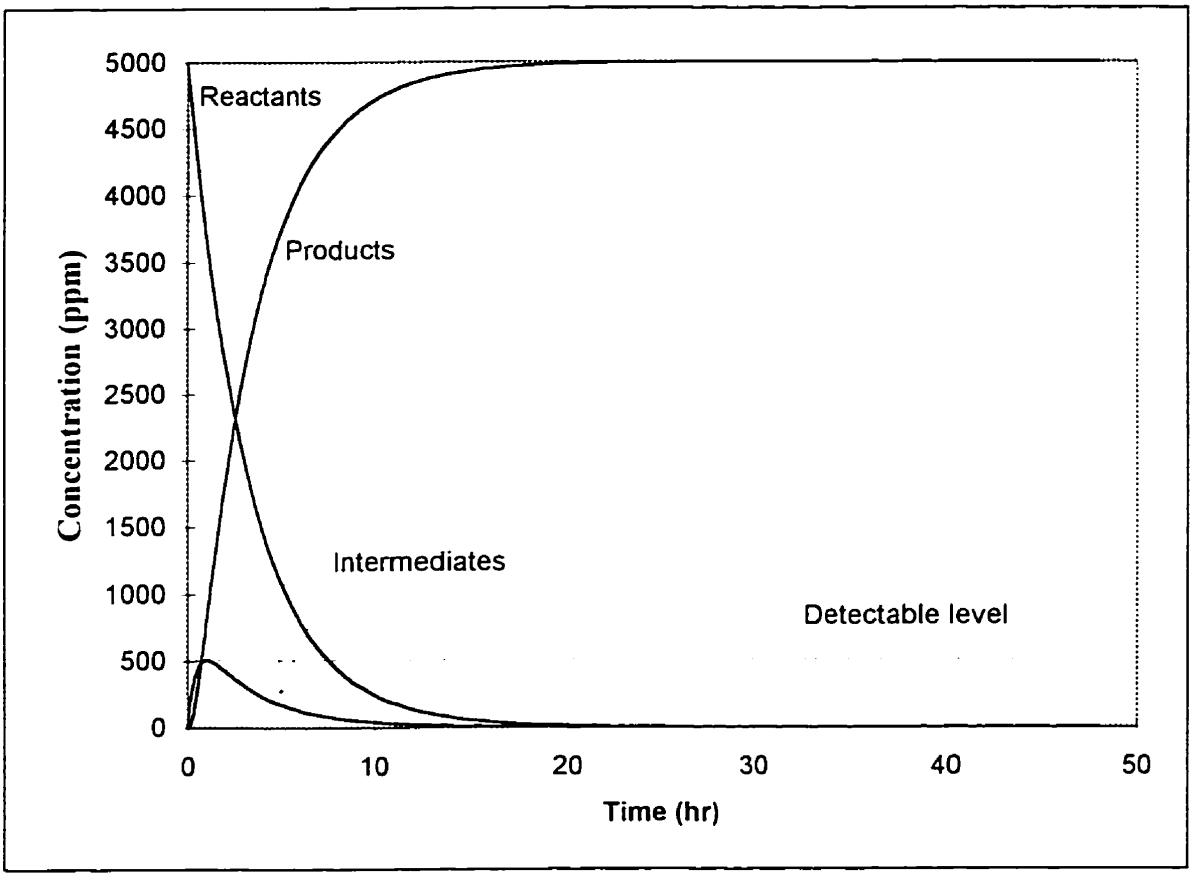

Figure 7.27: Simulated chemical species distribution for the following set of constants and operating conditions: k_1=0.3 (h^{-1}), k_2=2.2 (h^{-1}), and C_0= 18 $\mu g/cm^3$(5000ppm).

7.2.8 Catalyst Activity and Catalyst Activity Decay

There are some concerns in the photocatalytic literature about catalyst activity and eventual changes with time-on-stream [Luo and Ollis (1996), Jacoby *et al.*, (1996), and Peral and Ollis (1992)]. In the context of the present work, catalyst activity was examined by repeating experiments using a new filter mesh in each experiment. This was done for the first 16 experiments of the series at 100° C (refer to Table 7.2). However, to monitor catalyst activity decay, runs 29 to 32 were conducted with the same mesh which amounted to a filter being used for 90 h. Conversion remained at a steady level (15-20%), and on this basis it was concluded that there was no deactivation of the TiO_2 particles during the 90 h of utilization.

As well, as described in Section (7.2.4.3), the water effect on the catalytic activity in the context of the present study was tested. It was found that the values of the kinetic constant for toluene photo-oxidation at the high water concentration (runs 20-32) are slightly higher than the ones for the runs at low water concentration (runs 1-16). Thus, it was demonstrated that in Photo-CREC-Air, with a plate heating the mesh minimizing water adsorption, there was no negative effect of water on the catalytic activity.

7.2.9 Error Analysis

An error analysis was developed as to allow the estimation of the propagation of errors in the kinetic constant which is related directly to the following measured quantities: toluene concentration, time, and light intensity. Method followed was described in Mickley *et al.*, (1957). Error calculations associated with the kinetic constant were

performed assuming a maximum of 7% error associated with toluene concentration measurements, 1% on the experimental time and 10% on the measured UV light intensity. A Qbasic program, Appendix E, helped in analyzing 40 samples with errors randomized with respect to toluene concentration measurements, experimental time as well as the measured UV light. Typical standard error in the kinetic constant as calculated in the present study is 15% (Figure 7.28).

Note that the potential sources of errors as identified in the experimental runs were associated with the following: (i) imperfect injection of samples into the GC, (ii) diffusion of the sampling bags contents to the atmosphere, and (iii) eventual toluene condensation when warm samples were cooled to room temperature after being stored in the bags for a couple of hours.

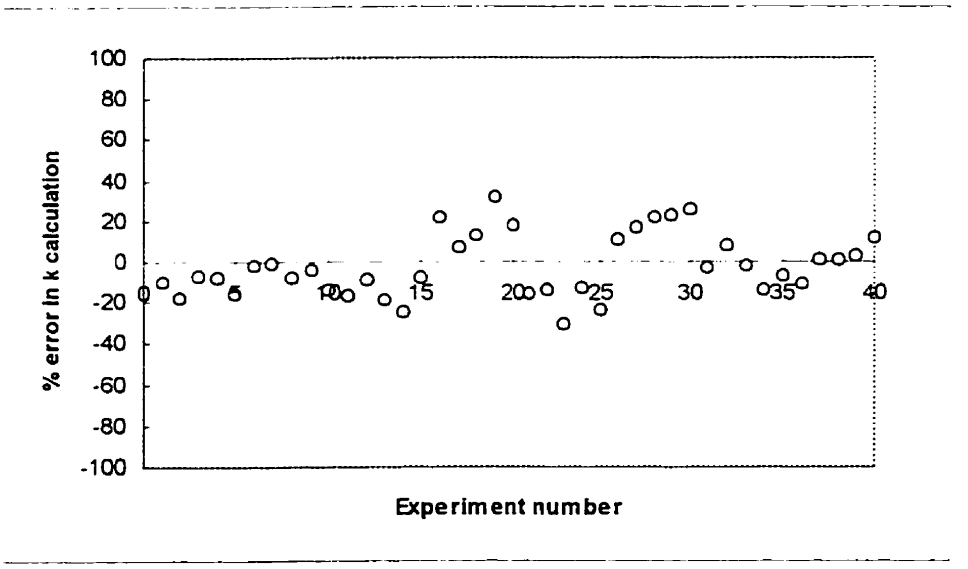

Figure 7.28:Estimated errors of the kinetic parameter associated with the different measured variables

7.3 Conclusions

Systematic runs developed in Photo-CREC-Air prototype demonstrated the excellent performance of the unit while performing runs with the heating plate at 100° C. The heating plate supporting the TiO_2 mesh, minimizes condensation/adsorption on the TiO_2 mesh surface and eliminates the potential influence of water content on catalytic activity.

Under these conditions it was found that first order kinetics (based on a pseudo-homogeneous model of the photoreaction with low/minimum adsorption of pollutants) is adequate for the description of the reaction data. Using the kinetic constants and the light absorbed by the mesh, apparent quantum yields in the 60-450 % range were obtained and this confirmed the special character of the photoconversion in Photo-CREC-Air, where every photon is involved in more than one photoconversion event.

CHAPTER 8

CONCLUSIONS AND RECOMMENDATIONS

The following are the conclusions of the present study:

- Photo-CREC-Air is designed with unique features such as the Venturi section, the heating plate supporting the TiO_2 mesh, and the focused illumination section. All of these characteristics optimized the unit performance in terms of fluid dynamic characteristics, TiO_2 mesh loading, illumination and quantum yield.
- Photo-CREC-Air displays high energy efficiency (high apparent quantum yields) being able to photoconvert significant amounts of pollutants with minimum light power.
- On the basis of the reported data, it is demonstrated that Photo-CREC-Air provides valuable performance in terms of toluene photodegradation in the range of concentration studied using minimum light power.
- Carbon dioxide and water were the only products observed from the photodegradation of toluene under the conditions studied. Intermediate species were below the detectable limits.
- It was demonstrated that a perforated heating plate supporting the TiO_2 mesh, a special Photo-CREC-Air feature, was very effective in minimizing water adsorption and condensation at 100° C. Under those conditions no catalyst activity decay was observed.

- It was found that pollutant adsorption at 100° C was not very significant, and on this basis a first order pseudo homogeneous model rate was considered. This model was adequate for representing the photo-oxidation rate of toluene under the experimental conditions tested.
- Apparent quantum yields assessed, in the course of study, were very promising. Values obtained were as high as 450% indicating the involvement of one photon in more than one photocatalytic event.

From the preceding conclusions and results, the following recommendations can be advanced:

- In Photo-CREC-Air reactor insulation is needed for better performance of the heating plate and the complete system. This will minimize heat losses around the plate section and heat removal to the surrounding environment. In addition, better insulation will keep the air enclosed in the recirculation loop at higher temperature minimizing toluene condensation.
- In Photo-CREC-Air, rate of pollutant photodegradation can be greatly improved including increasing the number of lamps, increasing the lamps power and changing the windows to Pyrex glass.
- Future experimentation of the existing photoreactor should incorporate an on-line GC injection for samples analysis. This will greatly reduce the inaccuracy in samples collection and data measurements.

- A more comprehensive study of the adsorption phenomena at 100° C and higher temperatures is needed for better assessment of the rate equations and this will provide more accurate kinetic modeling of the photo-oxidation rate.
- Evaluation of the heat of formation of the ·OH and/or other potentially involved radicals in the photocatalytic process is required to allow further application of the thermodynamic principles for energy efficiencies.
- A more detailed study of apparent quantum yields, found as described here almost in all cases above 100%, and its connection with the photocatalytic reaction mechanism is very much needed.

REFERENCES

Akimoto, H., Hoshino, M., Inove, G., Okuda, M., and Washida, N., "Reaction Mechanism of the Photo-oxidation of the Toluene -NO_2-O_2-N_2 System in the Gas Phase", Bulletin of the Chemical Society of Japan, v51(9), 2496-2502, **1978**.

Anderson, M., Yamazaki-Nishida, S., and Cervera-March, S., "Photodegradation of Trichloroethylene in the Gas Phase Using TiO_2 Porous Ceramic Membrane", in Photocatalytic Purification and Treatment of Water and Air: Proceedings of the 1st International Conference on TiO_2, 405-420, D. Ollis and H. Al-Ekabi (eds.), **1993**.

Atkinson, R., Carter, W., Darnall, K., Winer, A., and Pitts, J., "A Smog Chamber and Modeling Study of the Gas Phase NO_x Air Photo-Oxidation of Toluene and the Cresols", International Journal of Chemical Kinetics, v7, 779-836, **1980**.

Berman, E., and Dong, J., "Photocatalytic Decomposition of Organic Pollutants in Gas Stream", in Chemical Oxidation Technologies for the Ninties, 183-189, W. Eckenfelder *et al.* (eds), **1994**.

Besemer, A., "Formation of Chemical Compounds from Irradiated Mixtures of Aromatic Hydrocarbons and Nitrogen Oxides", Atmospheric Environment, v16(6), 1599-1602, **1982**.

Bickley, G., Munuera, and Stone, F., "Photo Adsorption and Photocatalysis of Rutile Surfaces: Photocatalytic Oxidation of Iso-propanol", J. of Catalysis, v31, 398-407, **1973**.

Blanco, J., Avila, P., Bahamonde, A., Alvarez, E., Sanchez, B., and Romero, M., "Photocatalytic Destruction of Toluene and Xylene at Gas Phase on a Titania Based Monolithic Catalyst", Catalysis today, v29, 437-442, **1996**.

Bolton, J., Safarzadeh-Amiri, A., and Cater, S., "The Detoxification of Waste Water Streams Using Solar and Artificial UV Light Sources", in Alternative Fuels and the Environmental, 187-192, F. S. Sterret (ed.), **1995**.

Childs, L., and Ollis, D., "Is Photocatalysis Catalytic?", Journal of Catalysis, v66, 383-390, **1980**.

de Lasa, H., "Photocatalytic Reactor and Method for Destruction of Organic Airborne Pollutants", Canadian Patent Application N° 2202716, **1997**.

de Lasa, H., and Ibrahim, H., "Photocatalytic Reactor for the Destruction of Airborne Pollutant", Proposed Patent Application, **1998**.

Dibble, L., and Raupp, G., "Fluidized-Bed Photocatalytic Oxidation of Tricholoethylene in Contaminated Air streams", Environ. Sci. and Technol., v26(3), 492-495, **1992**.

Formenti, M., Juillet, F., Meriaude, P., and Teicher, S., "Heterogeneous Photocatalysis for Partial Oxidation of Paraffins.", Chem. Technol., v1, 680, **1971**.

Formenti, M., Juillet, F., and Teicher, S, "Photocatalytic Oxidation Mechanism of Alkanes over Titanium Dioxide: 2. Reaction Mechanism", Bull. Soc. Chem. Fr, v9-10, 1315-1320, **1976**.

Formenti, M., and Teicher, S., in "Catalysis v.2, Specialist Periodical Report", p87, Chemical Society of London Edition, London, **1979**.

Fox, M., and Dulay, M., "Heterogeneous Photocatalysis", Chemical Reviews, v93, 341-357, **1993**.

Fox, Marye Anne . "Photocatalytic Oxidation of Organic Substrates", in Photocatalysis and Environment: Trends and Applications, 445-467, Schiavello M. (ed.), **1988**.

Fujishim, A., and Honda, K., "Electrochemical Photolysis of Water at a Semiconductor Electrode", Nature, v238(5358), 37, **1972**.

Heuss, J., Nebel, G., and D'Alleva, B., "Effects of Gasoline Aromatic and Lead Content on Exhaust Hydrocarbon Reactivity", Environ. Sci. Technol., v8, 641-647, **1974**.

Ibusuki, T., and Takeuchi, K., "Toluene Oxidation on UV Irradiated Titanium Dioxide With and Without O_2, NO_2, or H_2O at Ambient Temperature", Atmospheric Environment, v20(9), 1711-1715, **1986**.

Ibusuki, T., Kutsuna, S., and Takeuchi, K., "Removal of Low Concentration Air Pollutants through Photoassisted Heterogeneous Catalysis", in Photocatalytic Purification and Treatment of Water and Air: Proceedings of the 1st International Conference on TiO_2, 375-386, D. Ollis and H. Al-Ekabi (eds.), **1993**.

Jacoby, W., Blake, D., Noble, R., and Koval, C., "Kinetics of Oxidation of TCE in Air via Heterogeneous Photocatalysis", Journal of Catalysis, v157, 87-96, **1995**.

Jacoby, W., Blake, D., Fennell, D., Boulter, J., Vargo, L., George, M., and Dolberg, S., "Heterogeneous Photocatalysis for Control of Volatile Organic Compounds in Indoor Air", Journal of Air and Waste Management Association, v46, 891-898, **1996**.

Lonneman, W., Kopczynski, S., Darley, P., and Suterfield,. F., " Hydrocarbon Composition of Urban Air Pollution", Environ. Sci. Technol., v8, 229-236, **1974**.

Luo, Y., and Ollis, D., "Heterogeneous Photocatalytic Oxidation of Trichloroethylene and Toluene Mixtures in Air: Kinetic Promotion and Inhibition, Time-Dependent Catalyst Activity", Journal of Catalysis, v163, 1-11, **1996**.

Matthews R., "Kinetics of Photocatalytic Oxidation of Organic Solutes Over Titanium Dioxide", Journal of Catalysis, v3, 264-272, **1988**.

McCabe, S., Smith, J., and Harriott, P., Unit Operations of Chemical Engineering. McGraw-Hill, Inc., Toronto, **1993**.

Mickley, H., Sherwood, T., and Reed, C., Chemical Engineering Series: Applied Mathematics in Chemical Engineering. McGraw-Hill, Inc., Toronto, **1957**.

Miller, R., and Fox, R., "Treatment of Organic Contaminants in Air by Photocatalytic Oxidation: A Commercialization Perspective", in Photocatalytic Purification and Treatment of Water and Air: Proceedings of the 1st International Conference on TiO_2, 573-578, D. Ollis and H. Al-Ekabi (eds.), **1993**.

Milne, T., and Nimlos, M., "Chemical Safety: Incomplete Photocatalytic Oxidation of TCE", Chem. Eng. News, v70(14-26), 2, (June,22) **1992**.

Muradov, N., T-Raissi, A., Muzzey, D., Painter, C., and Kemme, M., "Selective Photocatalytic Destruction of Airborne VOCs", Solar Energy, v56(5), 445-453, **1996**.

Muriel, M., Rueda, A., and Milow, B.(eds.), Plataforma Solar de Al-meria. Annual Technical Report., Spain, **1996**.

Obee, T., and Brown, R., "TiO_2 Photocatalysis Indoor Air Applications: Effects of Humidity and Trace Contaminant Levels on the Oxidation Rates of Formaldehyde, Toluene, and 1,3-Butadiene", Environmental Science and Technology, v29(5), 1223-1231, **1995**.

Ollis, D., "Photo Reactors for Purification and Decontamination of Air", in Photocatalytic Purification and Treatment of Water and Air: Proceedings of the 1st International Conference on TiO_2, 481-494, D. Ollis and H. Al-Ekabi (eds.), **1993**.

Peill, N., and Hoffmann, M., "Development and Optimization of a TiO_2 Coated Fiber Optic Cable Reactor: Photocatalytic Degradation of 4-Chlorophenol", Environ. Sci. Technol., v29, 2974-2981, **1995**.

Peill, N., and Hoffmann, M., "Chemical and Physical Characterization of a TiO_2 Coated Fiber Optic Cable Reactor", Environ. Sci. Technol., v30, 2806-2812, **1996**.

Peral, J., and Ollis, D., "Heterogeneous Photocatalytic Oxidation of Gas-Phase Organics for Air Purification: Acetone, 1-Butanol, Butyraldehyde, Formaldehyde, and m-Xylene Oxidation", Journal of Catalysis, v136, 554-565, **1992**.

Perry, R., and Green, D., Perry's Chemical Engineering Handbook. McGraw-Hill, Inc., Toronto, **1984**.

Raupp, G., Nico, J., Annangi, S., Changrani, R., and Annapragada, R., "Two Flux Radiation-Field Model for an Annular Packed Bed Photocatalytic Oxidation Reactor", AIChE, v43(3), 792-801, **1997**.

Sauer, M., and Ollis, D., "Acetone Oxidation in a Photocatalytic Monolith Reactor", Journal of Catalysis, v149, 81-91, **1994**.

Sczechowski, J., Koval, C., and Noble, R., "A Taylor Vortex Reactor for Heterogeneous Photocatalysis", Chemical Engineering Science, v50(20), 3163-3173, **1995**.

Serrano, B., and de Lasa, H., "Photocatalytic Degradation of Water Organic Pollutants. Kinetics Modeling and Energy Efficiency", Ind. Eng. Chem. Res., v36, 4705-4711, **1997**.

Shepson, P., Edney, E., and Corse, E., "Ring Fragmentation Reactions on the Photo-Oxidation of Toluene and O-xylene", The Journal of Physical Chemistry, v 88(18),4122-4126, **1984**.

Suzuki, K., Satoh, S., and Yoshida, T., "Photocatalytic Deodorization on TiO_2 Coated Honeycomb Ceramics", Denki Kagaku, v59(6), 521-523, **1991**.

Suzuki, K., "Photocatalytic Air Purification on TiO_2 Coated Honeycomb Support", in Photocatalytic Purification and Treatment of Water and Air: Proceedings of the 1st International Conference on TiO_2, 421-434, D. Ollis and H. Al-Ekabi (eds.), **1993**.

Tchobanoglous, G., and Burton, F. (Eds.). Wastewater Engineering Treatment, Disposal and Reuse. Toronto: Metcalf and Eddy Inc, **1991**.

Valladares, J., A New Photocatalytic Reactor for the Photodegradation of Organic Contaminants in Water, PhD Thesis, University of Western Ontario, **1995**.

Van Vlack, Lawrence. Materials for Engineering: Concepts and Applications. Addison. Wesley, **1982**.

Wang, K., and Marinas, B., "Control of VOC Emissions from Air Stripping Towers: Development of Gas-Phase Photocatalytic Process", in Photocatalytic Purification and Treatment of Water and Air: Proceedings of the 1st International Conference on TiO_2, 733-739, D. Ollis and H. Al-Ekabi (eds.), **1993**.

Yamazaki-Nishida, S., Nagano, J., Phillips, L., Cervera-March, S., and Anderson, M., "Photocatalytic Degradation of Trichloroethylene in the Gas Phase Using Titanium Dioxide Pellets", Journal of Photochemistry and Photobiology A: Chemistry, v70, 95-99, **(1993)**.

Yamazaki-Nishida, S., Read, H., Nagano, J., Jarosch, T., Eddy, C., Cervera-March, S., and Anderson, M., "Gas Phase Photocatalytic Degradation on TiO_2 Pellets of Volatile Chlorinated Compounds from a Soil Vapor Extraction Well", Journal of Soil Contamination, v3(4), 363-378, **1994**.

Yue, P., "Modeling, Scale-up and Design of Multiphasic Photoreactors", in Photocatalytic Purification and Treatment of Water and Air: Proceedings of the 1st International Conference on TiO_2, 495-510-, D. Ollis and H. Al-Ekabi (eds.), **1993**.

Zhang, N., Crittenden, J., Hand, D., and Perram, D., "Fixed-Bed Photocatalysts for Solar Decontamination of Water", Environ. Sci. Technol., v28, 435-442, **1994**.

APPENDICES

APPENDIX A: Fortran Program to Calculate the Venturi Length as a Function of Pressure Drop Across its Length

```
C-----------------------------------------------------------------------------------------
C This program was written as to aid in calculating the total length of the Venturi
C as a function of the total pressure drop across it and the throat to the pipe
C diameter. Variables definition is as follows:
C V2 is the velocity of the fluid at the throat, Dp is the pressure drop through the
C Venturi, L1 is the length of the up stream cone, L2 is the length of the
C downstream cone, Ltotal is the total length of Venturi including the straight
C section between the two cones, A1 is the upstream cone angle, A2 is the
C downstream cone angle, and B is the ratio of the inlet duct diameter to the
C diameter of the throat.
C-----------------------------------------------------------------------------------------
C234567
      IMPLICIT NONE
      REAL  V2,Dp,L1,L2,Ltotal,B,A1,A2
      PRINT*, "Please enter B, A1, A2"
      READ*,B,A1,A2
      V2=.152**2*3.6/(0.152*B)**2
      Dp=-(V2/0.98)**2*(1.2*(1-B**4)/2)
      L1=(15.2-15.2*B)/(2*TAN(A1))
      L2=(15.2-15.2*B)/(2*TAN(A2))
      Ltotal=L1+L2+B
      PRINT* V2,Dp,L1,L2,Ltotal
      END
```

APPENDIX B: GC Calibration Curves

GC calibration curves were prepared to help in assessing the actual amount of the reactant and product. Linear fits were adequate for toluene and carbon dioxide, whereas a quadratic fit was needed for water.

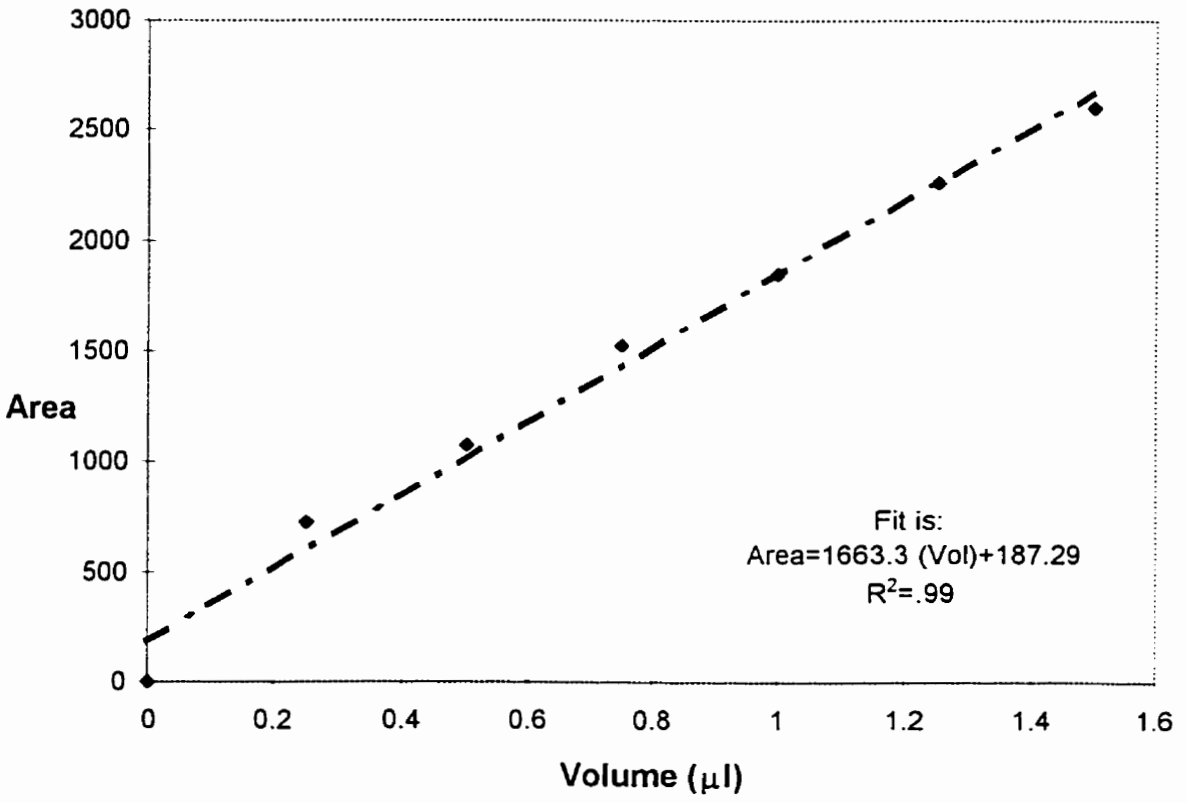

Figure B.1: Calibration curve of carbon dioxide.

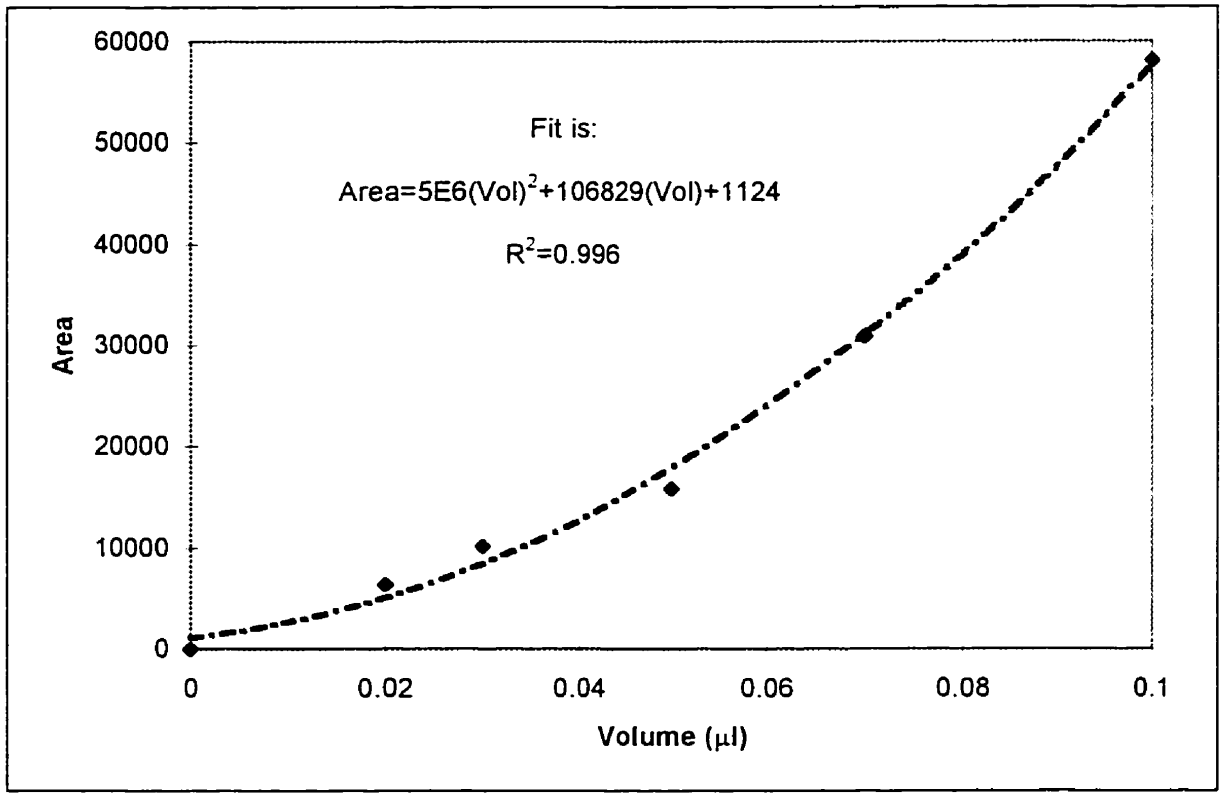

Figure B.2: Calibration curve of water.

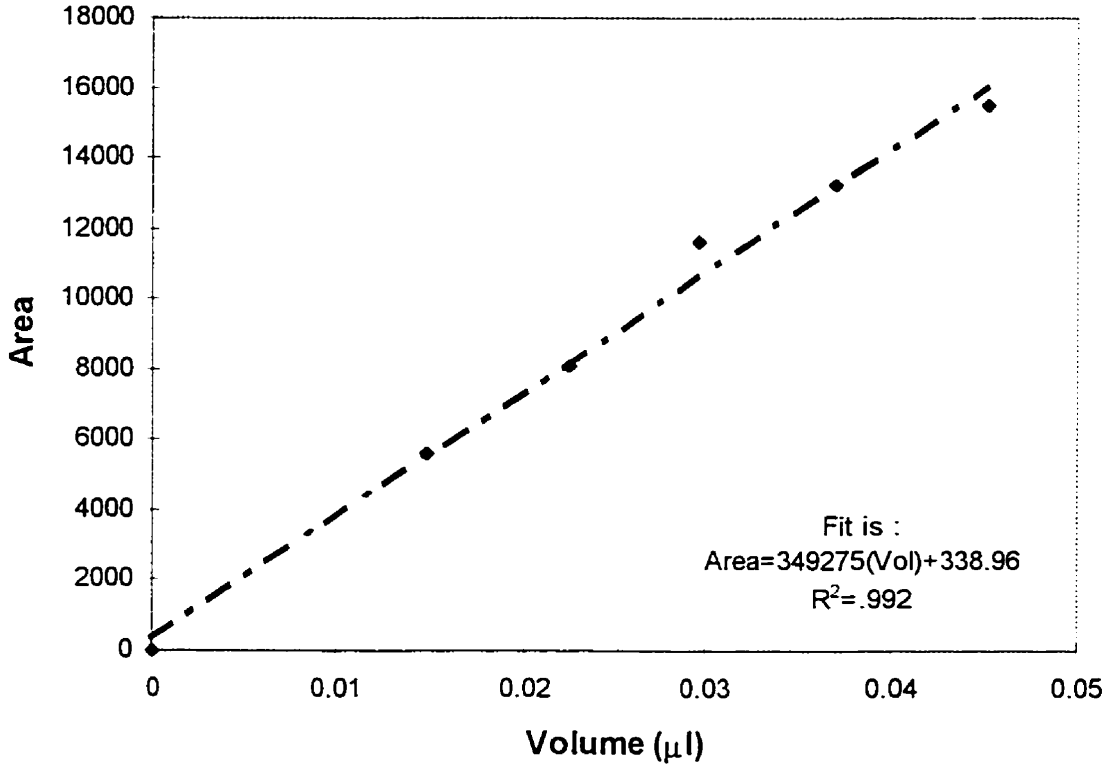

Figure B.3: Calibration curve of toluene.

APPENDIX C: Carbon and Hydrogen Mass Balances

This appendix gives a listing of typical carbon and hydrogen mass balances.

Temperature (°C)		100			75	50	20	100
Concentration ($\mu g/cm^3$)	5.2	7.78	10.4	13	10.4	10.4	10.4	10.4
water vapor ($\mu g/cm^3$)	<25	<25	<25	<25	<25	<25	<25	>25
Before								
CO_2 (g)	1.8E-06	1.5E-06	1.6E-06	1.7E-06	1.1E-06	1.5E-06	1.1E-06	1.1E-06
water (g)	6.2E-05	5.1E-05	5.17E-05	3.8E-05	3.9E-05	3.5E-05	3.9E-05	7.2E-05
toluene (g)	1.3E-05	2E-05	2.9E-05	3.3E-05	2.6E-05	2.6E-05	2.2E-05	2.9E-05
After								
CO_2 (g)	1.9E-06	1.6E-06	1.7E-06	1.8E-06	1.1E-06	1.6E-06	1.1E-06	1.2E-06
water (g)	6.6E-05	5.60E-05	5.58E-05	5.1E-05	3.8E-05	3.3E-05	3.6E-05	7.9E-05
toluene (g)	9.1E-06	1.2E-05	2E-05	1.8E-05	1.6E-05	1.7E-05	1.4E-05	2.1E-05
Net CO_2 increase (g)	1.3E-07	7.9E-08	1.5E-07	1.6E-07	7E-08	7.9E-08	5.3E-08	5.3E-08
Net Water increase (g)	3.6E-06	4.9E-06	4.1E-06	1.2E-05	-1.4E-06	-1.6E-06	-2.7E-06	6.8E-06
Net toluene decrease (g)	4.3E-06	7.8E-06	8.9E-06	1.4E-05	9.6E-06	9.2E-06	7.7E-06	7.8E-06
Net hydrogen balance (g)	-2.6E-08	1.4E-07	3.2E-07	-1.2E-07	9.9E-07	9.8E-07	9.7E-07	-8.2E-08
Net carbon balance(g)	3.9E-06	7.1E-06	8.1E-06	1.3E-05	8.7E-06	8.4E-06	7E-06	7.1E-06
Net hydrogen balance (%)	-2.19313	8.02662	12.6962	-4.23708	43.8897	43.8034	50.9451	-3.23985
Net Carbon balance (%)	31.7444	39.2172	30.9963	43.8522	36.7423	35.6746	35.1211	26.8936

APPENDIX D: Fortran Program for Data Simulation

```
C-----------------------------------------------------------------------------------------
C This program was written as help in providing some simulated data regarding
C the intermediates level that can be detected and the experimental time required
C under the different operating conditions  Variables definition is as follows:
C T is the time, DT is the change in time, CA is the concentration of reactant A,
C CB is the concentration of intermediate B, CC is the concentration of product C,
C DCA is the change in the reactant concentration, DCB is the change in the
intermediate C concentration, and DCC is the change in the product concentration,
K1 is the reaction rate constant for the reactant A reaction, K2 is the reaction rate
C constant for the intermediate B reaction.
C-----------------------------------------------------------------------------------------
C234567
      IMPLICIT NONE
      REAL T,DT,CA,CB,CC,K1,K2,DCA,DCB,DCC
      CA=5000
      CB=0
      CC=0
      K1=.2
      K2=20
      T=0
      DT=0.05
      OPEN(UNIT=1, FILE='OUTPUTS')
```

```
 10 T=T+DT
      IF (T.GT.24) GO TO 20
      DCA=-K1*CA*DT
      DCB=K1*CA*DT-K2*CB*DT
      DCC=K2*CB*DT
      CA=CA+DCA
      CB=CB+DCB
      CC=CC+DCC
      WRITE (1,901) T,CA,CB,CC
      PRINT*, T,CA,CB,CC
901     FORMAT (4(5X,F8.3))
      GO TO 10
 20 CONTINUE
   CLOSE (UNIT=1)
   END
```

APPENDIX E: Qbasic Program for the Calculation of the Error Involved in the Kinetic Constant Estimation as a Result of the Error Associated with the Measured Variables

---

This QBASIC program was written to help in estimating the propagation of errors of the measurable variable on the kinetic parameter estimation. Variables definition is as follows: T is the experimental time, DT is the maximum error associated with the time measurement, DC is the maximum error associated with the toluene concentration measurement, DI is the maximum error associated with the UV intensity measurement, I_o is the incident UV light intensity, Z1 Z2 and Z3 are generate random numbers for the purpose of testing the different errors associated with the measured variables, and k_o kinetic constant. The main equation in the program was derived from the classical error propagation analysis as described in Mickely (1957):

$$k_o = f(C,t,I) = (I_o/I) \ln(C_T/C_{To})/t \qquad (E.1)$$

$$dk_o = \delta f/\delta C \, dC + \delta f/\delta t \, dt + \delta f/\delta I \, dI \qquad (E.2)$$

$$\Delta k_o/k_o \leq (I_o/Itk_o) \, \Delta C/C \, \gamma_1 - (I_o/I) \, \Delta t/t \, \gamma_2 - (I_o/I) \, \Delta I/I \, \gamma_3 \qquad (E.3)$$

where γ_1, γ_2, and γ_3 are random error functions oscillating between -1 and 1.

```
OPEN "A", #1, "ERROR"
T = 24
Ko = 0.03
```

```
DC = .07
DT = .01
DI = 0.1
RANDOMIZE TIMER
FOR I = 1 TO 5
Z1 = RND
Z2 = RND
Z3 = RND
Kerror = -DT * Z1 * 100 * .5 + DC * Z2 * 100 * .5 / Ko / T - .5 * DI * Z3 * 100

PRINT #1, I, Z1, Z2, Z3, Kerror
NEXT I
CLOSE #1
```

IMAGE EVALUATION
TEST TARGET (QA-3)

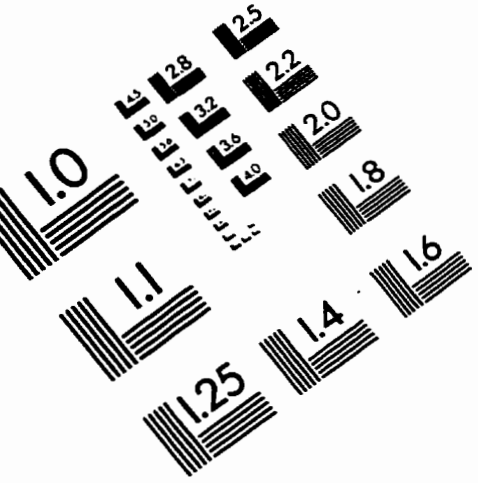

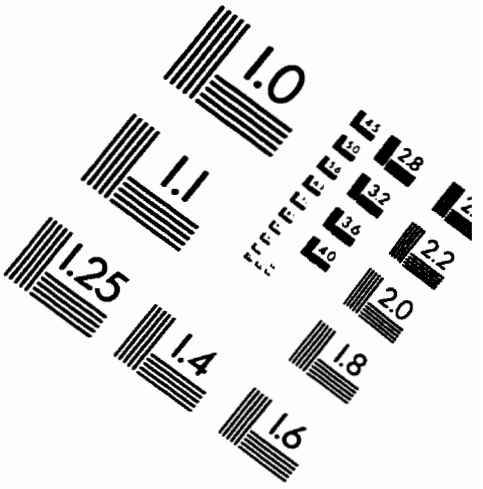

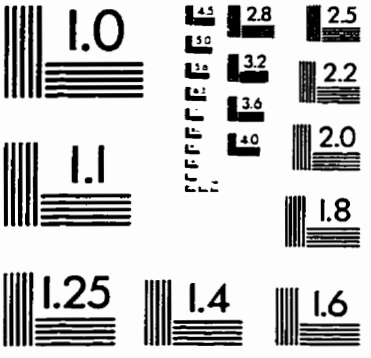

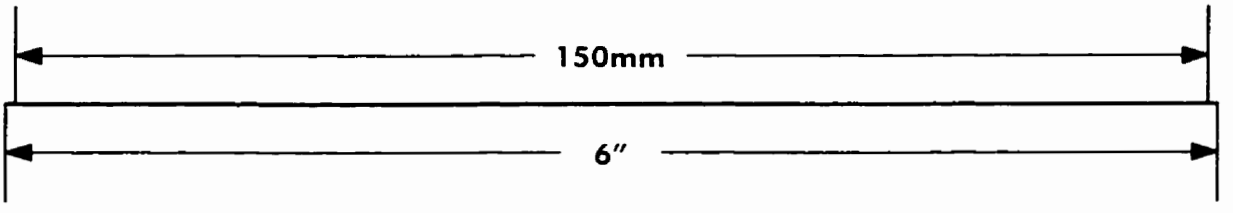

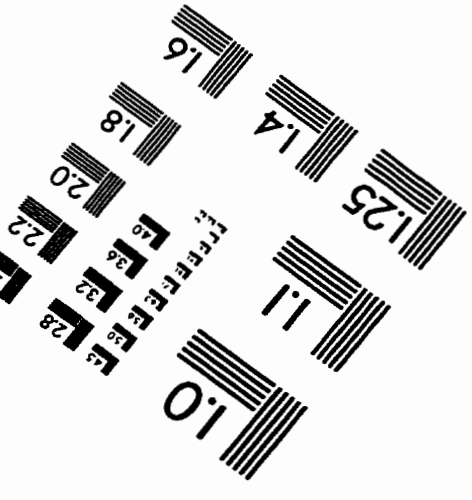

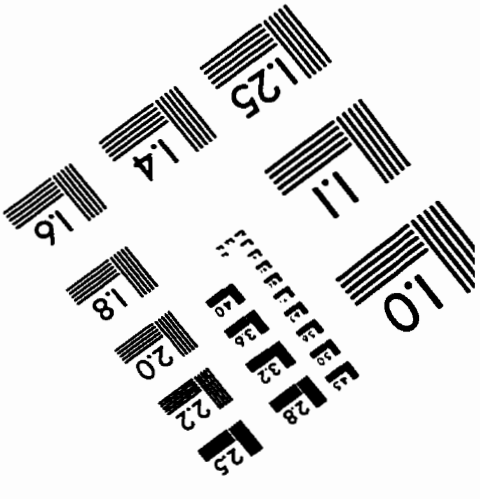

APPLIED IMAGE, Inc
1653 East Main Street
Rochester, NY 14609 USA
Phone: 716/482-0300
Fax: 716/288-5989

© 1993, Applied Image, Inc., All Rights Reserved